STUDIES OF CYCLODEXTRIN FUNCTIONALISED SILICA MATERIALS

A Thesis Submitted

To the College of graduate Studies and Research

in Partial Fulfillment of the Requirements

for the Degree of Master of Science

in the Department of Chemistry

University of Saskatchewan

Saskatoon

By

Sarker Tarek Mahmud

PERMISSION TO USE

In presenting this thesis in partial fulfillment of the requirements for a degree of Master of Science from the University of Saskatchewan, I, the author of the thesis, agree that the Libraries of this University may make it freely available for inspection. Permission for copying this thesis in any manner, in whole or in part, for scholarly purposes may be granted by Dr. Lee D. Wilson who supervised my thesis work or, in his absence, by the head of the Department of Chemistry or the Dean of the College of Graduate Studies and Research. Any copying or publication or use of this thesis, or parts thereof, for financial gain shall not be allowed without my written permission. Due recognition shall be given to the author and to the University of Saskatchewan in any scholarly use which may be made of any material in this thesis.

Requests for permission to copy or to make other use of material in this thesis in whole or part should be addressed to:

Head of the Department of Chemistry

University Of Saskatchewan

110 Science place, Saskatoon, S7N 5C9

Saskatchewan, Canada

ABSTRACT

Mesoporous silica materials containing microporous cavities provided by covalently bound β-cyclodextrin (CD ICS) were synthesized by co-condensation of a β-CD functionalized triethoxy silane (CD ICL) with tetraethyl orthosilicate (TEOS) by using neutral amine surfactants as structure directing agents (SDA). CD ICL was prepared by reacting β-CD with 3-isocyanatopropyltriethoxysilane. IR spectroscopy of CD ICL showed complete disappearance of isocyanato group at 2270 cm^{-1}. ^{1}H NMR results indicate an average of four isocyanate linkers covalently attached to random hydroxyl substituents of each molecule of β-CD.

Nine different CD ICS materials were synthesized using dodecylamine, tetradecylamine or hexadecylamine with β-CD (2, 4, and 6 mol %) with respect to TEOS. The incorporation of β-CD within the mesoporous framework was supported by IR, Raman, MALDI TOF MS, solid state ^{13}C NMR CP-MAS and TGA results. Small angle X-ray diffraction results showed a peak at $2\theta \approx 2.2^{0}$, supporting the presence of an ordered silica mesostructure framework. For materials with same CD loading, the surface area and pore volume doubled as the surfactant from dodecylamine to hexadecylamine. However, as the CD loading increased from 2% to 6%, the surface area decreases by a factor of ~ 1.5. MALDI TOF mass spectrometry showed two peaks at m/z 1157 a.m.u. and 1173 a.m.u. for $[\beta\text{-CD} + Na]^{+}$ and $[\beta\text{-CD} + K]^{+}$ respectively due to desorption of β-CD from the walls of the silica matrix. The ^{13}C NMR CP MAS results showed ^{13}C signals in the region δ=60-110 ppm due to the nuclei of β-CD. CD ICS materials

were found to be effective as a sorbent in both gas and aqueous phases, respectively. The sorption capacity (mmol/g) of p-nitrophenol increased from 61% to 84% with an increase of CD loading from 2% to 6% and as the alkyl chain length of the SDA increases from dodecylamine to hexadecylamine. The adsorption isotherm of CH_3Cl in the gas phase and that of p-nitrophenol in the aqueous phase at ambient temperature adopts a multilayer model of adsorption.

ACKNOWLEDGEMENTS

I express my deep and sincere gratitude to my supervisor, Dr. Lee D. Wilson, for his guidance, encouragement, wisdom and financial support during my work. His enthusiasm and patience helped me a lot during my studies. I would like to express my sincere gratitude to the Advisory committee member, Dr. Robert Scott, for his suggestions and advice.

I am indebted to my friend and lab member, Jae Hyuck Kwon, for his help during all my hard times. Thanks are due to the other lab members, Olumbunmi Fadeyi and Mohammed Hamid. Besides them I am also grateful to Adel Sudom, the undergraduate student, who helped me a lot during this research.

I am also grateful for the kind and friendly suggestions and assistance received from Zahid, Sunish, Vivek, Nagarjuna, Dorota, Umakanta, Xia and all my other friends. A special thanks to Sunish and Vivek for all of their support and help in difficult situations.

I thank my friends who were with me in all my cheerful and critical moments.

I would like to thank my family without whom I would not have been what I am now.

Finally, I would like to thank Allah for his mercy and love in my life.

DEDICATION

I dedicate my M.Sc. thesis to my younger brother Probal and my dearest wife, Doyel.

TABLE OF CONTENTS

LIST OF TABLES

LIST OF FIGURES

LIST OF SCHEMES

LIST OF ABBREVIATIONS

Å	Angstrom
APS	3-Aminopropyltriethoxysilane
APS β-CD	3-Aminopropyltriethoxysilane covalently attached to monochlorotriazinyl-β-cyclodextrin.
APS MCT	3-Aminopropyltriethoxysilane covalently attached to monochlorotriazinyl-β-cyclodextrin.
BET	Brunner-Emmet-Teller
cc	Cubic centimeter
cm	Centimeter
CD	Cyclodextrin
CD-HMS	Cyclodextrin incorporated hexagonal mesoporous silica
CD ICL	β-Cyclodextrin functionalized triethoxysilane where β-Cyclodextrin is covalently attached to 3-isocyantopropyl triethoxy silane via isocyanate carbamate linkage
CD ICS	β-Cyclodextrin composite hexagonal mesoporous silica where β-Cyclodextrin is covalently attached to silica network via urethane linkage
C, H, N analysis	Carbon, hydrogen, nitrogen elemental analysis
^{13}C NMR	^{13}C nuclear magnetic resonance
CP-MAS	^{13}C cross polarization and magic angle spinning
CTAB	Cetyltrimethylammonium Bromide
DMSO-d_6	Deuterated Dimethylsulfoxide
FID	Free Induction Decay
FT-IR	Fourier transform infrared spectroscopy
HMS	Hexagonal mesoporous silica synthesized by using neutral surfactant
Hz	Hertz
^{1}H NMR	proton nuclear magnetic resonance
IUPAC	International Union of Pure and Applied Chemistry
mL	Milliliter
mmol	Millimole
m/z	Mass to charge ratio
M41S	Periodic mesoporous silica
MCM-41	Hexagonal mesoporous silica synthesized by using ionic surfactant
M.W.	Molecular Weight
MALDI TOF MS	Matrix assisted laser desorption ionization time of flight mass spectrometry
nm	Nanometer
NMR	Nuclear magnetic resonance
ORMOSIL	Organically Modified Silica

pNP	p-nitrophenol
PMO	Periodic mesoporous organosilica
PAH	Poly Aromatic Hydrocarbon
PXRD	Powder X-ray Diffraction
SAXD	Small angle X-ray Diffraction
SDA	Structure directing agent
TEOS	Tetraethyl orthosilicate
TGA	Thermogravimetric analysis
UV-Vis	Ultraviolet-Visible
XRD	X-ray Diffraction

CHAPTER 1
INTRODUCTION
1.1 Mesoporous silica
1.1.1 Porous materials

Porous materials are widely used as adsorbents, catalysts, and catalyst supports due to their large surface area and pore volume characteristics. According to IUPAC, porous materials are classified into three types[1] namely: *i)* Microporous, with pore width below 2.0 nm, *ii)* Macroporous, with pore widths exceeding 50.0 nm, and *iii)* Mesoporous, with intermediate pore width between 2.0 and 50.0 nm. Microporous crystalline aluminosilicate materials, called zeolites, have uniform pores in the range of 0.5-2.0 nm and have well defined crystallographic sites, which enables them to be used as molecular sieves and catalyst, for example, cracking of crude-oil in the petroleum industry.[2] The general application of zeolites is limited due to their small pore size distribution. Consequently, a lot of effort was directed at the synthesis of "zeolite-like" materials with pores greater than 2 nm with a well defined and an ordered pore structure.

Table 1.1: Pore size regimes and representative porous inorganic materials[3]

Pore size regime	Size Domain	Examples	Actual size range
Macroporous	>50 nm	glasses	> 50 nm
Mesoporous	2-50 nm	Aerogels	>10 nm
		M41S	1.6-10 nm
Microporous	<2 nm	Zeolites	<1.4 nm
		Activated Carbon	0.6 nm

1.1.2 Periodic mesoporous silica

In 1992 Beck *et al.*[4] first reported the synthesis of a new family of ordered mesoporous molecular sieves designated as M-41-S. One member of the family, MCM-41, exhibited a hexagonal arrangement of uniform mesopore whose pore dimension was engineered in the range of 15Å to greater than 100 Å. Through the self-assembly of surfactant micelles and a silica precursor, tetraethyl orthosilicate (TEOS), an ordered nanocomposite forms, in which silica replicates the shape of the phase of the cylindrical organic micelles. Removal of the surfactant template from the nanocomposite gives the periodic mesoporous silica, as outlined in scheme 1.1[5]

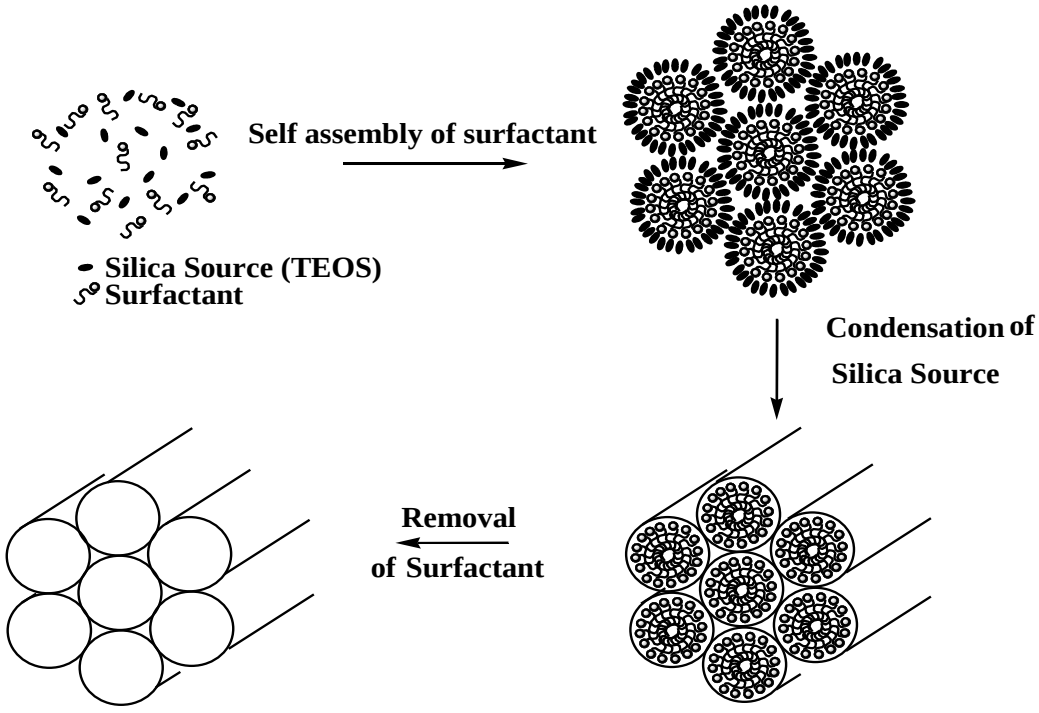

Scheme 1.1: Synthetic scheme for periodic mesoporous silica[5]

1.1.3 Organic functionalization of silica

Organically modified silica (ORMOSIL), where an organic group is incorporated within the network of a glass was reported by Schimdt *et al.*[6] in 1985. Mechanical and physical properties of ORMOSIL differ from traditional glasses and ceramics. Since the discovery of MCM-41 in 1992, considerable effort was directed toward new methods to incorporate organic functionalities in these ordered mesoporous materials. Organically functionalized silica is of great interest in environmental remediation and chromatographic separations due to its high surface area. The incorporation of organic functionalities in silica allows changes in the surface properties, modification of the hydrophilic/hydrophobic balance of the silica surface, introduction of binding affinity towards an adsorbate molecule, modification of surface reactivity and bulk properties of the material, and stabilization of the material toward hydrolysis. There are three general ways to functionalize organic groups in ordered mesoporous silica, which are as follows:

1. Post synthetic grafting

2. Direct incorporation, or one-pot method, by co-condensation of TEOS with a terminal organosiloxane, $RSi(OEt)_{3,}$ where R = organic functional group.

3. Periodic Mesoporous Organosilica: Co-polymerization of a bridged silsequioxane, $(RO)_3Si\text{-}B\text{-}Si(OR)_3$ either with or without TEOS, where B = organic bridging group.

Post synthetic grafting and direct incorporation

Introduction of an organic functionality can be achieved either by postsynthetic grafting of organic groups onto the channel walls by reacting them with pendant silanol groups of the original silica matrix or by co-condensation TEOS with a terminal organosiloxane of the type $RSi(OEt)_3$.[7,8] Each of the respective methods has advantages and disadvantages, as outlined below:

Advantages[7, 8]

1) The co-condensation method gives a uniform surface coverage with an organic group.

2) The post-synthetic grafting method gives a structurally well-defined material than the co-condensation method. Furthermore, pore size control is easier for post synthetic grafting process since organic functionalization takes place in pre-formed silica matrix with well defined pore structure characteristics.

Disadvantages[5]

1) Since the organosiloxane co-assembles with TEOS to obtain a stable periodic mesostructure, the co-condensation method limits the organic content of the material to ~ 25% with respect to the silicon wall sites.

2) Both methods may lead to a non-uniform distribution of the organic functionality within the pores. In the post-synthesis grafting method, organic loading is limited by the number of reactive surface silanol groups present and by diffusion limitations.[7] On the other hand, the co-condensation method involves self-condensation of the terminal organosiloxane and may lead to an inhomogeneous distribution of organic functionality on the silica surface.

Periodic Mesoporous Organosilica [9-11]

Polymerization of bridged silsequioxane monomers, $(RO)_3Si\text{-}B\text{-}Si(OR)_3$, or copolymerization of TEOS with bridged silsequioxane monomers in the presence of a surfactant template produces MCM-41 related materials where the organic functionality becomes an integral part of the channel walls. Removal of the surfactant creates the periodic mesoporous organosilica (PMO). The organics in these copolymers do not block the channels.

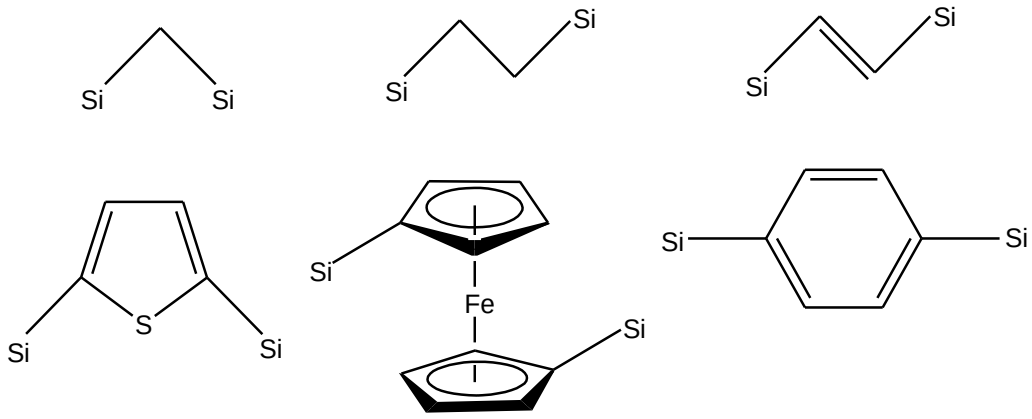

Figure 1.1: Structures of some typical organic bridging groups that were incorporated into first periodic mesoporous organosilica materials[5]

PMO has both advantages and disadvantages, which are as follows:

Advantages

1) Higher organic loading is possible.

2) Since the final periodic mesoporous organosilica contains entirely $O_3Si\text{-}R\text{-}SiO_3$ building blocks, pore blockage can be prevented.

3) A variety of organic bridging groups can be successfully incorporated by this method. A recent review[5] by Geoffrey A. Ozin on periodic mesoporous silica discusses a variety of bridging groups employed using this synthetic methodology.

Disadvantages

1) If a bridged silsequioxane monomer, $(RO)_3Si\text{-}B\text{-}Si(OR)_3$, does not self-assemble then the loading of the desired organic functionality decreases. If the bridged monomer does not self-assemble, it must be co-assembled with TEOS or bis(triethoxysilyl)ethane to provide an ordered porous material.

2) Co-condensation of a bridged monomer with TEOS or bis(triethoxysilyl)ethane, is often accompanied by phase separation. The result is, a well-ordered but nonfunctional inorganic silica phase, in addition to a functional disordered organosilica phase.

3) If the guest molecule is large, it cannot access the organic functionality because of potential pore blockage. Relatively small metal cations may access the organic groups within the walls of the pore, however, as the size of the guest molecule increases the functional groups becomes relatively inaccessible.

1.2 Cyclodextrin functionalized silica materials

1.2.1 Cyclodextrins

Cyclodextrins are a family of cyclic oligosaccharides composed of six to twelve D-glucopyranose units connected by α-(1, 4) linkages. The most widely studied cyclodextrins are those composed of six-, seven- and eight-glucopyranose units denoted by α-CD, β-CD, and γ-CD, respectively. They are produced by intramolecular transglycosylation reaction during the degradation of starch by cyclodextrin glucosyl transferase (CGTase) enzyme.[12]

Discovery of cyclodextrins

Villiers[13] isolated about 3 g of a crystalline cyclodextrin as degradation byproduct of starch in 1891 and determined its empirical composition to be $(C_6H_{10}O_5)_7.3H_2O$. The preparation and properties of these cyclodextrins were described by Schardinger in 1911.[12] Between 1942 and 1948 the structures of α-, β- and γ-cyclodextrin were elucidated by X-ray crystallography.[14]

Molecular structure of cyclodextrins

The average conformational structure of a cyclodextrin is that of a truncated cone, with the primary hydroxyl groups (C_6) situated at the narrow rim and the secondary groups (C_2 and C_3) at the wide one. The apolar C-H bonds at positions C_3 and C_5 and the ether-like oxygen at the glycosidic bonds are at the interior of the CD torus. The exterior rim of the torus is polar in nature because of the numerous hydroxyl groups at the periphery of the annulus, while the cavity is considered to be apolar, (see Figure 1.2).[14]

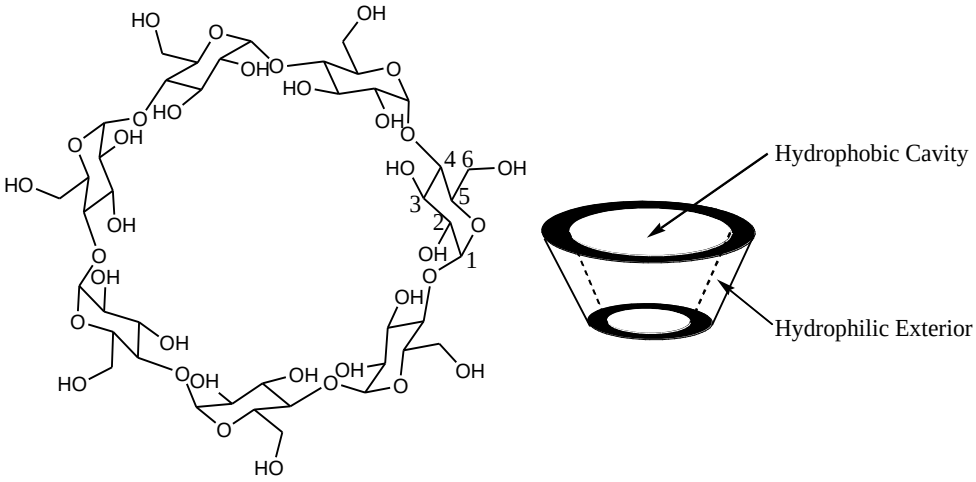

Figure 1.2: Molecular structure of β-cyclodextrin and its schematic toroidal three-dimensional shape. The numbering scheme of each glucose atom is included.

Properties of cyclodextrins

Table 1.2 below lists some of the physical and chemical properties of α-CD, β-CD and γ-cyclodextrin.[15]

Table 1.2: Physical Properties of α-CD, β-CD and γ-cyclodextrin.[15]

CD	Glucose units	M.W. (anhydrous)	V (in $Å^3$)	Water solubility at 25 ^{0}C (g/100 mL)	pK_a at 25 ^{0}C	Hydrate composition (w/w %)
α-CD	6	972	174	14.5	12.33	10.2
β-CD	7	1135	262	1.85	12.20	13.2-14.5
γ-CD	8	1297	427	23.2	12.08	8.13-17.7

V = Volume of the CD cavity

Formation of inclusion complex by cyclodextrin

Since the cavity of a cyclodextrin molecule is apolar, it provides a microenvironment into which appropriately sized non-polar moieties can enter to form inclusion complexes.[16] Figure 1.3 schematically depicts the formation of an inclusion complex between β-cyclodextrin and p-nitrophenol (pNP).

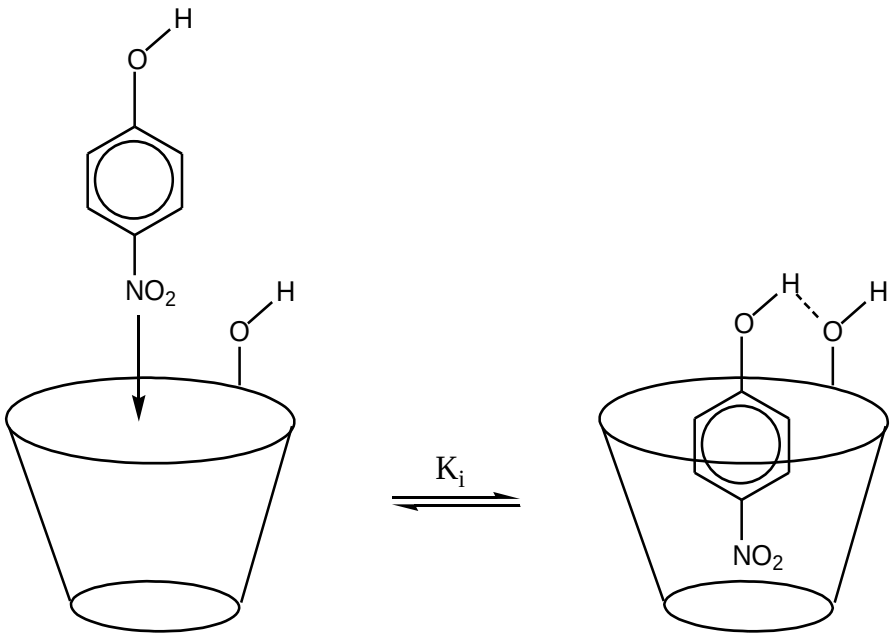

Figure 1.3: A schematic illustration of formation of inclusion complex between a β-cyclodextrin and p-nitrophenol (pNP) in aqueous solution[16] (Note: Solvent has been omitted for clarity purposes) where K_i is the equilibrium binding constant and the dashed line represents a hydrogen bond.

During the inclusion process, the nonpolar portion of the guest makes maximum contact with the apolar cavity while its polar region interacts with the hydrophilic surface of the cyclodextrin molecule.[15]

The formation of an inclusion complex between a cyclodextrin and a guest molecule is mediated by several contributing factors, as follows:

a) Hydrophobic effects,[17] induce the nonpolar groups of guest molecules to enter into the nonpolar CD cavity for an inclusion process in aqueous solution.

b) van der Waals interactions involve the interaction between permanent and induced dipoles and London dispersion forces.

c) Hydrogen bonding between the guest molecule and the hydroxyl groups of the cyclodextrin molecule. With an increase of the polarity of the guest molecule, the contribution from hydrogen bonding increases.

d) Steric factors also influence the inclusion process. The stability of the inclusion complex depends on the shape and size of the guest molecule.

e) Solvent effects involve the release of enthalpy-rich hydrophilic water molecules from the lipophilic cavity of cyclodextrin. Lipophilic guest molecules present in solution displace the hydrophilic water molecules to achieve an optimal apolar-apolar association and a decrease of the cyclodextrin ring strain resulting (applicable for α- and γ-cyclodextrin only) to a more stable lower energy state.

The binding of the guest molecule within the cavity of cyclodextrin is not a static process, but rather, is a dynamic equilibrium. In solution, the complex formation between the cyclodextrin (CD) host molecule and the guest (G) molecule can be represented by following equilibrium expression.[16]

$$CD + G \underset{k_r}{\overset{k_f}{\rightleftharpoons}} CD \bullet G \qquad \text{..... (1.1)}$$

$$K_i = \frac{k_f}{k_r} = \frac{[CD \bullet G]}{[CD\,]\;\;[G]} \quad \text{where } i = 1{:}1 \qquad \text{..... (1.2)}$$

where, the equilibrium constant K_i depends on k_f and k_r which are forward and reverse rate constants, respectively. The higher the value of equilibrium constant the more stable is the cyclodextrin inclusion complex.

Bertrand *et al.*[18] estimated the equilibrium constants using isothermal titration calorimetry and the standard enthalpies for the formation of the complexes of α-cyclodextrin and β-cyclodextrin with substituted phenols in aqueous solutions at 298.15K. The complex formation of a substituted phenol with α-cyclodextrin is more exothermic than that observed for β-cyclodextrin (see Table 1.3).

Table 1.3: Thermodynamic parameters for complexes of *p*-substituted phenols with β-cyclodextrin at 298.15K (Data obtained from reference 18).

Phenol	Molar Volume (mL/mol)	β-cyclodextrin		
		Equilibrium Constant, K_i (L/mol)	Enthalpy, ΔH^0 (kJ/mol)	Entropy, ΔS^0 (kJ/mol-K)
Hydroquinone	87.8	113 ± 5	-17.1 ± 0.5	-18 ± 2
Phenol	89.4	94 ± 3	-12.2 ± 0.2	4 ± 1
p-chlorophenol	102.2	410 ± 60	-11.9 ± 0.4	10 ± 2
p-nitrophenol	102.7	260 ± 30	-13.4 ± 0.6	1 ± 2
p-bromophenol	105.5	860 ± 160	-12.2 ± 0.3	15 ± 2
p-cresol	106.9	250 ± 10	-12.5 ± 0.2	4 ± 1

Applications of cyclodextrins

The ability of cyclodextrin molecules to form inclusion complexes results in changes to the physiochemical properties of the guest molecule such as: *i)* changes in the apparent solubility, *ii)* increases in the stability of the guest in the presence of heat, light, and oxidizing conditions, and *iii)* decreases in the volatility of the guest compound. Due to these properties, cyclodextrins are widely used in pharmaceutical, food and flavors, cosmetics, packing, textiles, fermentation and catalysis, agriculture, environment protection, separation process and chromatographic techniques. This is evidenced by a large number of review articles[19-30] on cyclodextrins and their applications.

A wide variety of toxic organic compounds e.g. substituted phenols,[31-35] benzene derivatives[36-40] are produced by different industrial processes (e.g. manufacturing industry, hospitals, forestry, agriculture). These compounds are found in trace quantities in industrial waste water and constitute health and environmental concerns. Since many of these compounds are not biodegradable they persist in the environment and may create serious concerns on public health

by contaminating the soil and groundwater supplies. To address this problem cyclodextrin compounds may be implemented as novel sorbents by functionalization of silica based materials with cyclodextrins. The following discussion gives an overview of the functionalization of silica by β-cyclodextrin.

1.2.2 Functionalization of silica by cyclodextrins

Cyclodextrins are highly water soluble and can be processed into solid forms before they can be employed in solid state separation technologies. This strategy creates insoluble cyclodextrin host compounds and purification becomes easier due to the ability to remove the guest impregnated cyclodextrin host compounds simply by filtration and solid phase extraction processes.

Silica is widely used as an inorganic solid support and its surface may be used for chemical immobilization of cyclodextrin molecules. The following properties of silica make it suitable for use as a solid support.[41]

1) It has high specific surface area.

2) It has sufficient mechanistic stability (silica is an inorganic silicon-oxygen polymer)

3) It is stable to water, chemical reagents, and radiation.

4) It does not swell in contact with solvents and results in favorable/predictable kinetic properties of sorption.

5) It can be processed into different forms, porous or nonporous powders, films, granules and micro spheres.

6) The surface contains silanol groups (Si-OH group) which serve as an active site for adsorptive processes and chemical modifications with inorganic, organic and organsilicon compounds.

There are four main methods for preparing cyclodextrin-functionalized solid materials. These are described in the following pages according to the type of silica-based materials: *(1)* Cyclodextrin polymers, *(2)* Coating or grafting of cyclodextrin onto a stationary phase, *(3)* Molecular imprinting of cyclodextrin on silica gel, and *(4)* Incorporation of cyclodextrin within the framework of mesoporous silica.

***(1)* Cyclodextrin polymers**

Insoluble derivatives of cyclodextrin can be formed by the chemical reactivity of hydroxyl groups at carbon positions 2-, 3- and 6- positions of the glucose units within cyclodextrin (see Figure 1.2). A variety of cross linking agents can provide water-insoluble polymers of cyclodextrin by reacting with any number of the 21 hydroxyl groups. The first of these involve the incorporation of cyclodextrin into polymers by connecting cyclodextrin moieties using chemical linkers such as aldehydes, ketones, isocyanates, epichlorohydrin to the backbone of polymer chains[38, 39, 42-46] (see Figure 1.4).

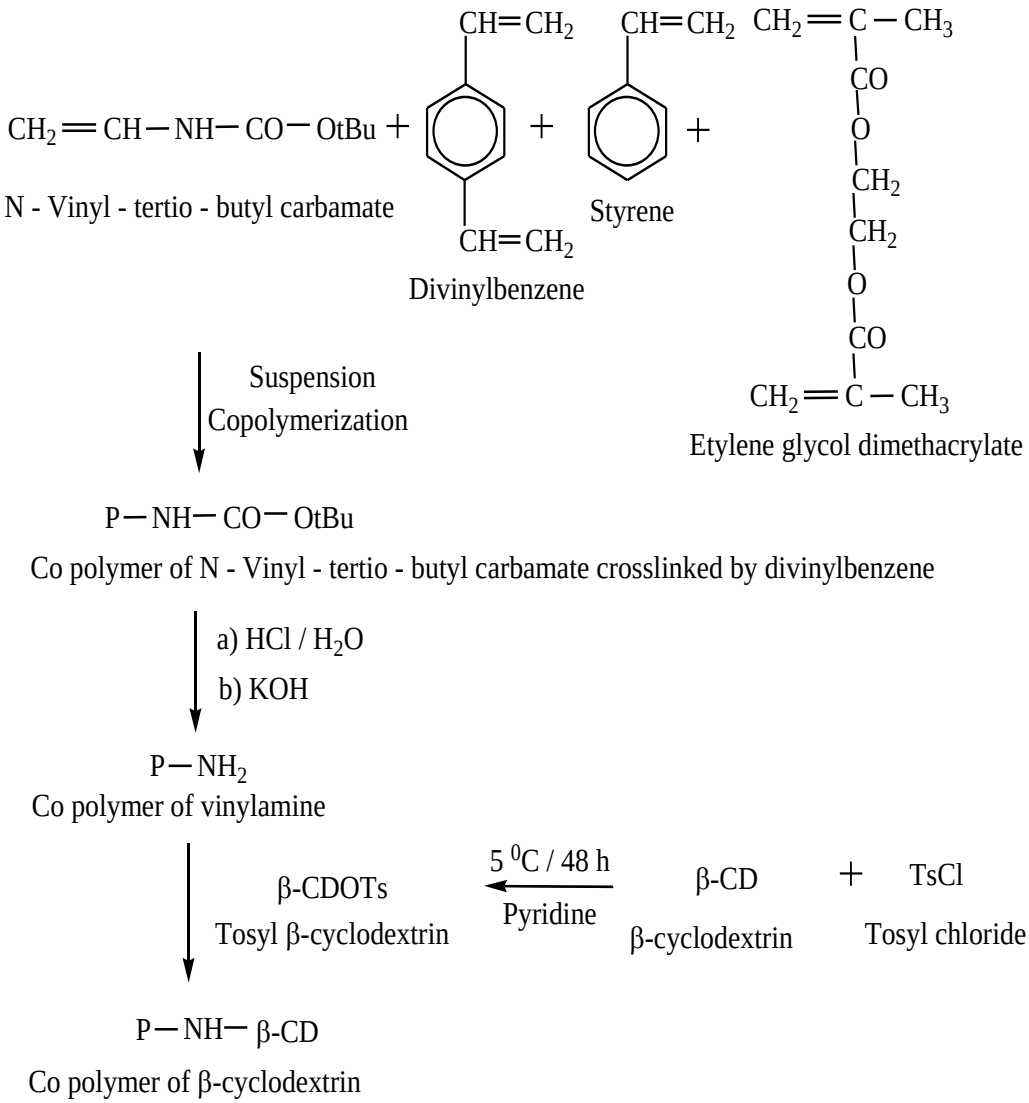

Figure 1.4: Synthesis of a copolymer containing β-cyclodextrin[39]

***(2)* Coating or grafting of cyclodextrin onto stationary phase**

Cyclodextrin moieties are coated or grafted onto stationary phases such as organic polymers[47, 48] or silica gel[49-56] according to the strategy outlined in Figure 1.5.

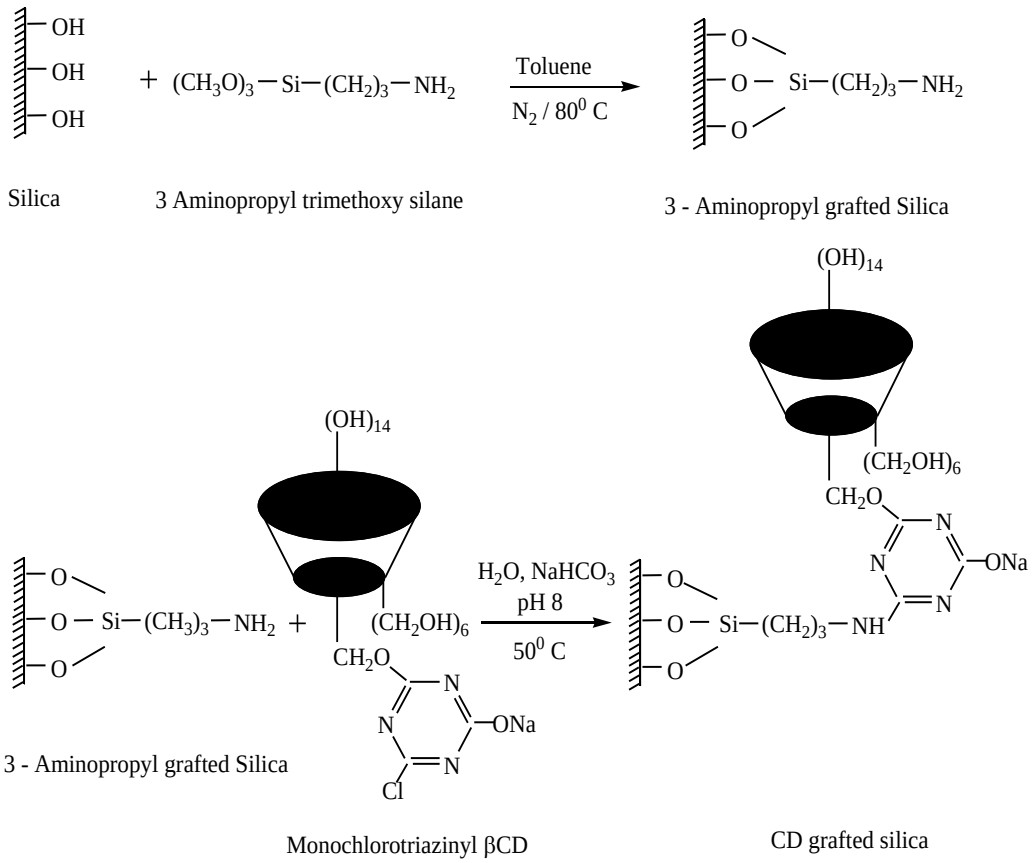

Figure 1.5: Grafting of β-cyclodextrin on to the surface of silica gel[57]

***(3)* Molecular imprinting of cyclodextrin on silica gel**

Molecular imprinting methods are based on the molecular recognition property of a cyclodextrin host toward a specific sized guest molecule. Tomohiro Akiyama *et al.*[58] cross linked vinyl monomers of cyclodextrin with N, N´-methylenebisacrylamide in the presence of different template molecules involving the multiple recognition sites of cyclodextrin. The resulting polymer successfully recognized the template in aqueous solution (see Figure 1.6).

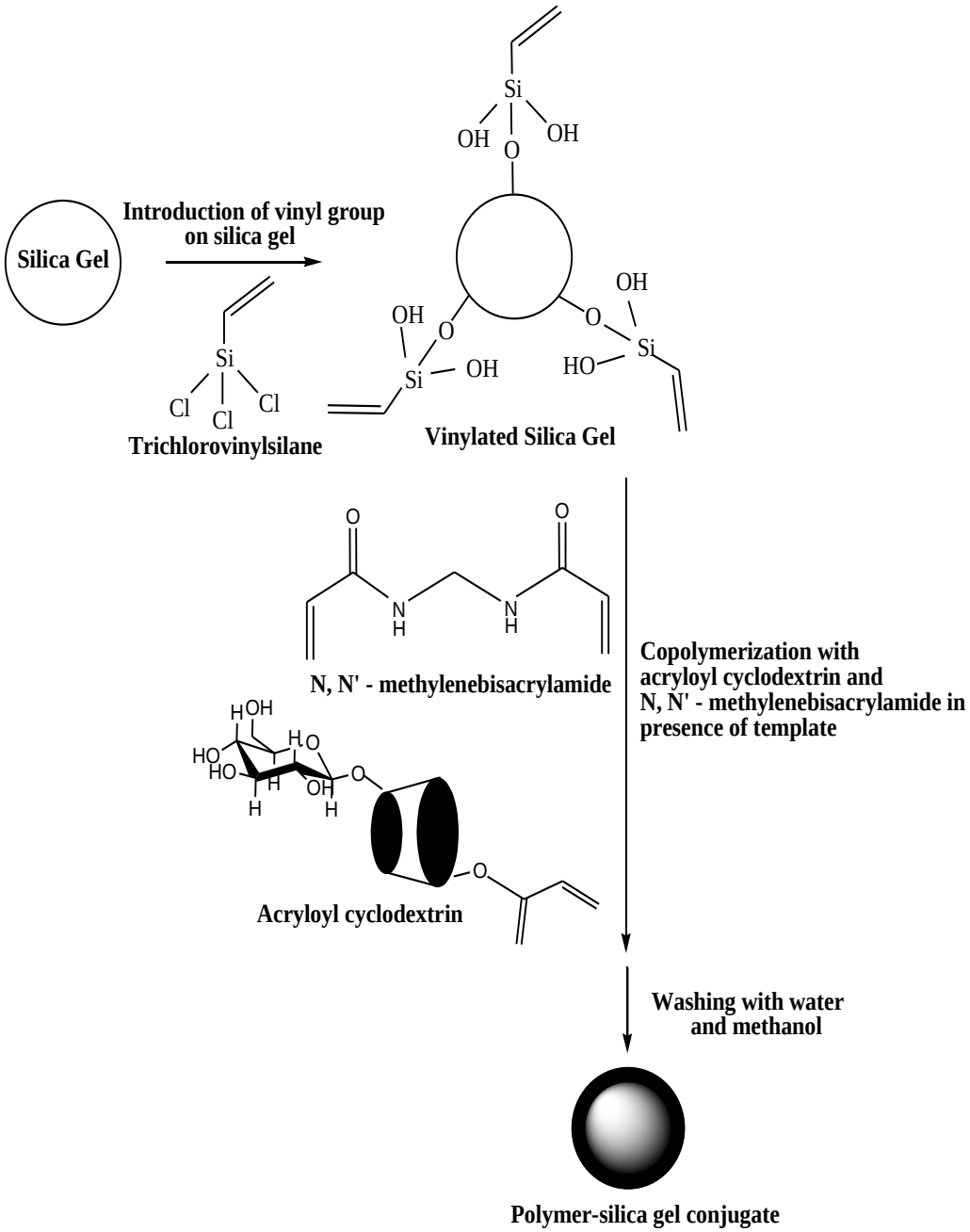

Figure 1.6: Immobilization of an imprinted β-cyclodextrin polymer on silica gel according to the synthetic scheme by Tomohiro Akiyama *et al*.[58]

The following molecules were used as templates (see Figure 1.7) for molecular imprinting strategies.

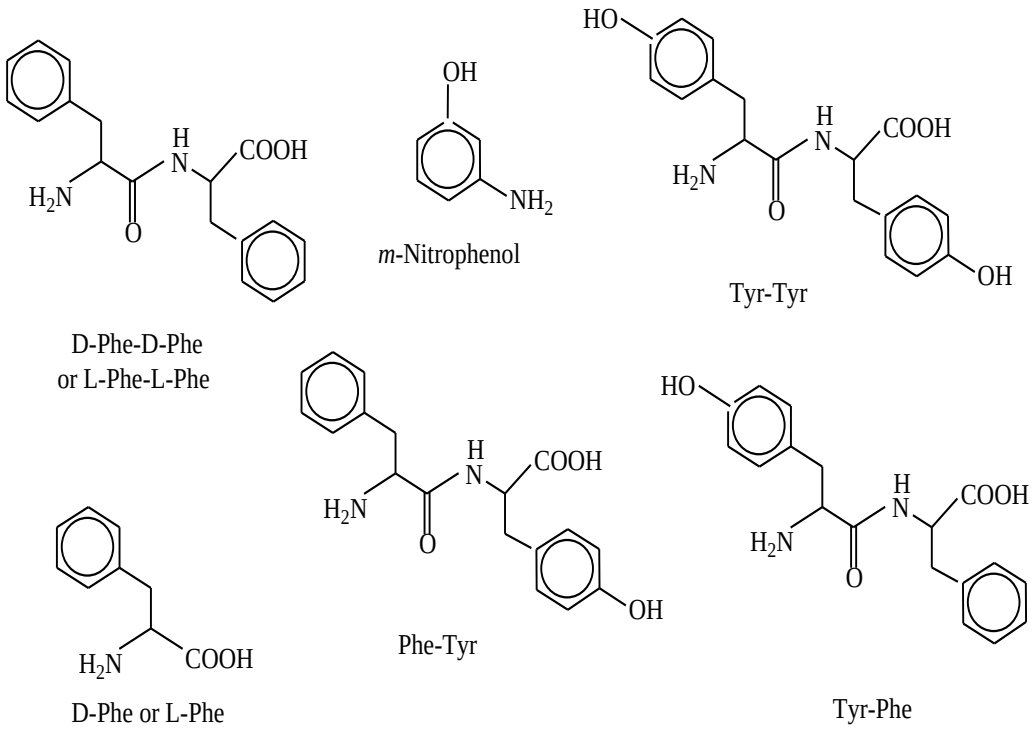

Figure 1.7: Template molecules used by Tomohiro Akiyama *et al.*[58]

The following bioactive molecules were used as substrates (see Figure 1.8) by Tomohiro Akiyama *et al.*[58] for molecular imprinting strategies.

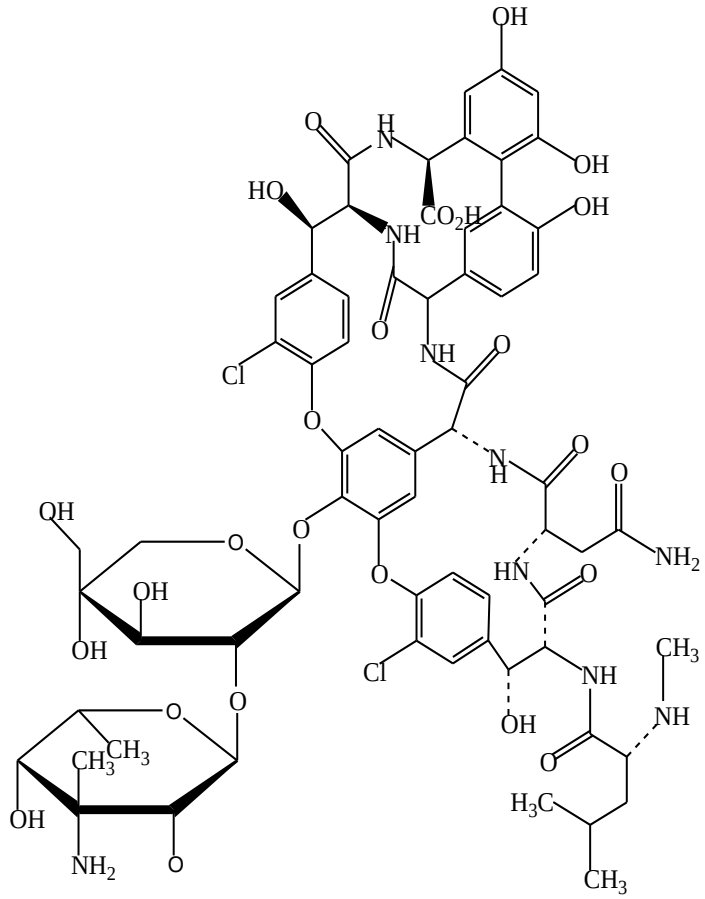

Vancomycin

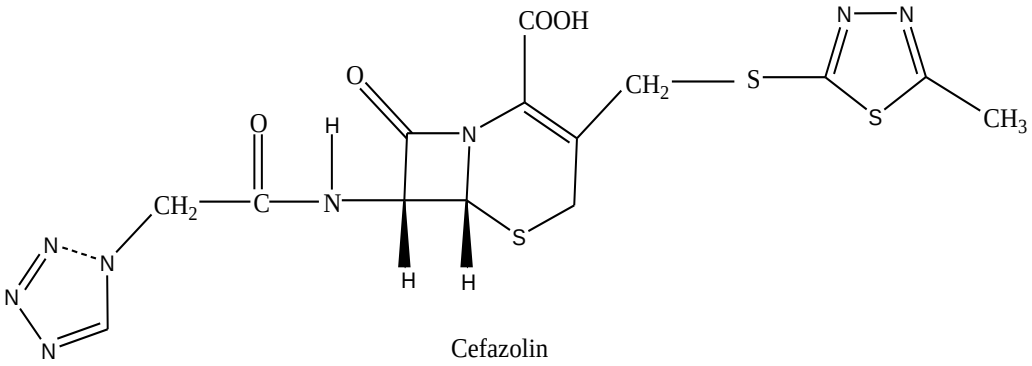

Cefazolin

Figure 1.8: Substrate molecules used by Tomohiro Akiyama *et al.*[58]

Although cyclodextrin polymers may have high cyclodextrin content, they generally have very low specific surface areas[59] (1.0-2.0 m^2/g). Adsorbate molecules cannot easily enter into the crowded cyclodextrin sites within the microporous network of polymer chains resulting in incomplete sorption and slow diffusion kinetics of adsorption. Moreover, the reduced thermal and chemical stability of cross linked polymers makes them unsuitable for industrial applications.

Cyclodextrin-coated (or grafted) silica materials offer improved access to the CD cavity sites since the cyclodextrin moieties are located on the external surface of the support. Furthermore, they have improved mechanical stability due to the robust character of the substrate and also have high surface areas compared to conventional CD polymers. Grafted materials show limited sorption due to the relatively low content of cyclodextrin incorporation.

The major drawback of cyclodextrin grafted silica materials is the use of amorphous silica as a solid support. Since the discovery of MCM-41 and periodic mesoporous organosilica, more efficient ways of grafting organic functionalized silica have been developed.[49-56]

***(4)* Incorporation of cyclodextrin within the framework of mesoporous silica**

Cyclodextrin (CD) or CD derivatives can be incorporated within the framework of mesoporous silica.[60-65] Cyclodextrin-silica hybrid mesoporous materials have an open framework structure with pore sizes 3-25 nm so that the organic guests can access the surface bound cyclodextrin binding sites.[62-64] The introduction of mesoporosity provides enhanced access because of the increased surface area

and accessibility of the organic guests to the internal cavity of the cyclodextrin host molecule.

There are two different synthetic strategies for preparing cyclodextrin-silica hybrid mesoporous materials. The first method is the direct synthesis by co-condensation of cyclodextrin functionalized trialkoxysilane with tetraethoxysilane (TEOS) in the presence of a structure directing agent (SDA; such as cetyltrimethyl ammonium bromide or dodecylamine). Removal of the SDA by solvent extraction produces a mesoporous silica material containing cyclodextrin. The second method is surfactant templated copolymerization of TEOS with cyclodextrin-bridged silsequioxanes monomers $(RO)_3Si\text{-}B\text{-}Si(OR)_3$ where B is a bridging compound (e.g. cyclodextrin). Removal of the surfactant produces periodic mesoporous organosilica material (PMO) in which cyclodextrin acts as an integral part of the channel wall.

Method 1

Direct synthesis by co-condensation of organosilane and tetraalkoxysilane: In this one-pot method,[66] the organosilanes are co-hydrolyzed and condensed with other silica reagents, e.g. tetraalkoxysilanes, water, and the appropriate SDA molecules to create the desired mesoporous material (see Figure 1.9).

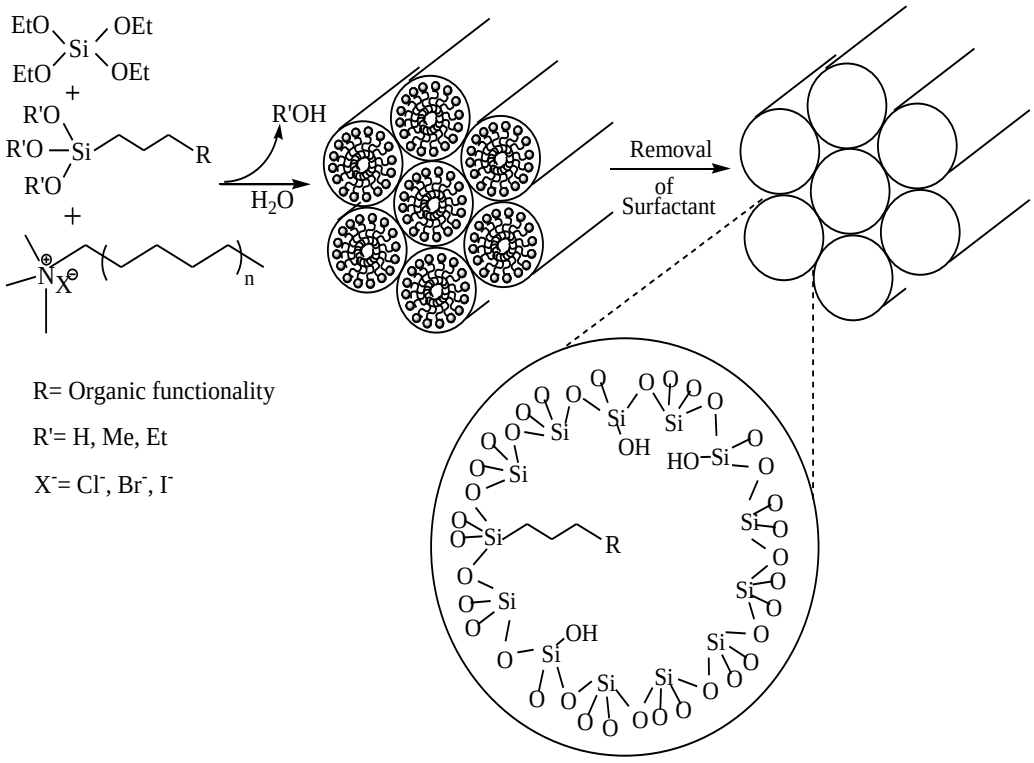

Figure 1.9: Direct Synthesis Method, Co-condensation of Organosilanes and Tetraalkoxysilanes for the Assembly of Ordered, Mesoporous, Organic-Inorganic Hybrid Solids[66]

The use of a non-electrostatic templating pathway (using neutral surfactant or non-ionic surfactant) is a promising strategy for the rapid and convenient synthesis of functionalized mesoporous silica materials. A general disadvantage of electrostatic S^+I^- assembly (S^+= structure directing alkylammonium ion surfactant and I^- = framework forming silicate oligomers) for direct functionalization is incomplete removal of the charged surfactant molecules from the framework. Extraction may be problematic in some instances because the functionalized mesostructure decomposes by acid leaching.[67]

Mercier and coworkers[60] prepared cyclodextrin containing hexagonal phase mesoporous silica (CD-HMS) materials by a direct synthetic process (see Figure

1.10). Transmission electron microscopy (TEM) images, nitrogen sorption and small angle x-ray diffraction patterns reveal a wormhole morphology with an approximate 40 Å pore diameter pores. The material with the highest CD incorporation level studied was, CD-HMS 8%, which contained 8% cyclodextrin. No PXRD reflection was observed for CD-HMS 8% which was attributed to contrast matching caused by the presence of high cyclodextrin loading in the pore channels. Broadening of the pore size distribution of CD-HMS 8% showed highest CD loading resulted in a mesoporous framework that suffered from severe structural perturbation and mechanical instability.

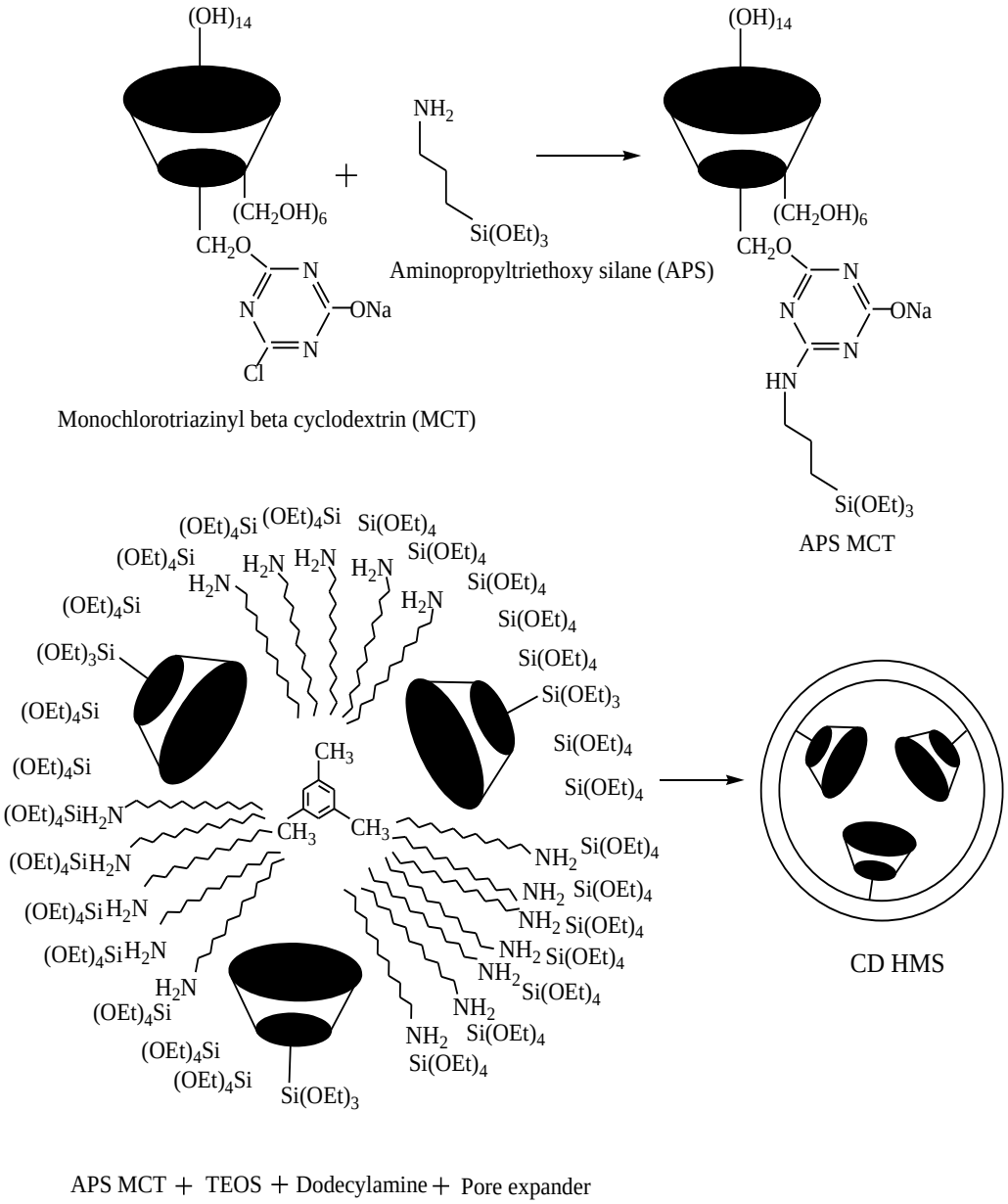

Figure 1.10: Synthesis of Cyclodextrin incorporated Hexagonal Mesoporous Silica CD-HMS materials, according to Mercier *et al*.[60]

Method 2

Periodic Mesoporous Organosilica: Lambert and coworkers[61] prepared β-cyclodextrin containing mesoporous polymers using cetyltrimethylammonium bromide (CTAB) as the surfactant where the cross linking of the polymer occurred from a cyclodextrin monomer that was completely functionalized containing up to 42 hydrolysable (7×6 OEt groups from the cyclodextrin functionalized tri-ethoxy silane where every glucose unit of one cyclodextrin molecule contains six $Si(OEt)_3$ units (see Figure 1.11), groups as compared with only four in the case of TEOS.

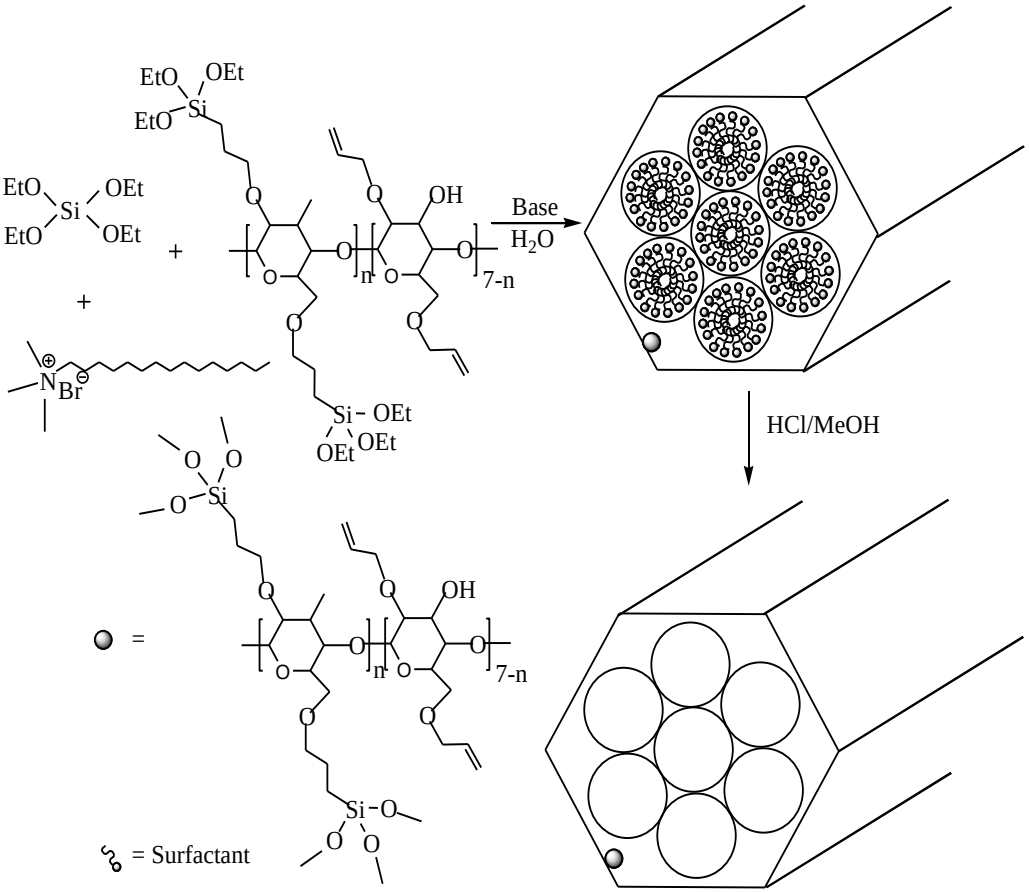

Figure 1.11: Synthesis of CD-functionalized periodic mesoporous materials according to Lambert *et al.*[61]

Small angle XRD measurements of the synthesized CD- functionalized periodic mesoporous silica (Figure 1.11) by Lambert *et al.*[61] showed no ordering or periodicity. As the proportion of TEOS decreases and the cyclodextrin monomer content increases, the long range order is lost. The peak at 2.2° decreased in intensity as the percentage of TEOS decreased from 90 to 50% and was absent when the percentage of TEOS was 25% or less. With the decrease of the percentage of TEOS, the formation of silica framework is hindered because TEOS is the principal component for silica network formation.

Chunqing Liu[62-65] prepared β-cyclodextrin hybrid mesoporous silica from a monomer of cyclodextrin having an isocyanate carbamate linkage both in the absence of a surfactant[62] and also in the presence of a surfactant (CTAB).[64] The same author also reported the synthesis of β-cyclodextrin hybrid mesoporous silica using a tri-block copolymer[65] as the SDA.

General drawbacks

A general drawback occurs with all of the β-cyclodextrin hybrid mesoporous silica reported. As the loading of CD increases, the framework mesoporosity and mechanical stability tend to decrease. On the other hand, the high CD loading is expected to increase the sorption capacity of these composite materials. This is an important factor to consider for their successful utilization as sorbents for applications involving water purification. An increase in the CD loading not only disrupts the framework mesoporosity but also lowers the surface area of the materials. For these reasons an increase in the CD loading decreases the accessibility of the organic host.

Problems with compounds reported by Lambert *et al.*[61]

Although the CD loading of CD HMS materials reported by Mercier *et al.*[60] are lower than that reported by Lambert *et al.*[61] (8% for CD HMS and 25% for Lambert *et al.*[61]), the reported p-nitrophenol sorption capacity for both types materials are comparable. With an increase in CD loading, we expect a theoretical increase in the sorption capacity for such compounds, as reported by Lambert. However, this was not observed. With an increase in CD loading, the framework mesoporosity and surface area, both decrease. As well, p-nitrophenol diffuses more slowly to enter the CD binding sites. Most of the abundant CD hosts deep in the collapsed mesopore remain inaccessible to the p-nitrophenol guest.

Problem with compounds reported by Mercier *et al.*[60]

Although the p-nitrophenol sorption properties of both types of materials are comparable, the direct synthetic process ("one-pot method") followed by Mercier is considered more convenient. The cyanuric chloride linker used by Mercier is sensitive to alkaline pH due to hydrolysis[41] of APS MCT. Hence, these linkers are ineffective in materials that involve aqueous phase adsorption of p-nitrophenol because of the hydrolysis of the APS MCT linker from the silica framework. The decrease in sorption is related to cleaving off the surface bound CD moieties.

The general concept, "more CD, more sorption", does not hold at all for materials containing the MCT linker because of the easily hydrolyzed CD functionalities. Consequently, it is necessary to develop a synthetic scheme that

utilizes a robust linker which will solve the problem of CD accessibility, as well as, the versatile attachment of CD to the silica framework. To accomplish this goal, the following research was proposed to address the aforementioned problem.

1.2.3 Outline of the Research

The objectives of this research were to synthesize, characterize and study the sorption properties of cyclodextrin hybrid porous silica materials prepared by different synthetic strategies. The direct synthesis method of Mercier *et al.*[60] was exploited with some important modifications.

a) **Change of Linker:** The cyanuric chloride linker used by Mercier (see Figure 1.10) is sensitive to alkaline pH due to hydrolysis.[41] Instead of the cyanuric chloride linker an isocyanate-based linker will be used (see Figure 1.12). Since urethane bonds are less susceptible to hydrolysis, they are considered more favorable method for connecting the cyclodextrin to the silica framework.

The isocyanate linker was synthesized by reacting cyclodextrin with 3-isocyanatopropyltriethoxysilane according to a synthetic strategy as outlined by Liu *et al.*[64] (see Figure 1.12). This synthetic method was modified in order to increase the number of hydrolysable functionalities: 4 moles of 3-isocyanatopropyltriethoxysilane was used instead of 3 moles.

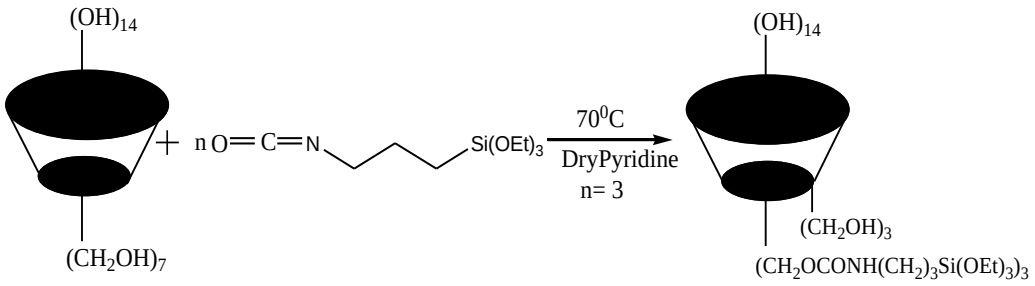

Figure 1.12: The synthesis of isocyanate based CD monomer[64]

The CD-based monomer from Figure 1.12 was co-condensed with TEOS using dodecylamine as SDA and 1,3,5-trimethylbenzene (TMB) as pore expander following the basic synthetic strategy of Mercier and coworkers.[60]

b) **Change of Surfactant:** The size of framework confined mesopore is equal to the diameter of the framework channels or to the diameter of the parent rod-like micellar phase and can be varied by tuning the surfactant alkyl chain length.[68] The alkyl chain length of the surfactant was increased using $C_nH_{2n+1}NH_2$ where n = 12, 14 or 16.

FT-IR, Raman spectroscopy, elemental analysis, solid state ^{13}C-NMR spectroscopy, MALDI TOF MS, and nitrogen porosimetry were used to characterize the CD-containing silica materials. The sorption properties of the materials were studied using p-nitrophenol as an adsorbate in aqueous solution and also with the gaseous adsorbate CH_3Cl. The results were evaluated using the Langmuir,[69] Freundlich,[70] and Brunauer-Emmet-Teller[71] models of adsorption. The composite materials are expected to contribute positively to future industrial applications related to sorption phenomena and chemical separations involving the removal of organic compounds from aqueous media or from the gas phase.

CHAPTER 2
EXPERIMENTAL

2.1 Preparation of CD functionalized silane

2.1.1 Introduction and Background Theory

Cyclodextrin functionalized silane CD ICS was prepared by reacting one mole of β-cyclodextrin with four moles of 3-isocyanatopropyltriethoxysilane according to the following reaction scheme (see Scheme 2.1).

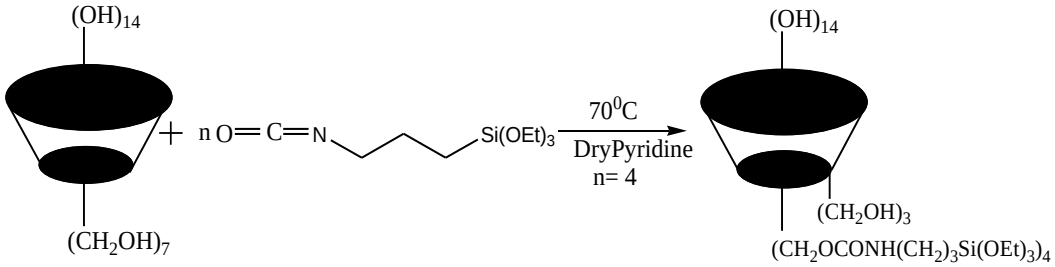

Scheme 2.1: Synthesis of an Isocyanate based linker CD ICL, where n=4. According to this synthetic scheme CD is bonded to Si by an isocyanate linkage

CD ICL is co-condensed with TEOS in the presence of a structure directing agent (SDA) (i.e. surfactant) and pore expander (TMB) following a direct synthesis pathway.[72,73] Then the surfactant and pore expander are removed by solvent extraction from the surfactant containing ("as synthesized") material using ethanol as the extraction solvent. Finally, after drying at 80^0C at high vacuum, CD ICS is found as a white powder.

2.1.2 Materials and methods

Materials

3-isocyanatopropyltriethoxysilane was purchased from Gelest Inc., USA. All other chemicals were purchased from Aldrich Inc., Canada. Pyridine was dried over potassium hydroxide pellets for 24 h. The decant was collected and distilled from calcium hydroxide at atmospheric pressure. The dried pyridine was stored over 4Å sieves in screw capped bottles. β-cyclodextrin was dried in an Abderhalden[74] pistol drier at using acetone as the refluxing solvent.

Methods

Preparation of CD ICL

4.95g (20.0 mmol) of 3-isocyanatopropyltriethoxysilane was added to a stirred solution of dried β-CD (5.74 g, 5.0 mmol) in 70 mL of dried pyridine. The solution was stirred at 70 °C under N_2 for 48 h. The solvent was removed under reduced pressure under N_2. The product CD ICL was obtained as a light yellow solid.

Preparation of CD ICS from CD ICL

CD ICL (X mmol where X=0.61, 1.21, 1.81) was stirred in 10 mL of water for 30 min. The mixture is then added to the surfactant (dodecylamine, tetradecylamine or hexadecylamine) solution (6.7 mmol in 10 mL of ethanol and 90 mL of water) and stirred for 30 s after which TEOS (30.3X mmol) was added. After the mixture was further stirred for 30s, TMB (6.7 mmol) was added as pore expanding agent. The mixture was then stirred for 24h and the resulting powder was filtered and washed by ethanol and then by water. The "as-

synthesized" material was dried overnight under vacuum and was washed by Soxhlet extraction using ethanol for 24h. The material obtained was labeled as CD ICS Y (Z) where Y=100X/30.3 or 2, 4, 6 respectively and Z= number of carbon atoms of the alkyl chain in the neutral surfactant (for example, 12, 14 or 16 for dodecylamine, tetradecylamine or hexadecylamine, respectively).

2.2 Characterization of Materials

2.2.1 Introduction

The ^{1}H NMR spectra provides useful structural information for determining the average degree of substitution of CD by ICL from the integration of ^{1}H NMR line intensities. Since a CD molecule has 7 primary and 14 secondary hydroxyl groups, it can be theoretically substituted at any of the 21 hydroxyl groups. Depending on the mode and number of substitution of the hydroxyl groups, the CD functionalized triethoxysilane can be in different isomeric forms according to Wenz and others.[75] The ratio of the native cyclodextrin and linker can be determined from the ratio of the intensity of the unreacted proton H-1 of cyclodextrin and the intensity of the unreacted proton of the linker.

Small angle X-ray diffraction patterns of hexagonal mesoporous silica show reflections between $2\theta = 2^{0}$ to 5^{0} due to ordered hexagonal array of parallel silica tubes. For cyclodextrin incorporated silica materials, the reflection for only (100) plane of a hexagonal unit cell has been reported.[60, 61] The incorporation of a large cyclodextrin moiety in the hexagonal channel results in reduced ordering of the silica channel and the signals at higher angles are lost.

Solid State ^{13}C NMR CP-MAS Spectra of can provide structural information about the CD functionalized silica material. This allows confirming the incorporation of CD into the mesoporous silica network by demonstrating peaks in the region δ = 60-110 ppm region for CD.

Matrix assisted laser desorption ionization time of flight (MALDI TOF) mass spectrometry can give information on the incorporation of cyclodextrin within the mesostructure silica framework. Due to desorption of the grafted species by laser irradiation, MALDI TOF mass spectrometry permits direct detection of cyclodextrin bonded to the silica network by direct measurement of oligosaccharide mass fragments desorbed from the surface.

Infrared spectra were acquired using the diffuse reflectance technique where the sample was mixed with potassium bromide. Reflection does not occur at exactly the same frequency as absorption for strong bands, which causes shifts and distortions. The Kubelka-Munk method is the proper method for representing the intensity of the diffuse reflectance spectra. This method corrects the transmission spectra for the wavelength dependence of the IR absorption bands. The Kubelka-Munk function ($f(R_\infty)$) is the ratio of absorption (k) and the scattering coefficient (s) of the sample:

$$f(R_\infty) = \frac{(1- R_\infty)^2}{2R_\infty} = \frac{k}{s} = \frac{2.303a}{s} \bullet c = k^* \bullet c \quad .....(2.1)$$

where, R_∞ is the reflection of the sample with infinite thickness. In practice the experimentally observed reflection ($R_\infty = R_{\infty, exp}$) is the ratio of the reflection of the sample ($R_{\infty, s}$) and the reference material ($R_{\infty, r}$).[76] According to the equation

(2.1), $k = 2.303\ ac$ where a and c are the absorptivity and concentration of the analyte, respectively. If s is constant $f(R_\infty)$ is linear with the sample concentration and k^* can be related to the sensitivity of the analytical method[77].

Raman spectroscopy provides complementary information to Infrared spectroscopy because the selection rules for Raman Scattering are different from those of IR; some transitions are observed only through Raman Scattering, some only in IR and some both in IR and Raman.[78]

UV-Vis spectrophotometry can be used to get quantitative information of p-nitrophenol adsorbed in CD ICS. From the molar adsorptivity of p-nitrophenol the analytical unknown concentration of p-nitrophenol can be determined using the Beer Lambert Law:

$$\log\left(\frac{I_0}{I}\right) = cl\varepsilon = \frac{A}{cl} \ldots\ldots\ldots\ldots (2.2)$$

where I_0 is the intensity of the incident light (or the light intensity passing through a reference cell), I is the light transmitted through the sample solution, log (I_0/I) is the absorbance (A) of the solution, c is the concentration of the solute (in mol/dm^3), l is the path length of the sample (cm), ε is the molar absorptivity (unit M^{-1}cm^{-1}).[79]

Nitrogen porosimetry can give information about the surface area, pore volume and pore size distribution of the CD ICS materials. From the type of hysteresis loop observed, it is possible to predict the different types of adsorption and desorption processes that may occur in mesoporous materials.[80]

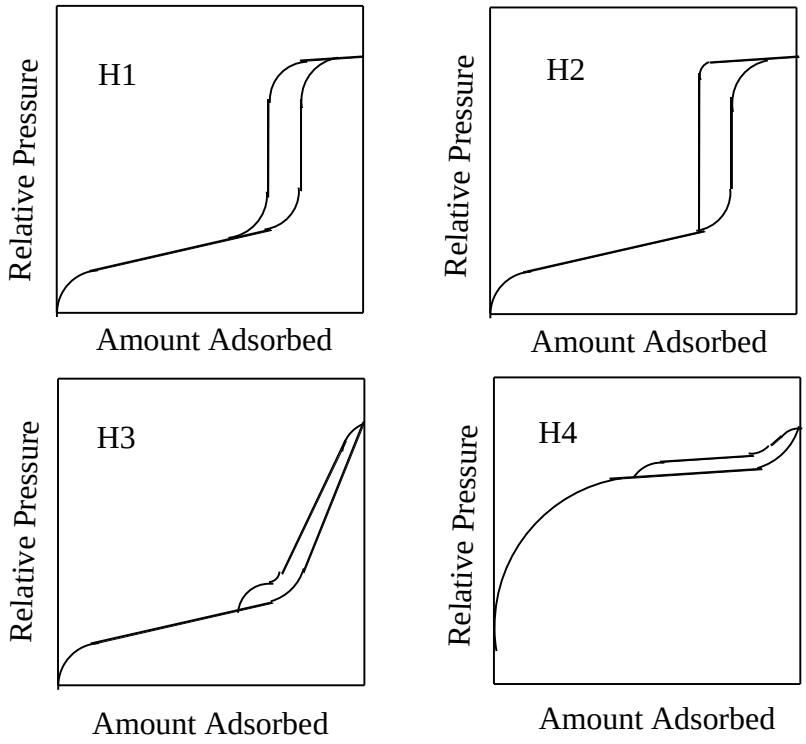

Figure 2.1: Different types of hysteresis loops for microporous and mesoporous materials observed in gas porosimetry experiments[80]

Type H1 is associated with porous materials with narrow pore size distribution, type H2 loop occurs in pores with narrow neck and wide bodies (called "ink bottle" pores), type H3 hysteresis loop is observed with aggregates of plate-like particles giving rise to slit shaped pores and type H4 loop is reported to be associated with narrow slit-like pores.[80]

Theromogravimetric analysis[4, 8, 11] provides quantitative information because this method provides information on weight loss over a specified temperature range. Because of the difference in thermal stability between organic and inorganic materials, it is anticipated that the TGA profile gives information on the CD loading. Information about CD loading, removal of (SDA) surfactant[68, 87] and pore expander may be obtained, from the percentage weight loss and

differential thermogravimetric profile. Physisorbed water is desorbed at temperatures less than 110^0C, the surfactant and pore expander losses are at ~ 100^0C to 250^0C and chemically-bonded cyclodextrin decomposes at ~320^0C. The various temperature ranges are categorized as low, medium, and high temperature regimes.

2.2.2 Instrumental analysis

2.2.2.1 ^{1}H NMR Spectroscopy

^{1}H-NMR (Bruker; 500 MHz Avance NMR spectrometer) spectra was obtained with 128 scans using DMSO-d_6 as the internal reference for chemical shift measurements at room temperature.

2.2.2.2 Small Angle X-ray Diffraction

Small Angle X-ray Diffraction data was obtained on a Rigaku Miniflex diffractometer using Cu Kα radiation (wavelength 1.5418 Å) from $2\theta = 2^0$ to 10^0. 2g of sample was dry mounted by pressing on an aluminum disc sample holder.

2.2.2.3 Solid State NMR

Solid state ^{13}C NMR with cross polarization ^{13}C {^{1}H} magic angle spinning spectra were run at 150.8 MHz on a Varian Inova 600 spectrometer with rotor size 3.2 mm, spinning rate 16 kHz with a CP ramp pulse program. The chemical shifts were externally referenced to hexamethylbenzene at 16.9 ppm at ambient temperature. Data were processed with a 100 Hz line broadening and left shifting FID (1-2 data points) to correct baseline.

2.2.2.4 MALDI TOF Mass Spectrometry

MALDI TOF Mass Spectrometry was taken in Voyager DE STR MALDI Mass Spectrometer operated in positive ion linear mode, calibrated with Angiotensin 1 (m/z 1296.6853) and spectra were acquired from m/z 700 to m/z 3000. Approximately, 2 mg of sample was placed in an eppendorf tube and ground with a 200 µl pipette tip. 50 µl of 75% acetonitrile with 0.1% aqueous trifluoro acetic acid was added to the tube. The sample was sonicated in a sonication bath for 30 minutes. 1 µl of the slurried sample and 1 µl of matrix solution (5mg/ml alpha-cyano-4-hydroxycinnamic acid) were mixed on the MALDI plate and air dried). Milli-Q grade water was used for the preparation of the aqueous solutions.

2.2.2.5 DRIFT Spectroscopy

IR spectra were obtained by DRIFT (Bio RAD FTS-40 spectrophotometer). KBr was used as both the background and matrix over the range of 400-4000 cm^{-1}. Samples were prepared by mixing with pure spectroscopic grade KBr in an approximately equal ratio (KBr : sample ~ 1:1), grinding together in a small crucible and finally and pressed with a spatula in the sample holder to make a uniform planar upper surface. The spectra were taken at room temperature with a resolution of 4 cm^{-1} with approximately 250 scans.

2.2.2.6 Raman Spectroscopy

Raman Spectroscopy measurements were obtained in a Renishaw system 2000 with an excitation wavelength of 514 nm in a 180^0 backscattering configuration

at room temperature. The calibration was performed by using silicon wafer at 520 cm^{-1}.

2.2.2.7 UV-Vis Spectrophotometry

UV absorbance and molar absorption coefficients of p-Nitrophenol were obtained by UV-Vis spectrophotometry (Varian Cary 100 SCAN) with spectral band width of 2 nm and data collection at intervals of 1 nm.

2.2.2.8 C, H, N Elemental analysis

C, H, N analysis was determined using an Elemental Analyzer (Perkin Elmer 2400 CHN Elemental Analyzer, the limit of detection was: ± 0.3%). Experimental results were corrected for H_2O content obtained from thermogravimetric analysis to correct for H and O contents arising from adsorbed water.

2.2.2.9 Porosimetry

Nitrogen adsorption-desorption isotherms of the adsorbents were measured at 77 K on a Micromeritics ASAP 2000 sorptometer. Samples were grounded in a small crucible and passed through 40 mesh size sieve. Prior to measurement, every sample was degassed at 110^0C at 10^{-6} mm Hg. Samples were analyzed from around 40 mm Hg pressure to 710 mm Hg pressure of nitrogen.

2.2.2.10 TGA

TGA analysis was performed on TG-DSC-1100 supplied by Setaram Scientific and Industrial Equipment, NJ, USA. 20 to 50 mg of sample was placed in a balance inside the analyzer. The sample was heated in flowing Ar gas from 20 to 600 ^{0}C with a heating rate of 10^oC/min.

2.3 Sorption Studies of CD functionalized Silica Materials

2.3.1 Introduction and Background Theory

To investigate the adsorption capacities of the materials, sorption experiments were performed in the gas phase and solution phase, respectively. Methyl chloride, a volatile organic compound, a major industrial pollutant,[81] was chosen as the adsorbate for gas phase adsorption. For solution phase adsorption, p-nitrophenol, a model compound to represent typical small sized aromatic organic contaminants of water, was chosen as the adsorbate for solution phase adsorption.

2.3.2 Adsorption Isotherms

The following adsorption isotherm equations were considered for fitting the experimental data from the sorption studies.

Table 2.1: Description of Adsorption Isotherm Models

Model	Equation	Comment
Langmuir	$\frac{C_e}{Q_e} = \frac{C_e}{Q_m} + \frac{1}{bQ_m}$	Describes maximum monolayer capacity
BET	$\frac{C_e}{Q_e(C_0 - C_e)} = \frac{1}{Q_m k} + \frac{C_e(k-1)}{C_0 Q_m}\left(\frac{C_e}{C_0}\right)$	Describes multilayer adsorption
Freundlich	$\log Q_e = \frac{1}{n}\log C_e + \log k_f$	Empirical

where, Q_e is the amount of adsorbate adsorbed (mol g^{-1}), C_e is the equilibrium concentration of adsorbate in solution (mol L^{-1}), Q_m is the maximum adsorption for monolayer coverage (mol g^{-1}), C_o is the initial concentration of adsorbate (mol L^{-1}), b is the adsorption equilibrium constant (L mol^{-1}), k is a constant

related to the heat of adsorption, k_f and n are Freundlich constants representing adsorption capacity and intensity.[82]

2.3.2.1 Solid-Gas Adsorption studies

CD ICS materials were grounded in crucible and passed through 40 mesh size. CH_3Cl gas adsorption was performed at room temperature using the Langmuir Gas Adsorption apparatus. Prior to measurement, every sample were degassed at 110^0C and 10^{-6} mm Hg.

2.3.2.2 Solid-Solution Adsorption studies

CD ICS was passed through 40 mesh size sieves. A stock solution of 10^{-4} M p-nitrophenol was prepared in 0.1M CH_3COOH/CH_3COONa buffer at pH= 5.0. Different masses of CD ICS were taken in 10 mL of adsorbate solution in different vials and were shaken for 24 hrs to achieve equilibrium. The suspension was filtered and the p-nitrophenol concentration in the filtrate solution was measured by UV-Vis spectroscopy.

Kinetics of Adsorption

CD ICS was passed through 40 mesh size sieves. 10^{-4} M p-nitrophenol solution was prepared in 0.1M CH_3COOH/CH_3COONa buffer at pH= 5.0. 10 mg of CD ICS in 10 mL of adsorbate solution was added in different vials and the vials were shaken for different time intervals. The suspension was filtered and the residual p-nitrophenol concentration in the filtrate was measured by UV-Vis spectroscopy to determine the amount of p-nitrophenol adsorbed.

CHAPTER 3
RESULTS AND DISCUSSION
3.1 Synthesis

3.1.1 Synthesis of CD functionalized triethoxy silane (CD ICL)

The CD functionalized triethoxysilane was synthesized according to the following procedure: According to this method the CD functionalized silane (CD ICL) was synthesized by reacting β-cyclodextrin with 3-isocyanatopropyltriethoxysilane according to the following reaction Scheme 3.1.

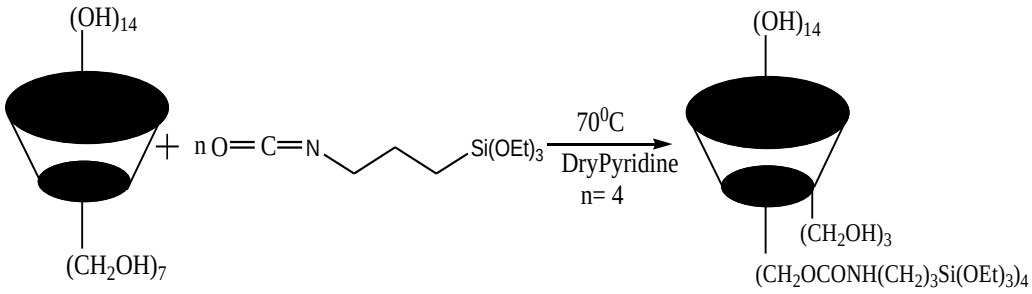

Scheme 3.1: Synthetic scheme of an isocyanate based linker CD ICL, where the degree of substitution n=4

The isocyanate linkage, CD ICL, is a relatively stable linker which can be preserved at room temperature and in the aqueous solution phase.

3.1.2 Synthesis of CD ICS (CD isocyanate carbamate linked hexagonal mesoporous silica)

CD ICL was cocondensed with TEOS in presence of a SDA and a pore expander (TMB) following the direct synthesis pathway.[72, 73] The surfactant and pore expander were subsequently removed from the "surfactant containing" or "as-synthesized" material by solvent extraction using ethanol as the solvent. Finally

after drying CD ICS was isolated as a white powder (see Schemes 3.2 and 3.3).

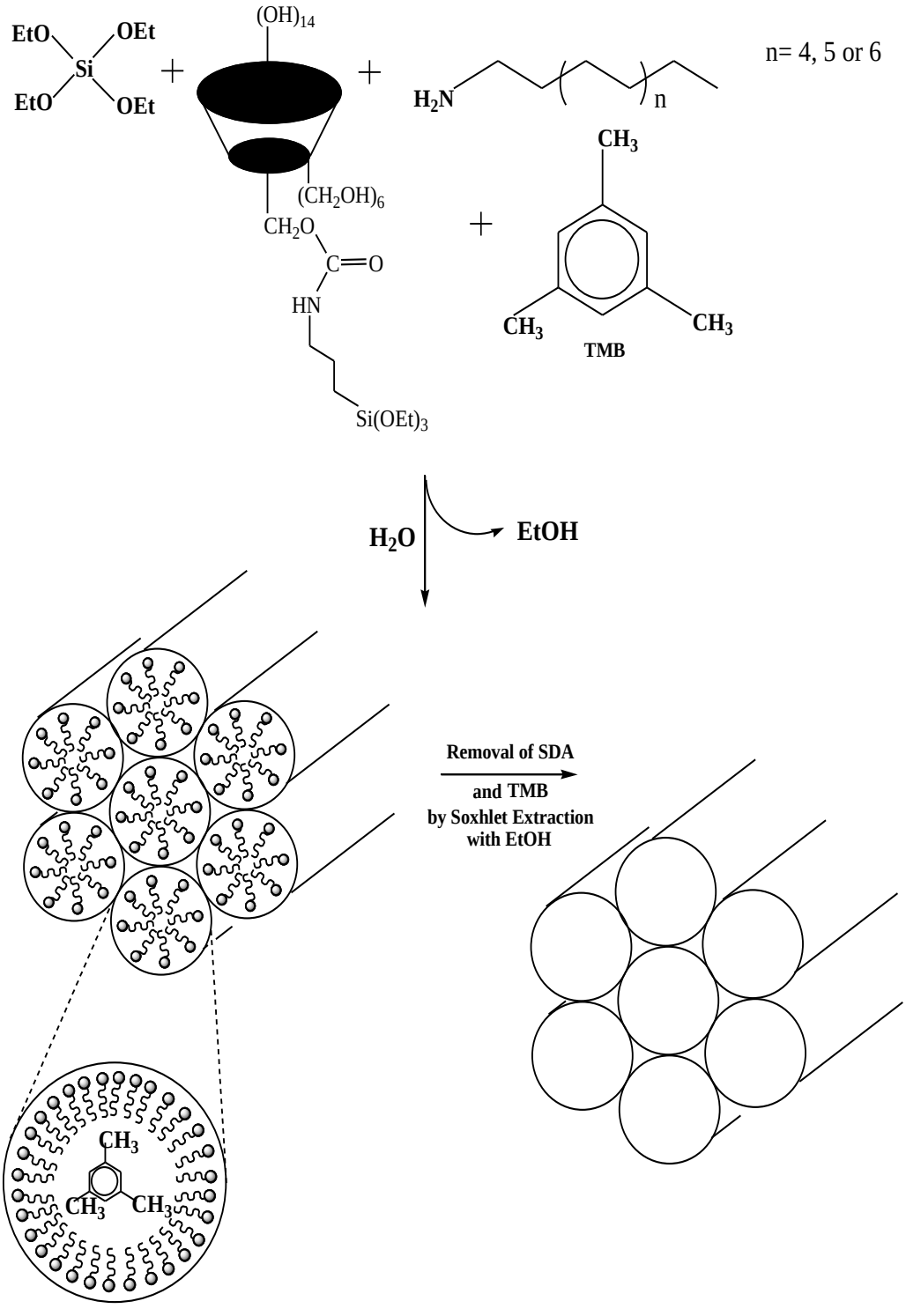

Scheme 3.2: Synthesis of CD ICS from CD ICL (This drawing is not to scale).

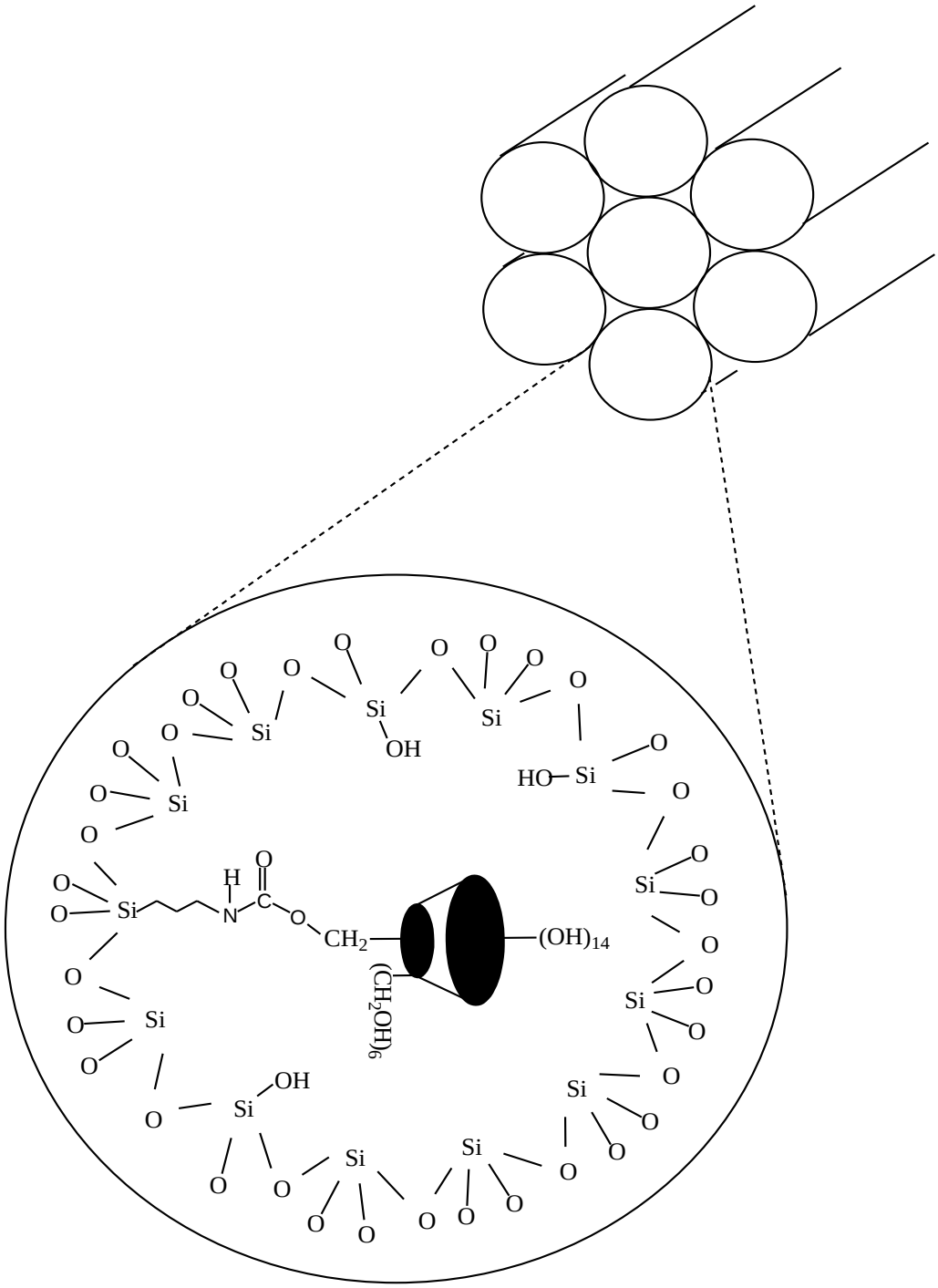

Scheme 3.3: A schematic representation of the structure of the final CD ICS material where β-cyclodextrin is attached to the silica matrix via an isocyanate linkage along the interior walls of the silica framework.

CD ICS materials were synthesized using different amounts of CD loading with three different types of neutral surfactants (SDA) which differ according to the

length of the alkyl chain. In total, nine types of CD ICS materials were synthesized and were named as follows (see Table 3.1).

Table 3.1: Synthesis of CD ICS Materials.

Material	β-CD (mol %) with respect to TEOS	SDA
CD ICS 2 (12)	2%	
CD ICS 4 (12)	4%	Dodecylamine
CD ICS 6 (12)	6%	
CD ICS 2 (14)	2%	
CD ICS 4 (14)	4%	Tetradecylamine
CD ICS 6 (14)	6%	
CD ICS 2 (16)	2%	
CD ICS 4 (16)	4%	Hexadecylamine
CD ICS 6 (16)	6%	

Here, 2, 4 or 6 represent the molar percentage of β-CD with respect to TEOS, the bracketed values 12, 14 or 16 represent the number of carbon atoms of the hydrophobic chain in the SDA used during synthesis. For example, CD ICS 2 (12) means 2% CD-incorporated mesostructured silica prepared using dodecylamine and CD ICS 6 (16) represents 6% CD-incorporated mesostructured silica prepared using hexadecylamine as the SDA.

Since the size of framework-confined mesopore is equal to the diameter of the framework channels or to the diameter of the parent rodlike micelles and can be varied by the SDA alkyl chain length,[68] and an increase of the alkyl chain length of the SDA results in larger mesostructures with greater surface areas and pore volumes.

3.2 Characterization

3.2.1 ^{1}H NMR

The ^{1}H NMR spectrum of the native β-cyclodextrin in DMSO-d_6 at 293K was similar to that already reported in the literature and was assigned according to Schneider *et al.*[83]

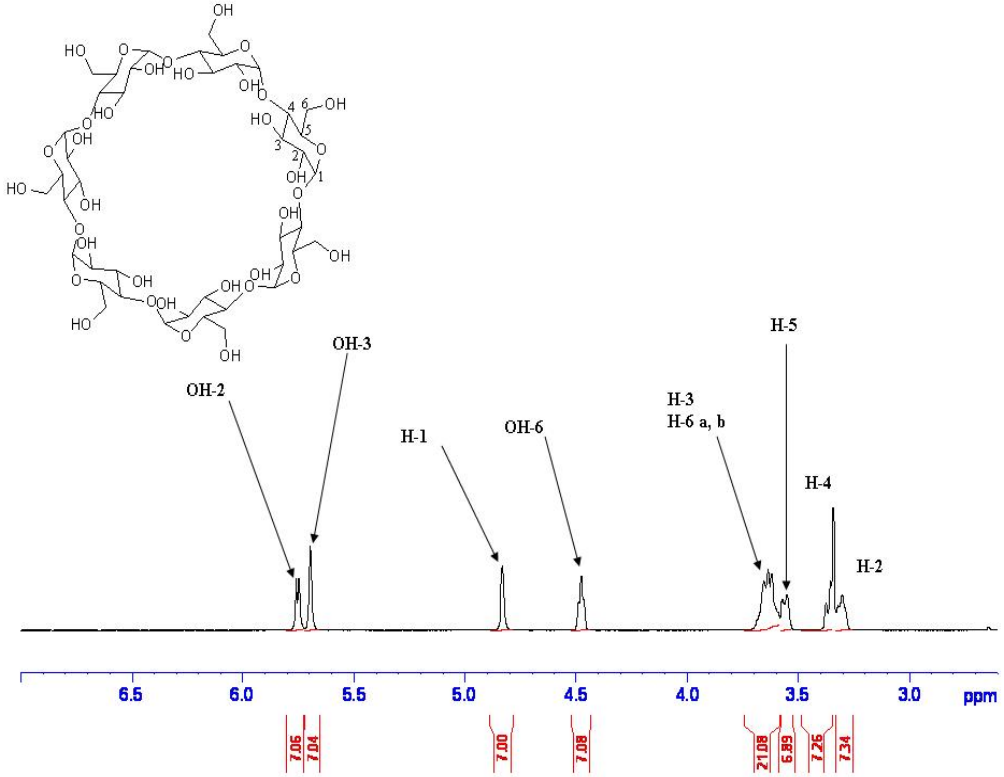

Figure 3.1: ^{1}H NMR spectrum of β-cyclodextrin in DMSO-d_6 obtained at room temperature and 500 MHz. (The numbering of C atoms of glucose unit in the β-CD macrocycle has been shown in the inset).

^{1}H NMR (DMSO-d_6) δ 3.29 (m, 7H, H-2), 3.34 (m, 7H, H-4), 3.55 (m, 7H, H-5), 3.60-3.70 (m, 21H, H-3, H-6 a, b), 4.45 (m, 7H, OH-6), 4.82 (s, 7H, H-1), 5.68 (s, 7H, OH-3), 5.75 (m, 7H, OH-2).

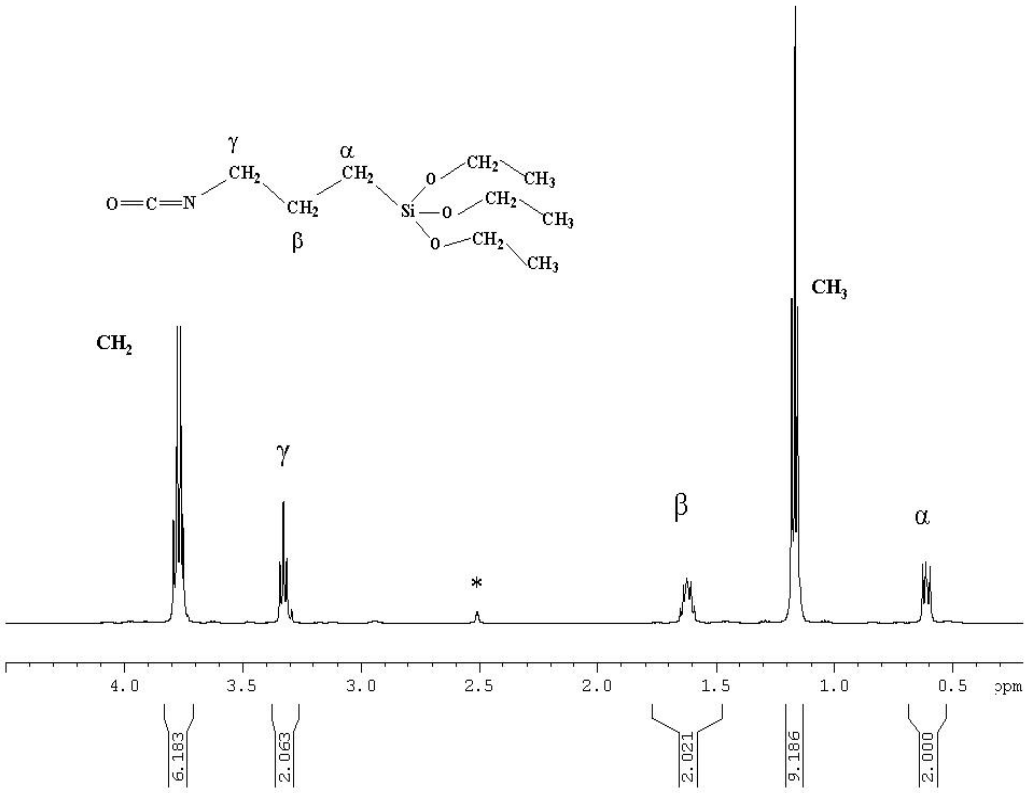

Figure 3.2: ^{1}H NMR spectrum of 3-isocyanatopropyltriethoxysilane in DMSO-d_6 obtained at room temperature and 500 MHz. (* denotes signal for DMSO-d_6).

The ^{1}H NMR spectrum of the 3-isocyanatopropyltriethoxysilane in DMSO-d_6 was assigned as below:

^{1}H NMR (DMSO-d_6) δ 0.60 (m, 2H, Si$\underline{CH_2}$), 1.15 (t, 9H, SiOCH$_2\underline{CH_3}$), 1.60 (m, 2H, SiCH$_2\underline{CH_2}$), 3.33 (m, 2H, SiCH$_2$CH$_2\underline{CH_2}$), 3.75(q, 6H, SiO$\underline{CH_2}$CH$_3$).

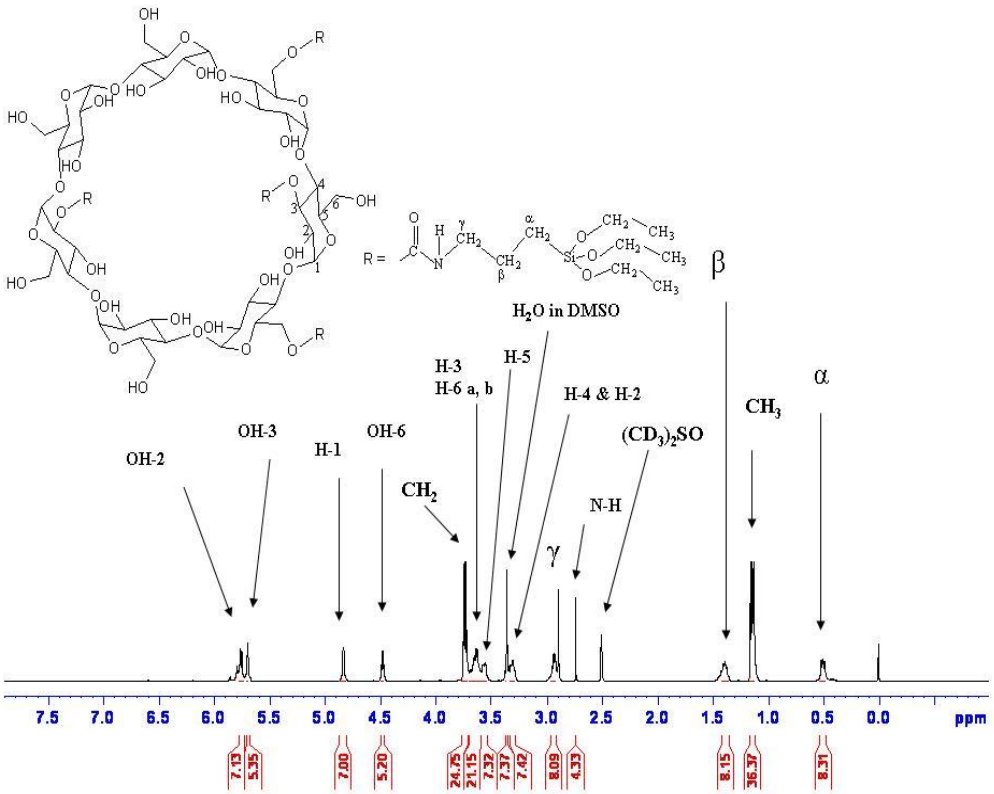

Figure 3.3: ^{1}H NMR spectrum of CD ICL in DMSO-d_6 obtained at room temperature and 500 MHz.

The ^{1}H NMR spectrum of CD ICL in DMSO-d_6 was assigned in the context of the results for the assignment of the ^{1}H NMR of the precursor's β-cyclodextrin and 3-isocyanatopropyltriethoxysilane. The assignment of the ^{1}H NMR resonance lines and integral intensities are in accordance with the molecular structure of the compound depicted in Figure 3.3 (see inset).

^{1}H NMR (DMSO-d_6) δ 0.50 (m, 8H, Si$\underline{CH_2}$), 1.15 (t, 36H, SiOCH$_2\underline{CH_3}$), 1.40 (m, 8H, SiCH$_2\underline{CH_2}$), 2.72 (s, 4H, N-H), 2.93 (m, 8H, SiCH$_2$ CH$_2\underline{CH_2}$), 3.29-3.34 (m, 14H, H-4 and H-2), 3.55 (m, 7H, H-5), 3.60-3.70 (m, 14H, H-3 and H-6 a,

b), 3.75 (q, 24H, SiO$\underline{CH_2}CH_3$), 4.48 (m, 5H, OH-6), 4.82 (s, 7H, H-1), 5.70 (s, 5H, OH-3), 5.75 (m, 7H, OH-2).

The chemical shift of α-, β- and γ- protons of the precursor 3-isocyanatopropyltriethoxysilane was 0.60, 1.60 and 3.33 ppm respectively. However, after the coupling reaction, the chemical shift of α-, β- and γ- protons in the final product, changed to 0.50, 1.40 and 2.93 ppm respectively. The measured change in chemical shift differences (Δδ) for α-, β- and γ- protons are (0.60-0.50) = 0.10, (1.60-1.40) = 0.20 and (3.33-2.93) = 0.40 ppm respectively. The α-, β- and γ- protons of the linker is connected to β-cyclodextrin via the urethane linkage where γ protons are the adjacent, followed by the β protons whereas the α protons are the most remote. Consequently, the change in chemical shift (Δδ) is the maximum for the γ protons (0.40 ppm), the medium for the β protons (0.20 ppm) and the lowest for the α protons (0.10 ppm), in accordance with the structure of the compound and the position of covalent attachment.

The H-1 proton is the unreacted proton of cyclodextrin. On the other hand the CH_3 protons of $SiOCH_2CH_3$ are the unreacted protons of the linker. Since one linker contains 9 CH_3 protons of $SiOCH_2CH_3$, the number of linkers attached to one molecule of cyclodextrin is 36.37/9 = 4. Since 4 linkers are attached to one cyclodextrin molecule, the number of α-, β- or γ- protons should be 4×2=8 which is in correspondence with the integration of the ^{1}H NMR data showing 8.31, 8.15 and 8.09 α-, β- and γ- protons respectively. Since 4 linkers are attached to one β- CD molecule, the number of CH_2 protons of $SiOCH_2CH_3$

should be 4×6=24, which is in correspondence with the integration of the ^{1}H NMR showing 24 CH_2 protons of $SiOCH_2CH_3$ protons.

Furthermore, if 4 linkers are attached to one β-CD molecule, the number of N-H protons should be 4 which are in correspondence with the integrated ^{1}H NMR showing 4.33 N-H protons. The integration of the ^{1}H NMR showed 5.20 and 5.35 protons of OH-6 and OH-3, respectively. The number of protons in both OH-6 and OH-3 in unsubstituted β-cyclodextrin is 7. In total, 4 protons have been substituted by the linker (2 protons from OH-6 and 2 protons from OH-3), the result of integration is 5 for both OH-6 and OH-3.

According to the ^{1}H NMR results, there are 4 isocyanate linkers attached to one cyclodextrin in CD ICL. A possible molecular structure for CD ICL is as follows.

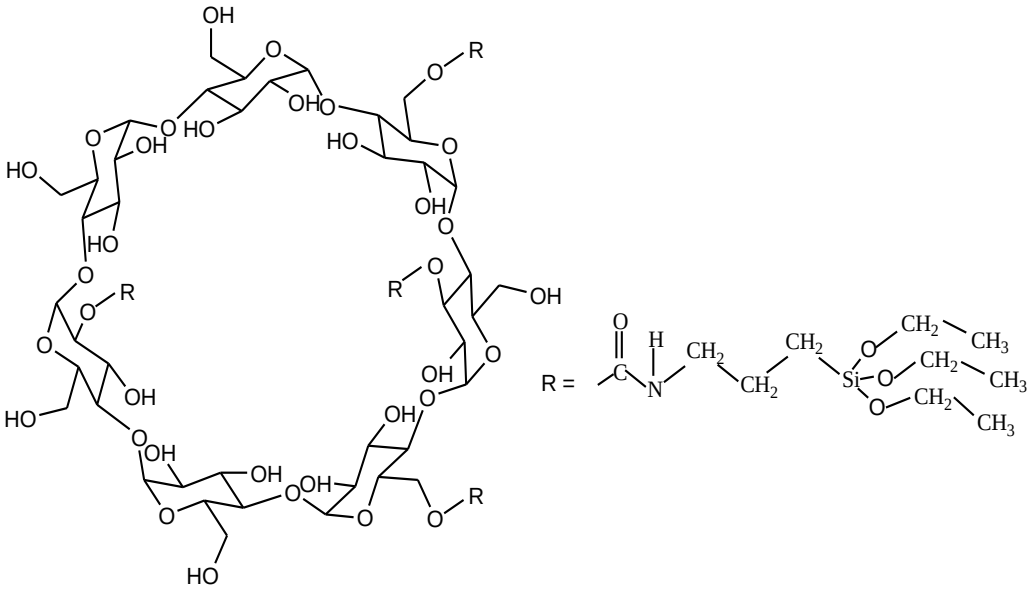

Figure 3.4: A schematic of one possible isomer of CD ICL where the linkers are bonded via OH-6 and OH-3 according to ^{1}H NMR data.

Since any 2 of the seven OH-6 protons and any 2 of the seven OH-3 protons could be substituted by the linker, the above structure is just one of the possible

isomers. It is also possible to have one molecule of cyclodextrin bonded to several linker molecules. Figure 3.4 shows just one of the several possible isomers of CD ICL where an average 4 linkers are attached to one molecule of β-cyclodextrin.

3.2.2 Infrared Spectra

According to the reaction Scheme 3.1 the molar ratio of β-CD to 3-isocyanatopropyltriethoxysilane was 1: 4 before reaction. According to the ^{1}H NMR results, four isocyanate linkers were attached to one cyclodextrin, i.e., reaction was complete. The completion of the reaction was supported by IR spectroscopy of CD ICL showing complete disappearance of the isocyanato group at 2270 cm^{-1} (see Figure 3.5).

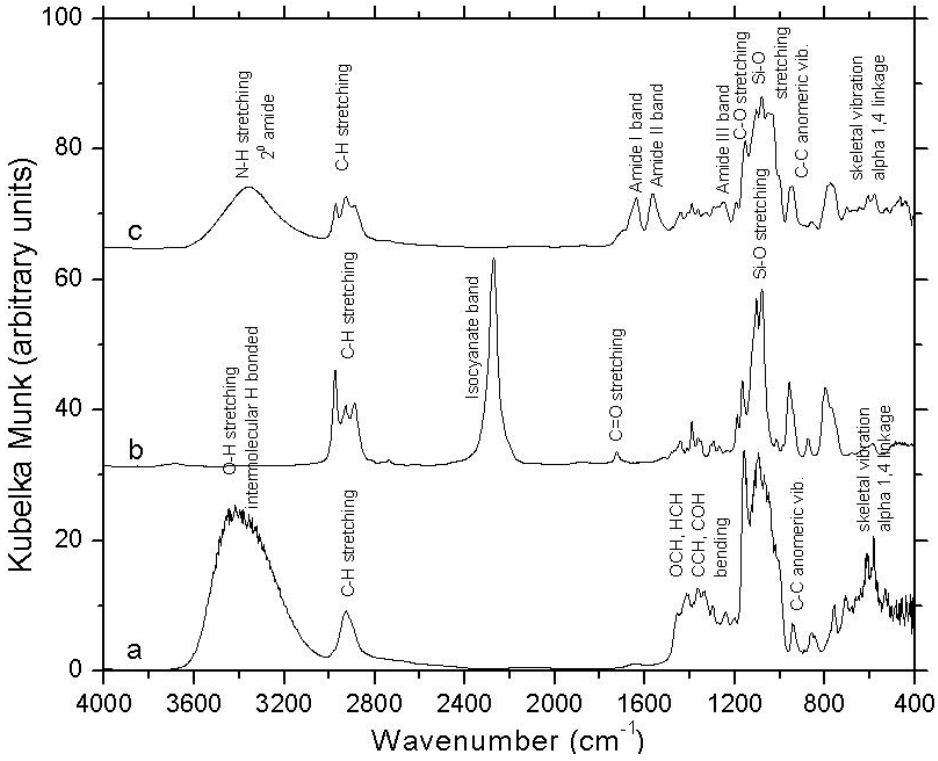

Figure 3.5: Infrared Spectra of a) β-cyclodextrin b) ICL and c) CD ICL at room temperature.

IR spectra of CD ICL (KBr, cm^{-1}): 3350 (N-H stretching), 2971 and 2924 (C-H stretching), 1634 (C=O stretching Amide I), 1560 (N-H bending Amide II), 1437-1280 (OCH, HCH, CCH, COH bending of β-cyclodextrin), 1260 (Amide III), 1150 (C-O stretching of β-cyclodextrin) 1090 (Si-O-C stretching), 870 (C-C anomeric vibration of β-cyclodextrin), 947 and 578 (skeletal vibration of α-1,4 linkage of β-cyclodextrin).

The IR spectra of CD ICL shows a single band around 3350 cm^{-1} which is due to N-H bond stretching of secondary urethane. Two bands around 1634 cm^{-1} and 1560 cm^{-1} are due to C=O stretching vibration (amide I) and N-H bending vibration (amide II) of secondary amides. The weak band at 1260 cm^{-1} is the amide III band due to coupling between N-H bending and C-N stretching of the C-N-H component. The bands observed in the IR spectra of the parent β-cyclodextrin,[84] overlaps with the characteristic bands of CDICL showing successful attachment of the β-cyclodextrin group with ICL.

Infrared spectra were taken for all nine CD ICS materials. The dominant peak in all cases was the Si-O-Si stretch at 1050-1150 cm^{-1}, which is characteristic of siloxane condensation.[85] The bands observed in the IR spectra of the CDICL, overlaps with the characteristic bands of CD ICS showing successful inclusion of cyclodextrin within the mesostructure.

Figure 3.6 below shows the infrared spectra of CD ICS 2(14), CD ICS 4(14) and CD ICS 6(14) as well as that of the synthetic precursor CD ICL.

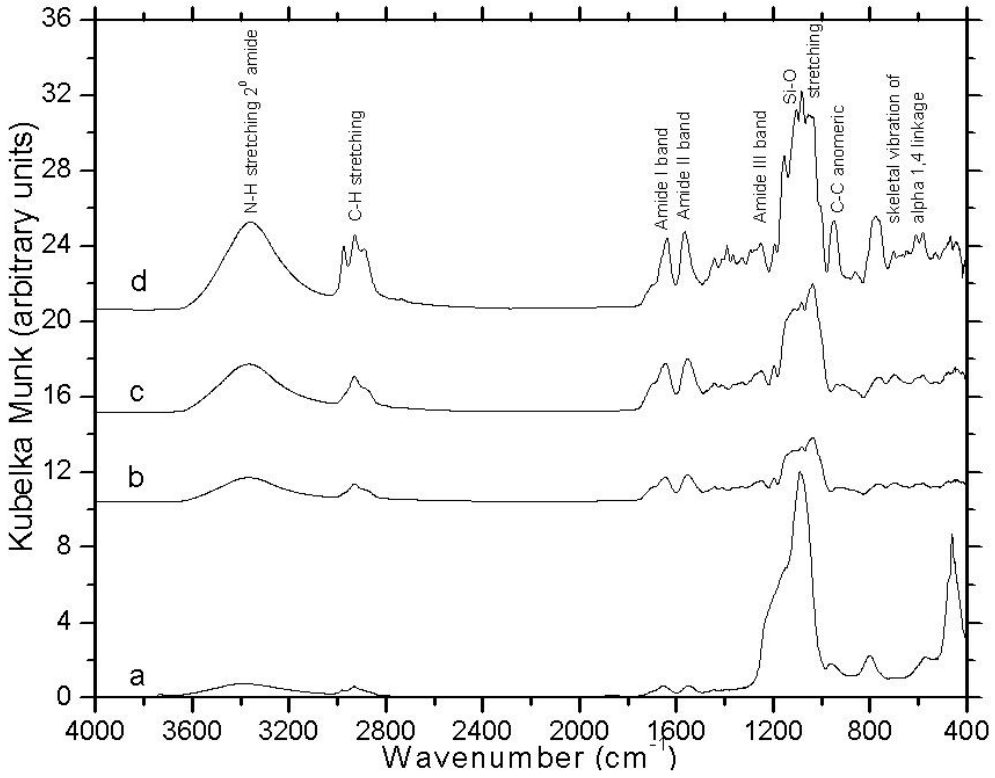

Figure 3.6: Infrared Spectra of a) CD ICS 2(14) b) CD ICS 4(14) and c) CD ICS 6(14) and d) CD ICL at room temperature.

IR spectra of CD ICS 4 (14) (KBr, cm^{-1}): 3350 (N-H stretching), 2920 (C-H stretching), 1637 (C=O stretching Amide I), 1545 (N-H bending Amide II), 1431-1300 (OCH, HCH, CCH, COH bending of β-cyclodextrin), 1240 (Amide III), 1078 and 1024 (Si-O stretching), 860 (C-C anomeric vibration of β-cyclodextrin), 910 and 570 (skeletal vibration of α-1,4 linkage of β-cyclodextrin).

Similar observations were found for all other CD ICS materials (see Figure A.16 and A.17 in the Appendices).

3.2.3 Raman Scattering of CD ICS

Raman spectra were taken for all nine CD ICS materials. The dominant peaks in all cases were the O-H stretch in 3650-3000 cm^{-1} and C-H stretch around 3000-2800 cm^{-1}.

Figure 3.7 below shows the Raman spectra of CD ICS 2(12), CD ICS 6(12) and β-cyclodextrin. The band around 1100-1000 cm^{-1} was assigned to Si-O-Si antisymmetric vibration[86] which is characteristic of siloxane condensation. With an increase of cyclodextrin loading from 2% to 6% the bands at 1442, 1398, 1315, 1209, 1125, 933, 841, 641 and 473 cm^{-1} due to cyclodextrin[87] increases in intensity.

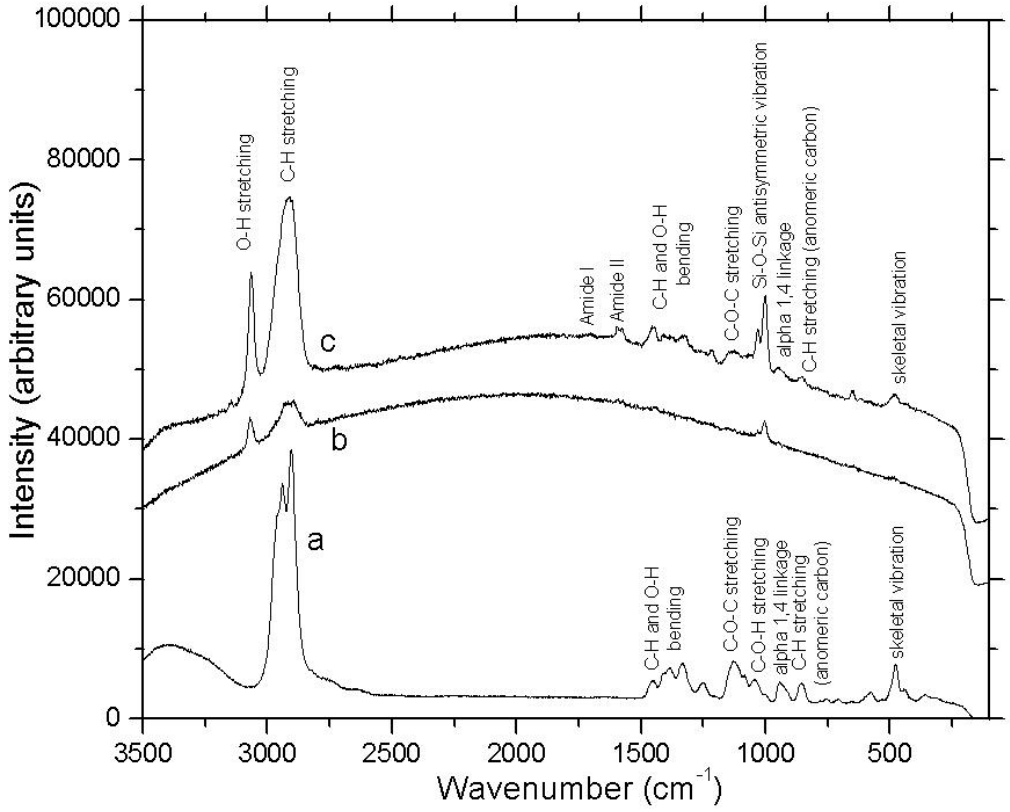

Figure 3.7: Raman Spectra of a) β-cyclodextrin b) CD ICS 2(12) and c) CD ICS 6(12) at ambient temperature with excitation wavelength 514 nm.

Raman spectra of β-cyclodextrin (λ_{ex} 514 nm, cm^{-1}): 2936 and 2931 (C-H stretching), 1442, 1374, 1324 and 1238 (C-H and O-H bending), 1115 (C-O-C stretching), 1032 (C-O-H stretching), 930 (α-1, 4 linkage), 847 (C-H stretching of anomeric carbon), 473 (skeletal vibration).

Raman spectra of CD ICS 2(12) (λ_{ex} 514 nm, cm^{-1}): 3083 (O-H stretching), 2900 (C-H stretching), 1578 (Amide II), 1430 (C-H and O-H bending), 1000 (Si-O-Si antisymmetric stretching).

Raman spectra of CD ICS 6(12) (λ 514 nm, cm^{-1}): 3065 (O-H stretching), 2900 (C-H stretching), 1650 (Amide I), 1570 (Amide II), 1442, 1315 and 1208 (C-H and O-H bending), 1130 (C-O-C stretching), 1000 (Si-O-Si antisymmetric stretching), 936 (α- 1, 4 linkage), 840 cm^{-1} (C-H stretching of anomeric carbon), 475 (skeletal vibration).

There is some question as to whether the CD hosts are embedded within the mesopore or dangling from the outer surface of silica network. According to the conclusions given by Lambert *et al.*[61] the degree of cross linking determines the position of CD. If cross linking occurs from all directions of CD unit, CD host will be embedded within the silica matrix. However, if CD polymers are not so extensively cross linked (*c.f.* Huq *et al.*[60] where CD was attached to 2.8 silicon atoms), polymerization moves away from the CD unit, leaving it to protrude into the mesopore. Since the CD ICS materials were synthesized from CD ICL that contains four polymerizable units, it is more probable that CD host is incorporated into the silica network rather than solely grafted on the silica surface. However, the present results cannot unequivocally differentiate between

surface-bound or matrix-bound β-cyclodextrin because the Raman excitation source (514 nm) employed is anticipated to penetrate the sample to 10^{-6}m or more in depth. Therefore, this would involve Raman signal from both contributions.

Figure 3.8 below shows the Raman spectra of CD ICS 6(14), CD ICS 6(16), CD ICS 4(12), CD ICS 2(16), CD ICS 4(16) as well as the β-cyclodextrin.

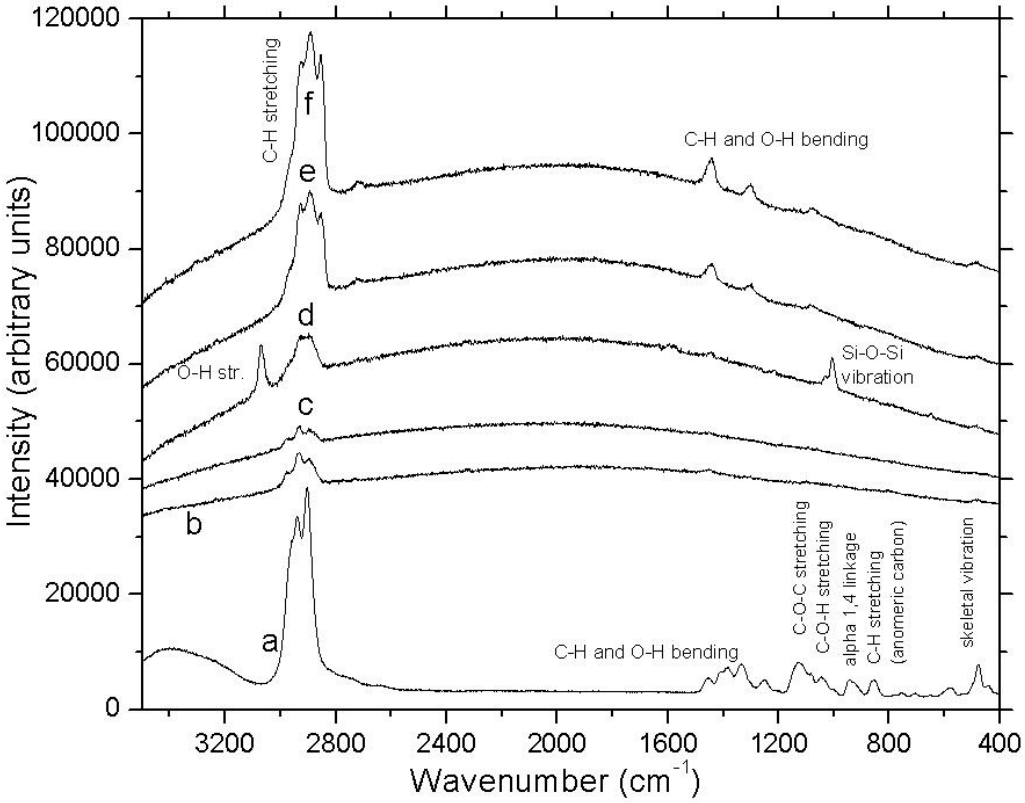

Figure 3.8: Raman Spectra of a) β-cyclodextrin b) CD ICS 6(14) and c) CD ICS 6(16) d) CD ICS 4(12) e) CD ICS 2(16) and f) CD ICS 4(16).

The dominant peak at 3000-2800 cm^{-1} was due to C-H stretch from cyclodextrin. However, the peaks around 1440-1240 cm^{-1} for C-H and O-H bending were less intense. The peaks at 1115 cm^{-1} for C-O-C stretching, 1032 cm^{-1} for C-OH stretching, 930 cm^{-1} for α-1, 4 linkage, 847 cm^{-1} for C-H stretching of anomeric

carbon and 473 cm^{-1} for skeletal vibration of cyclodextrin was very less intense or absent (see Figure 3.8).

3.2.4 MALDI TOF Mass Spectrometry

The incorporation of cyclodextrin within the mesostructure was supported by MALDI TOF mass spectrometry. Due to desorption of the grafted species by laser irradiation, MALDI TOF mass spectrometry permits the direct detection of the oligomers bonded to the silica network.[88-92]

Figure 3.9 below is shows the MALDI TOF MS of β-cyclodextrin where the two peaks at m/z 1157 and 1173 are due to $[\beta\text{-CD} + Na]^+$ and $[\beta\text{-CD} + K]^+$ respectively. Since the MALDI TOF MS spectrometer was operated in positive ion linear mode, ionization of fragmented species by Na^+ or K^+ is necessary in order to direct them towards the detector. For a specific fragment with a specific m/z value, there are differences in the peak intensity for a fragment associated with Na^+ and K^+ and this helps to detect a particular mass fragment. The peak due to $[\beta\text{-CD} + Na]^+$ is more intense than the peak corresponding to $[\beta\text{-CD} + K]^+$ by a factor of approximately 2. This can be attributed to abundance of residuals of these ions in the millipore water used for sample preparation.

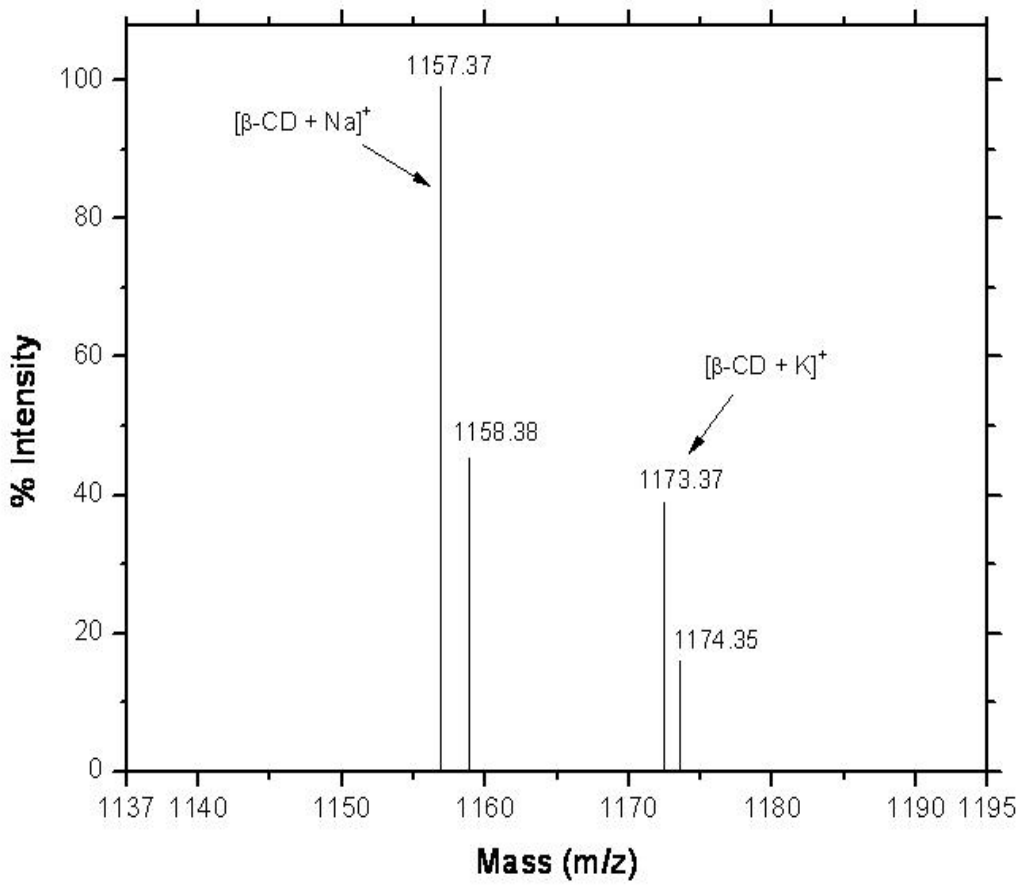

Figure 3.9: MALDI TOF MS of β-cyclodextrin.

MALDI TOF mass spectrometry of each CD ICS materials showed an intense peak at m/z 1157 and 1173 proving CD incorporation within the mesostructure. Besides these major peaks, there were also intense peaks due to various fragmentations of cyclodextrin into glucose fragments as well as a less intense peak due to $[\beta\text{-CD + linker +Na}]^+$. Figure 3.10 below shows the MALDI TOF MS of CD ICS 4(12) where the major peaks were assigned to the corresponding fragments.

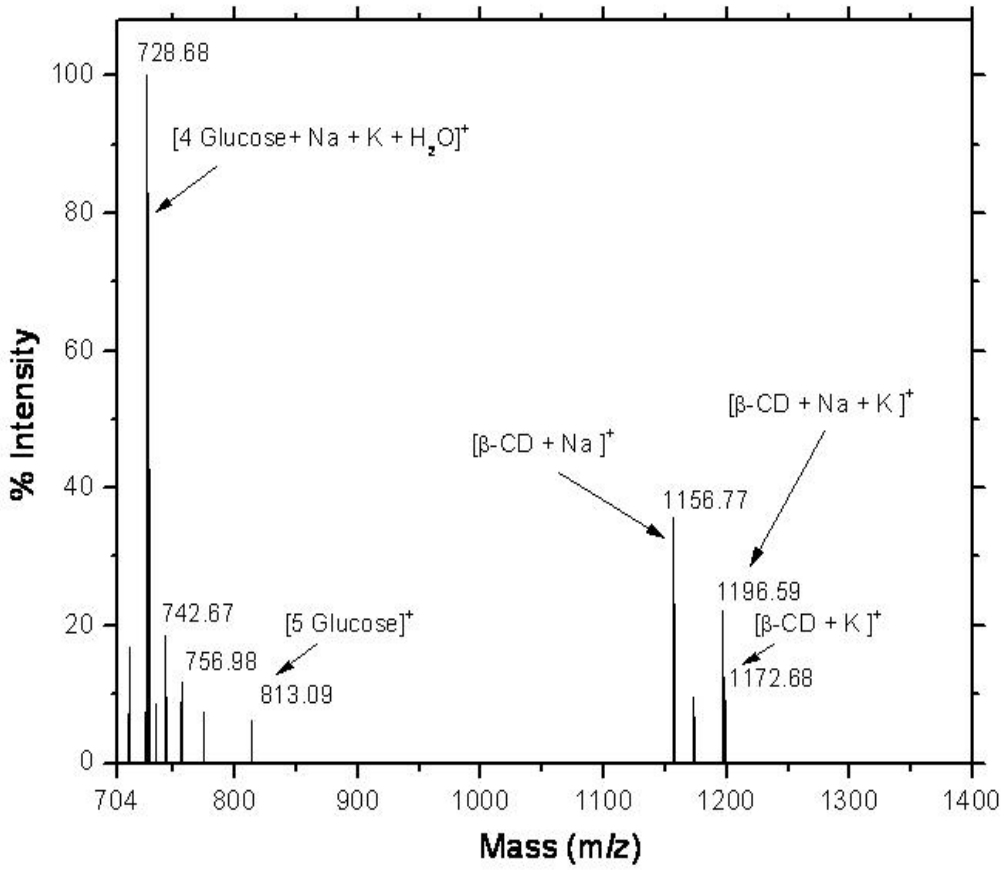

Figure 3.10: MALDI TOF MS of CD ICS 4(12).

A thorough search in literature was conducted[88-92]; no references were found where MALDI TOF MS was used to support CD incorporation within mesoporous silica framework. The MALDI results strongly support β-cyclodextrin attachment to the silica network and this may be the first such example in material chemistry for these types of composite materials.

MALDI TOF MS of other CD ICS materials also displayed peaks at m/z 1157 and 1173 due to $[\beta\text{-CD} + Na]^+$ and $[\beta\text{-CD} + K]^+$ proving the incorporation of β-cyclodextrin within the mesostructure (see Figures A.1 to A.7 in the Appendices).

3.2.5 Solid State ^{13}C NMR CP-MAS Spectroscopy

Solid State ^{13}C NMR CP-MAS Spectra of all the CD ICS were taken at 150.8 MHz on a Varian Inova 600 spectrometer with a spinning rate of 16 kHz. The carbon atoms in the urethane linkage (O**C**ONH) were found from δ = 160-170 ppm. The carbons in the linker (OCONH**C**H_2**C**H_2**C**H_2Si) were found in the region[93] δ = 9-50 ppm. The carbons in β-cyclodextrin were found in the region[83] δ = 60-110 ppm.

Figure 3.11 shows the solid state ^{13}C NMR CP-MAS Spectra of CD ICS 2 (14).

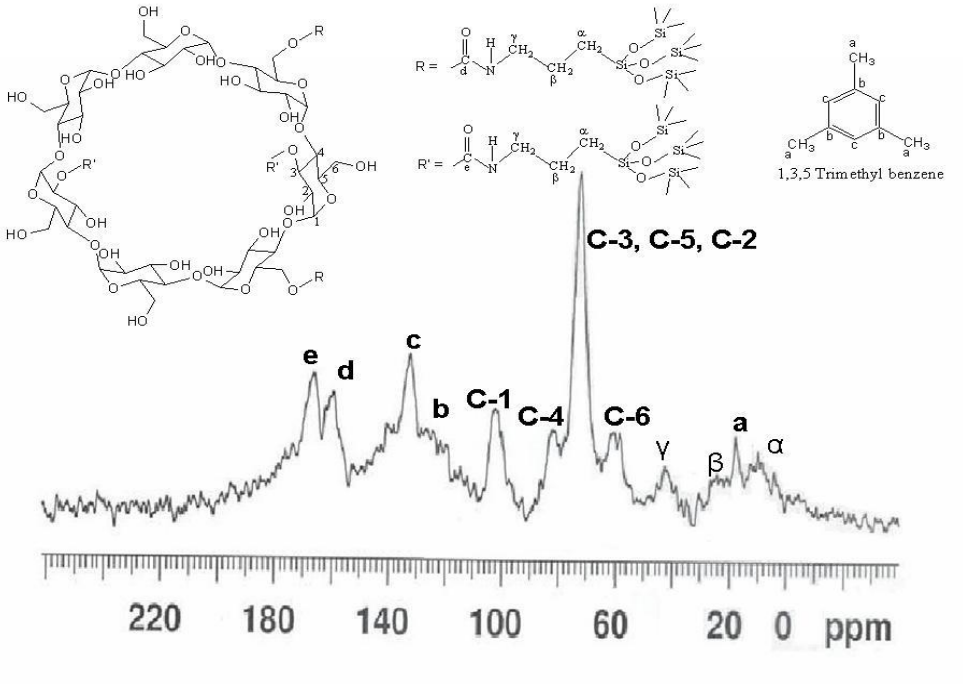

Figure 3.11: Solid state ^{13}C NMR CP-MAS spectrum of CD ICS 2(14) at room temperature. Included is the letter and the number scheme for identification of carbon atoms.

In addition to the expected peaks observed in the solid state ^{13}C NMR CP-MAS spectra, the peaks which correspond to the TMB (the pore expander) are indicated. This indicates that the pore expander was not completely removed by

Soxhlet extraction with ethanol following the procedure described by Huq *et al.*[60] This also reflects that the use of a pore expander for synthesizing such composite materials is not a suitable choice. Because the cyclodextrin itself has strong binding affinity towards aromatic compounds, there is a possibility that the pore expander was entrapped deep inside the silica network via non-covalent interactions with the hydrophobic interior of cyclodextrin. Soxhlet extraction for even 72 hrs could not completely remove the TMB. This supports the general conclusion that the pore expander can be occluded within the framework during synthesis. Solid State ^{13}C NMR CP-MAS Spectra of other CD ICS materials displayed ^{13}C NMR peaks in the region δ = 60-110 ppm due to the ^{13}C nuclei of β-CD and $\delta < 60$ ppm due to ICL, supporting the covalent attachment of β-CD with the silica framework. (see Figure A.8 to A.15 of the Appendices).

3.2.6 SAXD

Small angle X-ray diffraction spectra of the surfactant extracted CD ICS materials showed strong and sharp low angle diffraction peaks around $2\theta \approx 2.2^0$ indicating values of $d_{100} \approx 4.1$ nm and correspond to the presence of highly ordered mesoporous structure. Figure 3.12 below shows the SAXD patterns of CD ICS 4(12), CD ICS 4(16), CD ICS 6(16) and CD ICS 6(12). With an increase of CD loading from CD ICS 4(12) to CD ICS 6(12) the low angle peak at 2.2^0 decreases in intensity. A similar trend is observed for CD ICS 4(16) and CD ICS 6(16). Similar observations were reported by Lambert *et al.*[61] The authors reported loss of periodicity and decrease of intensity with an increase of CD loading: the peak at 2.2^0 decreases in intensity as the percentage of TEOS

goes from 90% to 50% and is absent at 25%. The increase of CD loading is associated with decrease of TEOS, as the proportion of TEOS decreases, the formation of silica framework is hindered because TEOS is the principal component for the silica network formation.

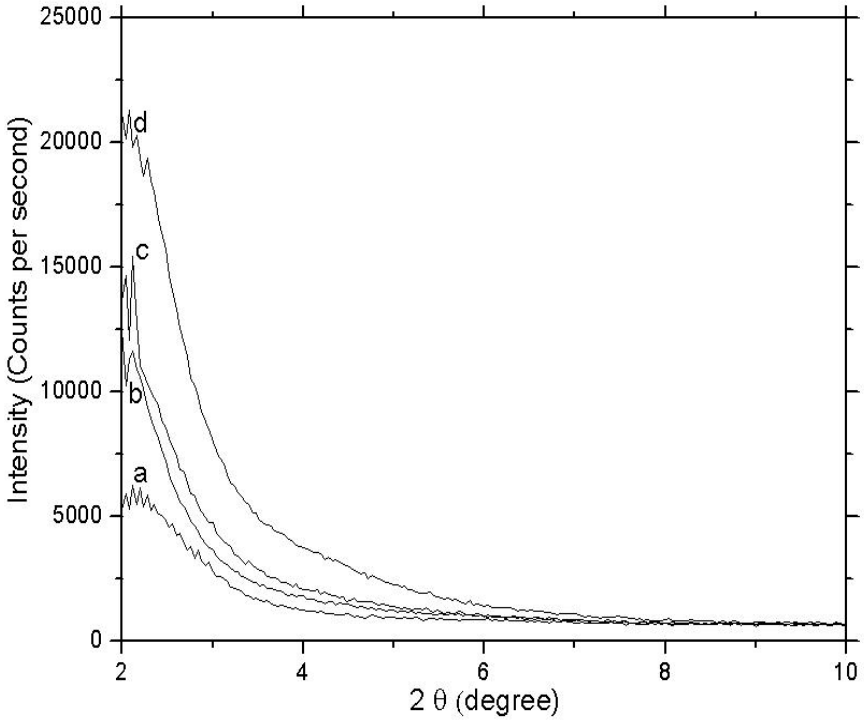

Figure 3.12: Powder X-ray diffraction pattern of surfactant-free CD based mesoporous materials containing different proportions of TEOS and CD (The inset is showing the SAXD pattern of CD composite silica materials reported by Lambert *et al.*[61]

The low angle peak is very sharp in intensity for the materials templated by hexadecylamine than those of dodecylamine. Similar observations were reported by Pinnavaia *et al.*[68] showing superior templating ability for neutral surfactants

with longer alkyl chain lengths as compared to their shorter alkyl chain length counterparts.

3.2.7 TGA

Figure 3.13 shows a typical thermogram obtained for β-cyclodextrin silica based materials with those corresponding to the CD ICL precursor. Mass losses were observed in the low, medium and high temperature regimes, for example, the samples lose physisorbed water at low temperatures ($<110^0$C). For the surfactant containing materials "as HMS" and "as CD ICS 6(12)", the weight loss from 100 to 200^0C (medium temperature) is due to decomposition of the surfactant and the pore expander. The comparison of the thermogram of "as HMS" with that of "as CD HMS" shows that the weight loss around 300^0C occurs for "as CD HMS" material. For the CD composite materials, CD ICL, CD ICS 6(12) and "as CD ICS 6(12)" the thermograms reveal an important weight loss around 300^0C, corresponding to the thermal decomposition of β-CD.

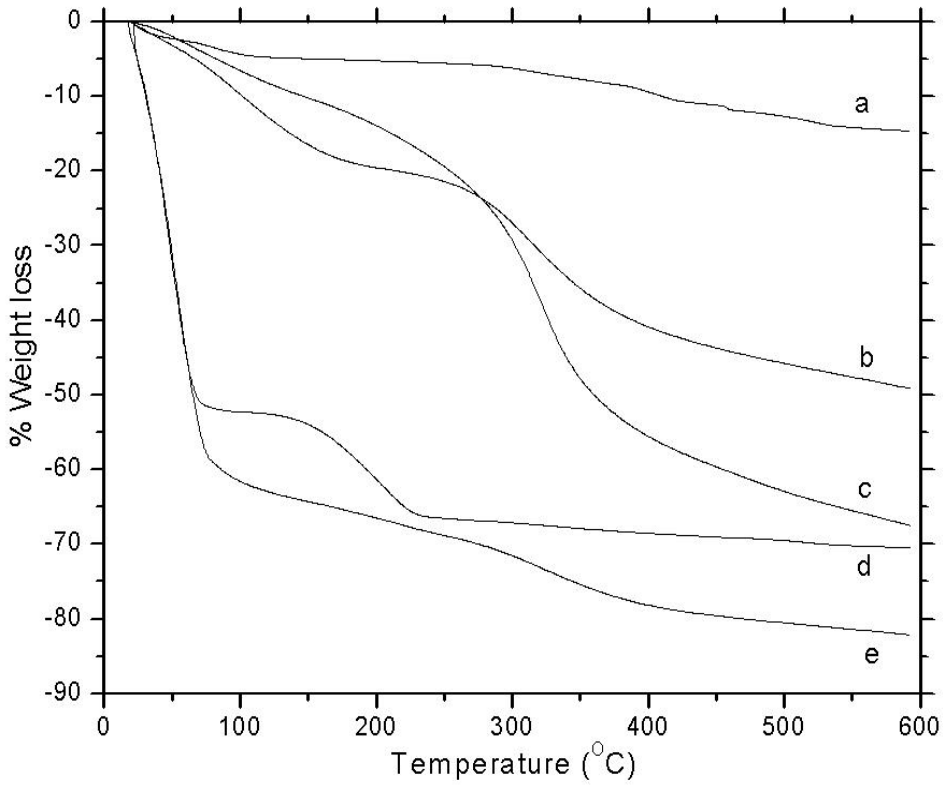

Figure 3.13: Thermogravimetric profiles of CD composite materials a) HMS b) CD ICS 6(12), c) CD ICL d) as HMS and e) as CD ICS 6(12). HMS stands for the hexagonal mesoporous silica without CD. The surfactant containing material is called "as synthesized" material hence the conventional notation "as" has been used for surfactant containing materials.

The differential thermogram of CD ICL and CD ICS 6(12) as shown in Figure 3.14 reveals that the decomposition temperature of cyclodextrin for CD ICL (324^0C) corresponds to that of CD ICS showing successful attachment of cyclodextrin with silica network. The decomposition temperature of CD ICL and CD ICS 6(12) is above 320^0C which is higher than the melting point (298^0C) of native β-cyclodextrin. This suggests that cyclodextrin is chemically bound to the silica network because extra energy is needed to break the bond between cyclodextrin and silica network.

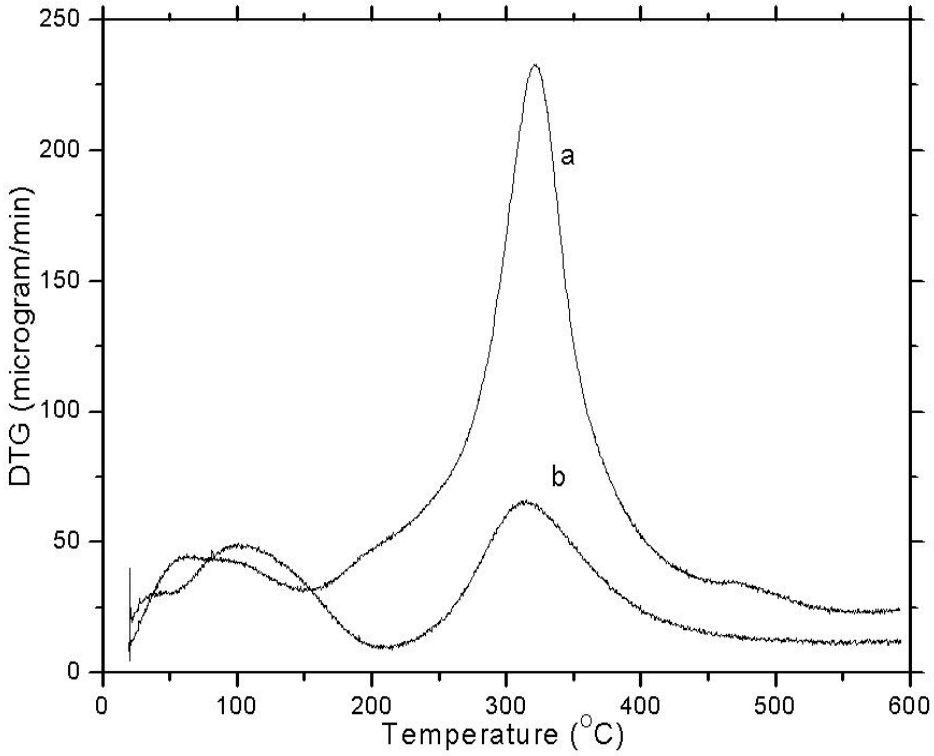

Figure 3.14: Differential thermogravimetric profile of a) CD ICL and b) CD ICS 6(12).

3.2.8 C, H, N Elemental Analysis

The elemental analysis result of CD ICL is as given below.

Table 3.2: Elemental (C, H, N) analysis of CD ICL 4.3.

Element	Calculated (%)	Experimental (%)
C	44.0	44.1
H	6.9	7.1
N	3.9	3.6

3.2.9 Porosimetry

Nitrogen adsorption-desorption isotherms of CD ICS materials (see Figure 3.15 to Figure 3.17) generally displayed Type IV isotherms with hysteresis loops arising from different adsorption and desorption mechanisms in the mesopore. Generally H4 hysteresis loops are observed. Isotherms with Type H4 hysteresis loops featuring parallel and almost horizontal branches have been ascribed to adsorption-desorption in narrow slit-like pores.[94] Loops of type H4 are often associated with narrow pore size distributions.

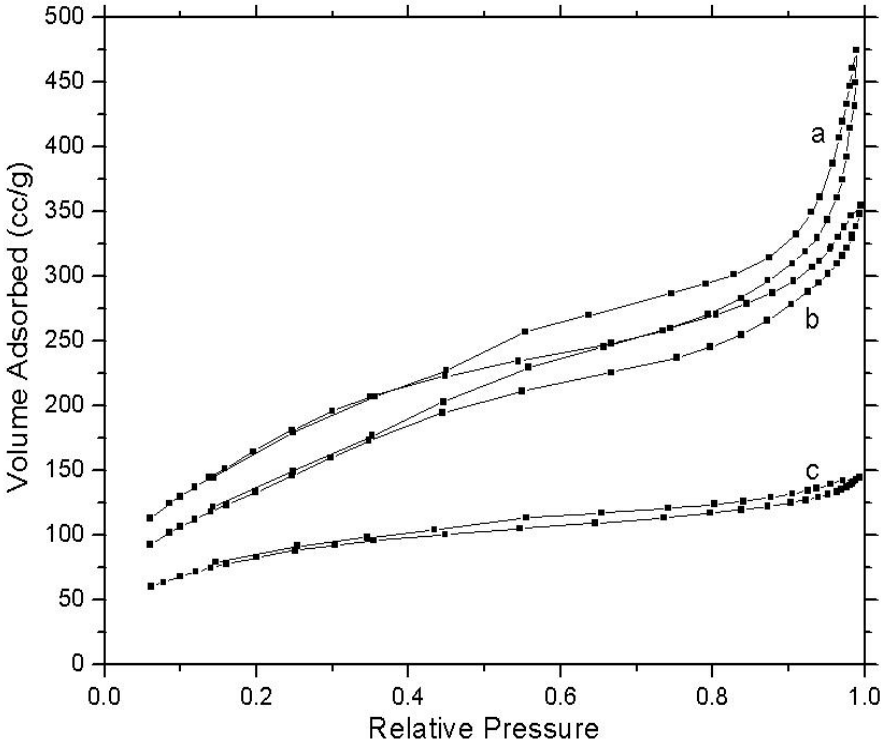

Figure 3.15: Nitrogen Adsorption-Desorption isotherm of a) CD ICS 2(12) b) CD ICS 4(12) and c) CD ICS 6(12) at 77 K.

For simplifying the following discussion it is required to define and differentiate the terms textural mesoporosity and framework mesoporosity. According to

Pinnavaia *et al.*,[67] the porosity which arises from the uniform channels of the templated framework is framework mesoporosity. The size of framework confined mesopore is equal to the diameter of the framework channels. Since the diameter of the framework confined mesopore varies with the parent rodlike micelles, it can be increased by increasing the length of the alkyl chain length of the surfactant or by the addition of organic compounds. The porosity which arises from non crystalline intraaggregate voids and spaces formed by interparticle contacts is called textural mesoporosity. The size of the textural mesopore depends on the size, shape and number of framework-confined mesopore.

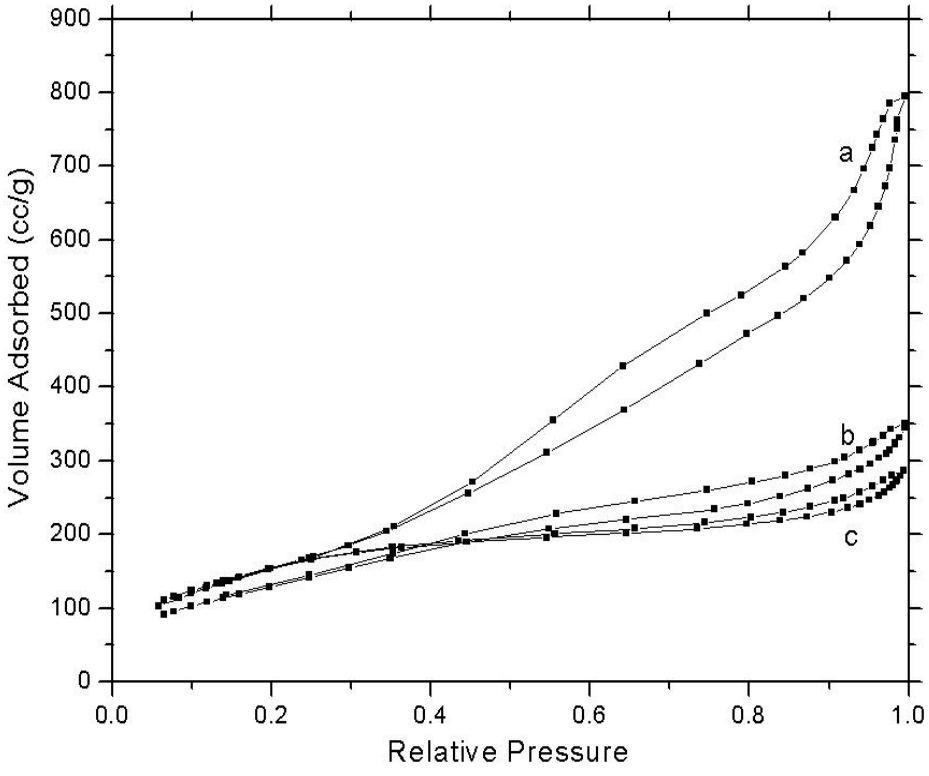

Figure 3.16: Nitrogen Adsorption-Desorption isotherm of a) CD ICS 2(14) b) CD ICS 4(14) and c) CD ICS 6(14) at 77 K.

The presence of framework confined mesoporosity is indicated by an adsorption step centered at the relative pressure region from around 0.05 to 0.3. From the height and slope of the sorption step in this region we can get a qualitative indication of the extent and the uniformity of the framework mesoporosity. For materials with less CD loading, e.g. CD ICS 2% or CD ICS 4%, adsorption in the region 0.05 to 0.3 is greater with a steeper slope (see Figure 3.15 to Figure 3.17). This indicates that the framework confined mesoporosity is well defined for the materials with a lower CD loading. On the other hand, with the increase

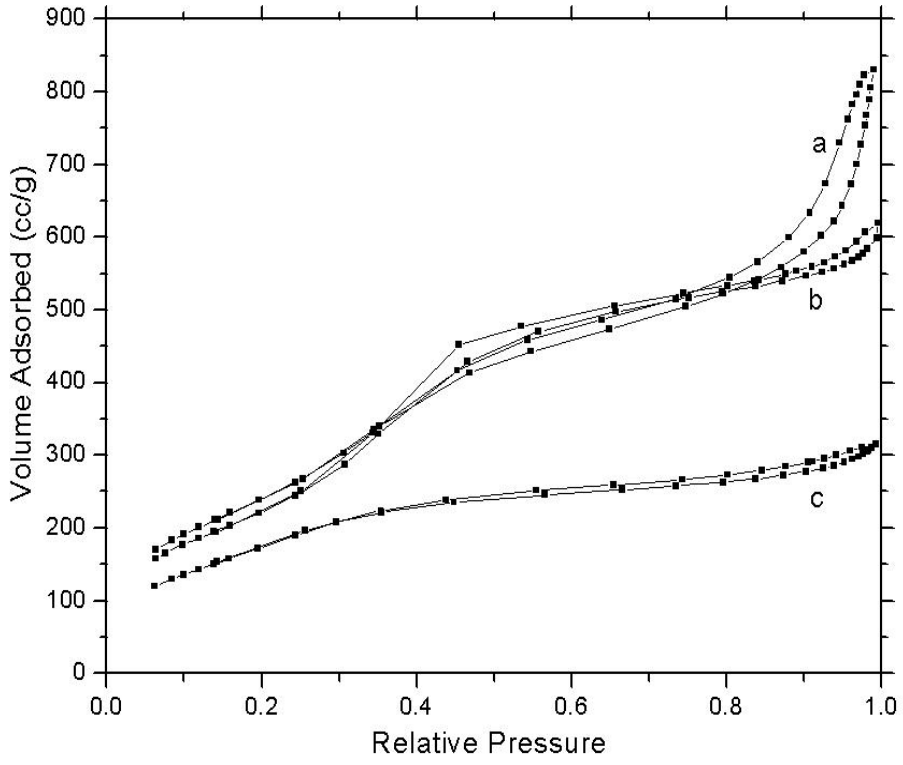

Figure 3.17: Nitrogen Adsorption-Desorption isotherm of a) CD ICS 2(16), b) CD ICS 4(16) and c) CD ICS 6(16) at 77 K.

of CD loading, adsorption in the region 0.05 to 0.3 decreases with a lower slope. This indicates that an increase of incorporation of large CD moieties within mesoporous framework, the uniformity of the mesoporous framework is degraded. Similar observations were reported by Huq *et al.*[60] observing structural perturbation of the framework caused by the inclusion of CD moieties within the mesoporous framework.

The presence of textural mesoporosity is verified by well defined hysteresis loop in the region from 0.3 to 1.0. If a comparison of the adsorption isotherms of different surfactant systems is made, it is found that CD ICS materials prepared by SDA with shorter alkyl chain length have more textural mesoporosity as compared to framework mesoporosity whereas the reverse is true for longer alkyl chain surfactants. Similar observations were reported by Pinnavaia *et al.*[68]

The following table shows the surface properties of CD ICS materials as determined from nitrogen porosimetry (see Table 3.3).

Table 3.3: Surface Properties of CD ICS Materials as determined from nitrogen porosimetry at 77 K.

Material	BET Surface Area (m^2/g)	Pore Volume (cm^3/g)
CD ICS 2(12)	630.3	0.67
CD ICS 4(12)	504.3	0.51
CD ICS 6(12)	307.0	0.21
CD ICS 2(14)	680.1	1.16
CD ICS 4(14)	505.4	0.52
CD ICS 6(14)	591.8	0.42
CD ICS 2(16)	906.5	1.18
CD ICS 4(16)	832.1	0.90
CD ICS 6(16)	656.8	0.47

Change of CD loading in same surfactant

With an increase of CD loading for CD ICS materials prepared by the same surfactant, the pore volume and surface area decreases. These changes in surface properties indicate the presence of the large CD moieties within the pore channels. Comparison of CD ICS 2(12), CD ICS 4(12), and CD ICS 6 (12) shows that with an increase of CD loading from 2% to 6%, a decrease of surface area from 630.3 m^2/g to 307.0 m^2/g occurs with a decrease of pore volume from 0.67 cm^3/g to 0.21 cm^3/g. Similar trends were observed for materials prepared in presence of tetradecylamine and hexadecylamine as the structure directing agents. (see Table 3.3)

Change of surfactant with same CD loading

With an increase of alkyl chain length of the surfactant, the size of framework mesoporosity increases. This intuitive prediction is observed for materials with different surfactant but the same CD loading.

For example, the comparison of CD ICS 2(12) and CD ICS 2 (16) shows that with an increase of alkyl chain length of the surfactant from dodecylamine to hexadecylamine results in increase of surface area from 630.3 m^2/g to 906.5 m^2/g which is associated with an increase of pore volume from 0.67 cm^3/g to 1.18 cm^3/g. Similar trends were observed for other materials. A comparison of CD ICS 4(12) with CD ICS 4(16), the SA and pore volume increases. A comparison of CD ICS 6(12) with CD ICS 6(16), the SA and pore volume increases.

3.3 Sorption Studies of CD functionalized silica

3.3.1 CH_3Cl Adsorption (Solid-Gas Adsorption)

CH_3Cl gas adsorption isotherm of CD ICS materials at ambient temperature was obtained by using a Langmuir adsorption apparatus. In order to find the dead volume the calibration curve was determined at first (see Figure 3.18).

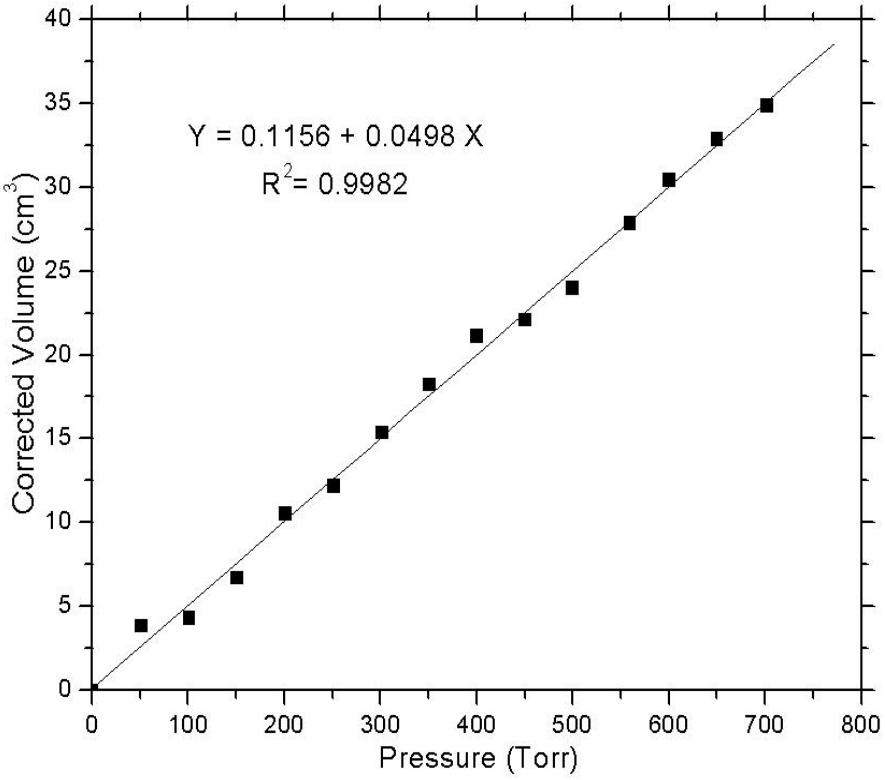

Figure 3.18: Calibration Curve for determination of dead volume for the Langmuir Gas Adsorption Apparatus at room temperature.

CH_3Cl gas adsorption isotherm of CD ICS materials were fitted by Langmuir, BET and Freundlich models. Figures 3.19 to 3.21 below show the nonlinear fitting for CD ICS 4(12) and CD ICS 6(14), respectively.

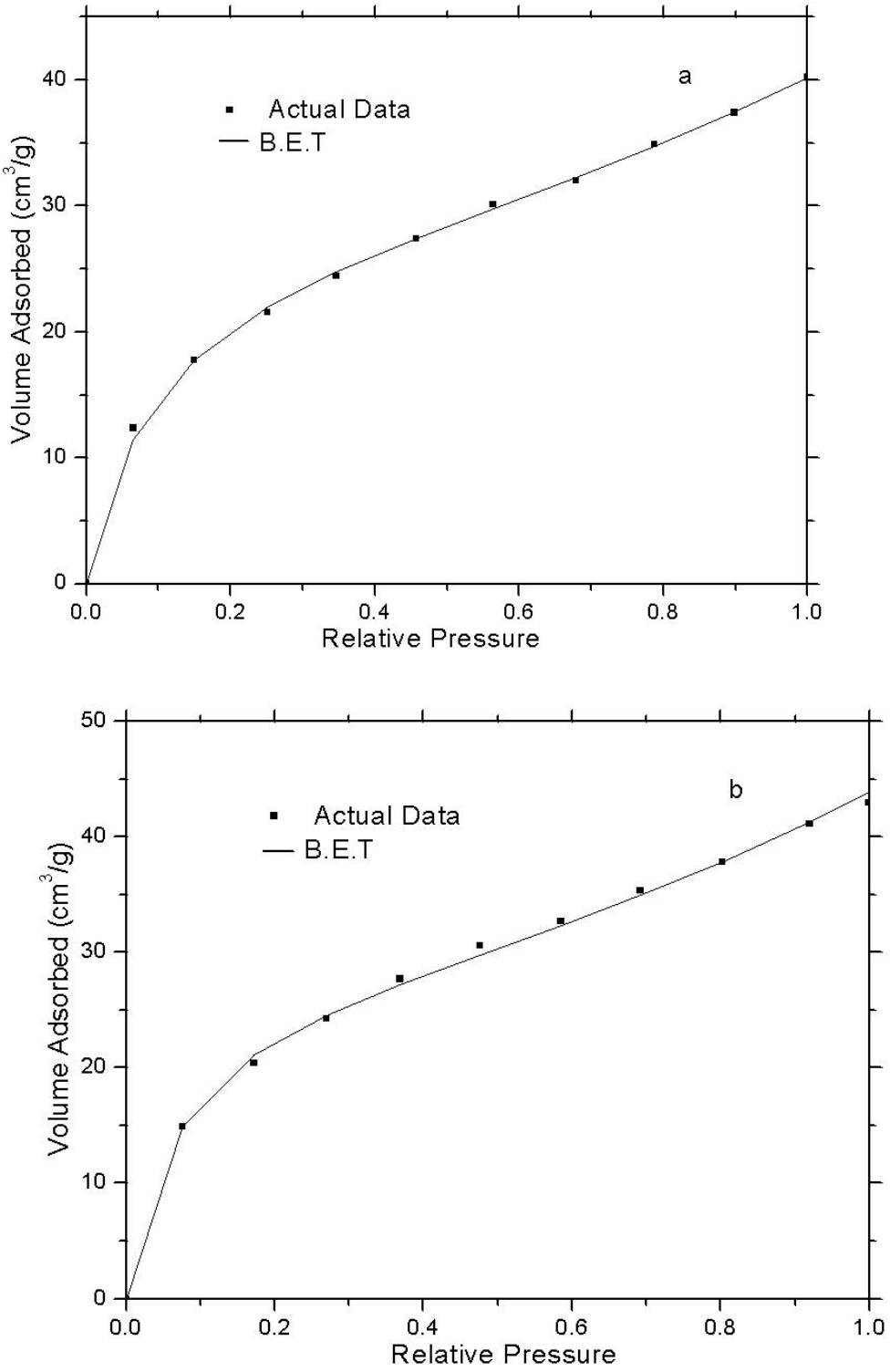

Figure 3.19: Experimental data and B.E.T. fitting of CH_3Cl adsorption of a) CDICS 4 (12) and b) CD ICS 6(14) at room temperature.

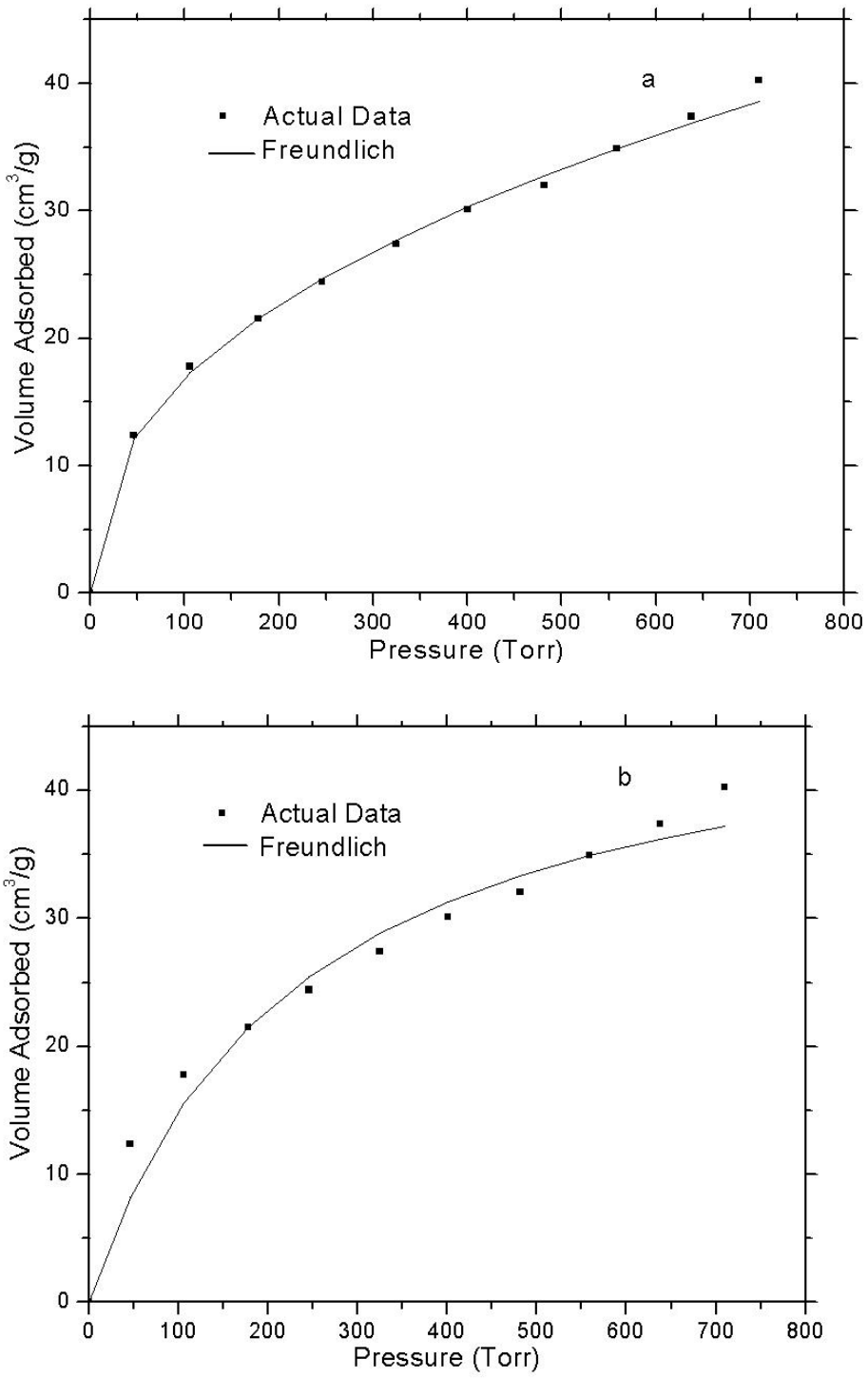

Figure 3.20: Experimental data and Freundlich fitting of CH_3Cl adsorption of a) CDICS 4 (12) and b) CD ICS 6(14) at room temperature.

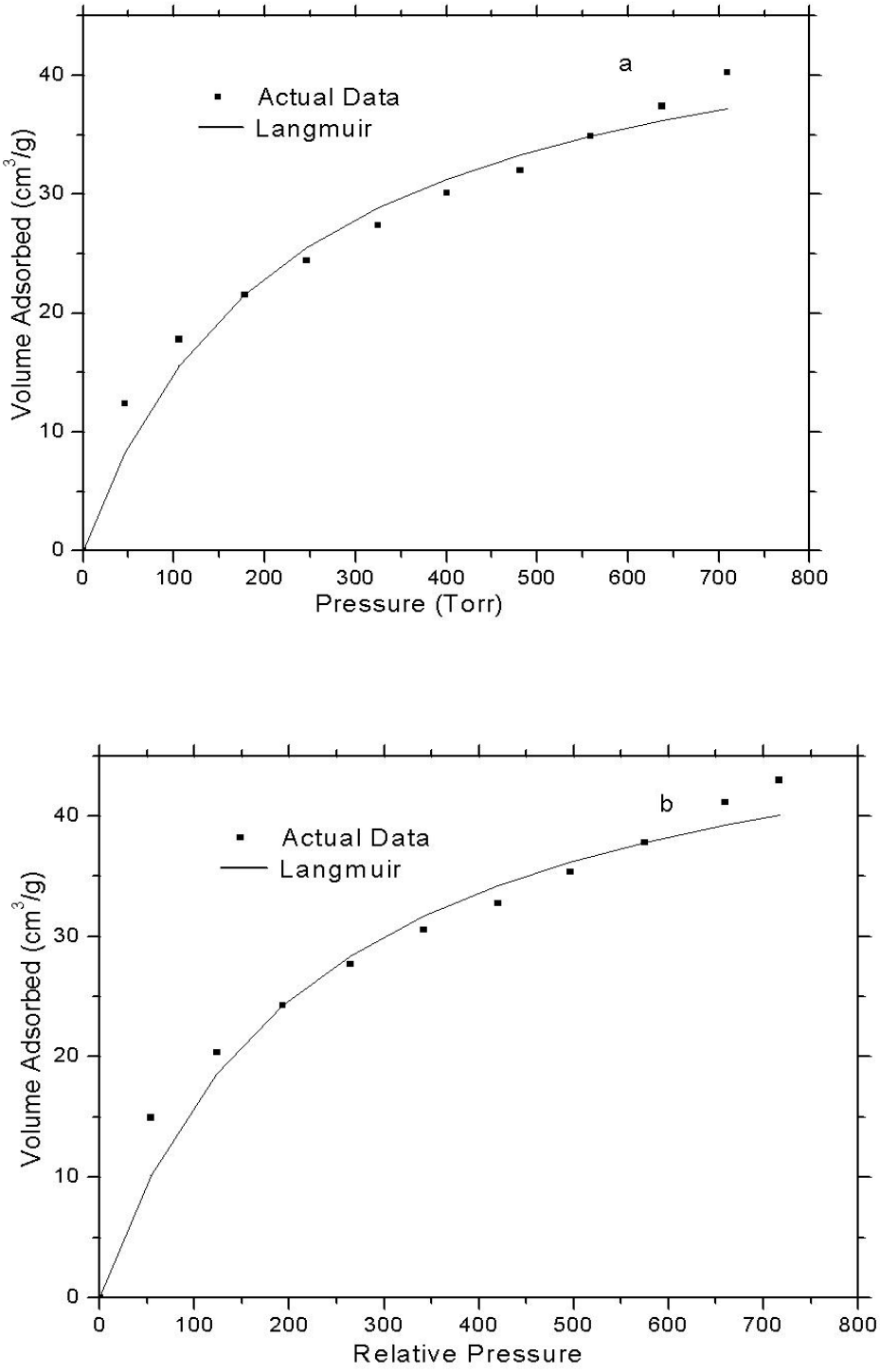

Figure 3.21: Experimental data and Langmuir fitting of CH_3Cl adsorption of a) CDICS 4 (12) and b) CD ICS 6(14) at room temperature.

Table 3.4 below shows the value of calculated fitting parameters for CH_3Cl adsorption of CD ICS 4(12) and CD ICS 6(14) fitted by Langmuir, BET and Freundlich model of gas adsorption. The goodness of the fit was assessed by evaluating the sums of square of residuals (SSR).

$$\text{SSR} = \sum_{i=1}^{N} (X_{i,\text{experimental}} - X_{i,calculated})^2 \text{.....} \quad (3.1)$$

where X_i represents data points at various pressure and volume co-ordinates for N data points.

Table 3.4: Calculated Fitting Parameters for CH_3Cl adsorption at room temperature.

Adsorption Isotherm	**Value of fitting parameter for CD ICS 4(12)**		**Value of fitting parameter for CD ICS 6(14)**	
Langmuir $\frac{P}{V} = \frac{P}{V_u} + \frac{1}{bV_u}$	V_u = 49.16 cm^3/g	b = 0.004 g/cm^3	V_u = 52.73 cm^3/g	b = 0.004 g/cm^3
BET $\frac{P}{V(P_0 - P)} = \frac{1}{V_u C} + \left(\frac{C-1}{V_u C}\right)\left(\frac{P}{P_0}\right)$	V_u = 8.04 cm^3/g	C = -3.61	V_u = 7.58 cm^3/g	C = -2.26
Freundlich $\ln V = \ln k_f + \frac{1}{n} \ln P$	n = 2.37	k = 2.41	n = 2.48	k = 2.92

V is the adsorbed volume of gas (cm^3/g of adsorbent) at pressure (P)

P_0 is saturation vapor pressure of the gas

V_u is volume of the monolayer (cm^3/g of adsorbent)

b is Langmuir constant characteristic of the system under study

C is the BET constant

n and k_f are the Freundlich constants

Deviation from the Langmuir isotherm occurs when its assumptions (monolayer coverage, non-interaction of species on the surface, equivalent surface sites) break down. Since the isotherms deviate from the Langmuir model, it is obvious that the adsorption process is not monolayer.

Since the BET and Freundlich models gave the best fit among the various models studied. Hence the nature of the adsorption can be interpreted as that of multi-layer adsorption. The negative value of *C* for BET constant is indicative of microporosity. The value of V_u determined from Langmuir fitting and that of BET fitting are different. A possible explanation for this could be due to the fact that BET isotherm often underestimates the amount of adsorption at low pressure and overestimates it at higher pressure values. As a result, the surface area values calculated from the BET isotherm are generally lower than the experimental values from nitrogen porosimetry. But the value calculated from Langmuir isotherm corresponds closely to the experimental value from nitrogen porosimetry.

Table 3.5: Calculation of the Surface Area for CH_3Cl sorption isotherm at room temperature.

Surface Area	**CD ICS 4(12) (m^2/g)**	**CD ICS 6(14) (m^2/g)**
Calculated from Langmuir isotherm	521	560
Calculated from BET isotherm	85	81
Experimental value from N_2 adsorption[a]	504	591

[a] BET surface area value obtained from Nitrogen porosimetry at 77 K

The BET surface area calculated from CH_3Cl adsorption is lower than the BET surface area value obtained from Micromeritics data (see Table 3.5). This difference in surface area can be attributed to the difference of adsorbate gas

(CH_3Cl and N_2) and also the difference in the temperature at which the experiments were performed. The adsorption of CH_3Cl occurs at room temperature; however, the adsorption of N_2 occurs at 77 K. The anticipated number of multilayers formed in case of CH_3Cl adsorption is much less than that formed in case of N_2 adsorption. Moreover, N_2 is a smaller molecule than CH_3Cl and the shape of the N_2 molecule is linear, whereas for CH_3Cl it is a pyramidal molecule. As a result the BET surface area value calculated from CH_3Cl adsorption is lower than that obtained from N_2 adsorption and may be attributed to the difference in micropore filling of each respective gas because of the Kelvin effect.

3.3.2. p-Nitrophenol Adsorption (Solid-Solution Adsorption)

The sorption isotherms in aqueous solution were determined from equilibrium adsorption of p-nitrophenol using UV-Vis spectrophotometry. The results were evaluated using the Langmuir, Freundlich and B.E.T. models of adsorption.

Figures 3.22 to Figure 3.26 show the fitting of the adsorption isotherms obtained for CD ICS 2 (12), CD ICS 4 (12), CD ICS 6 (12), CD ICS 6 (14) and CD ICS 6(16).

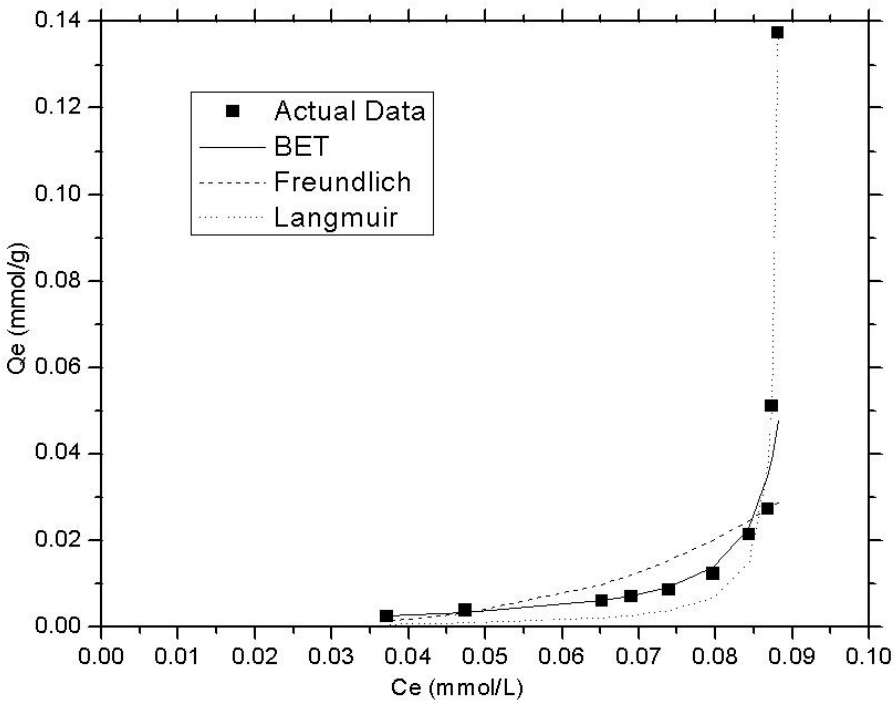

Figure 3.22: Experimental data and fitting of sorption isotherms CD ICS 2(12) using p-nitrophenol at pH 5.0 in 0.1 M CH_3COOH/CH_3COONa buffer.

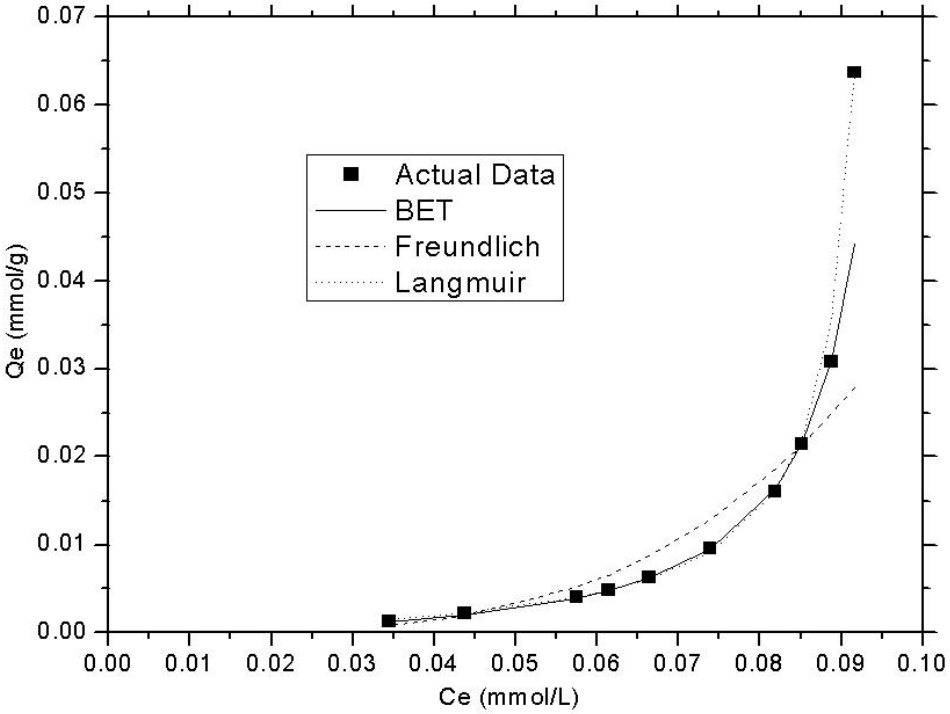

Figure 3.23: Experimental data and fitting of sorption isotherms CD ICS 4(12) using p-nitrophenol at pH 5.0 in 0.1 M CH_3COOH/CH_3COONa buffer.

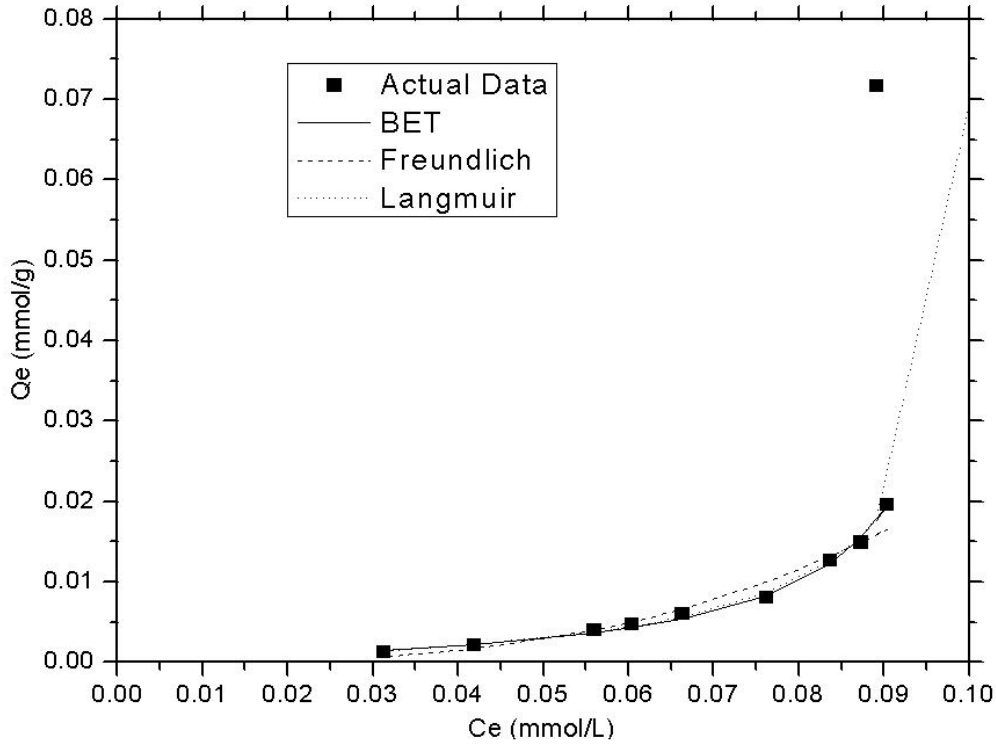

Figure 3.24: Experimental data and fitting of sorption isotherms CD ICS 6(12) using p-nitrophenol at pH 5.0 in 0.1 M CH_3COOH/CH_3COONa buffer.

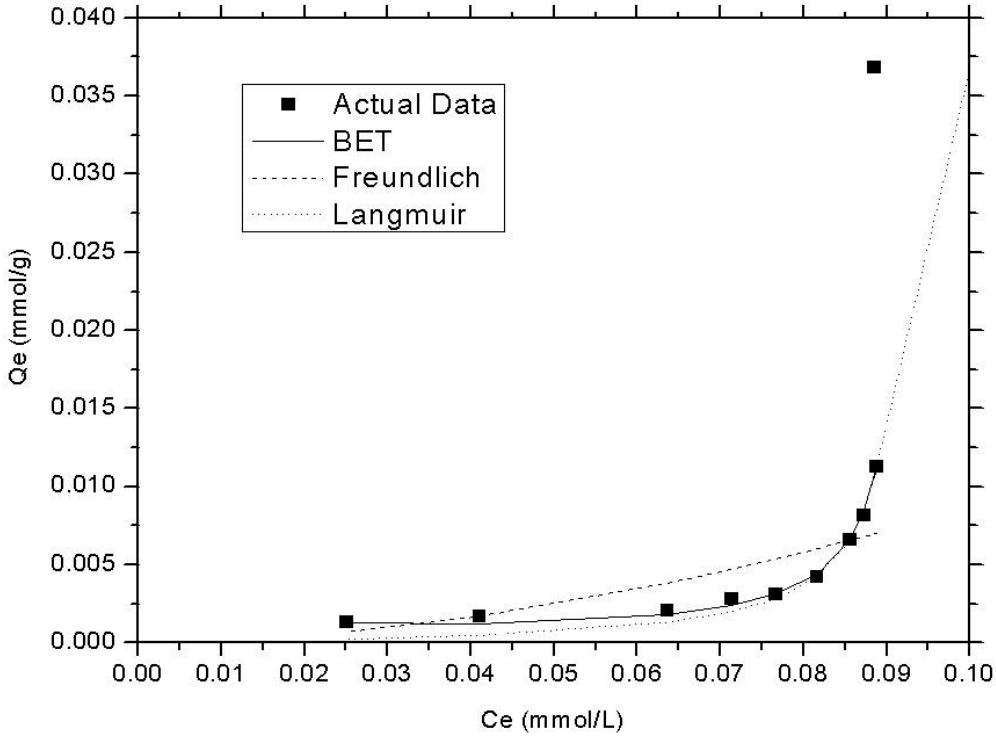

Figure 3.25: Experimental data and fitting of sorption isotherms CD ICS 6(14) using p-nitrophenol at pH 5.0 in 0.1 M CH_3COOH/CH_3COONa buffer.

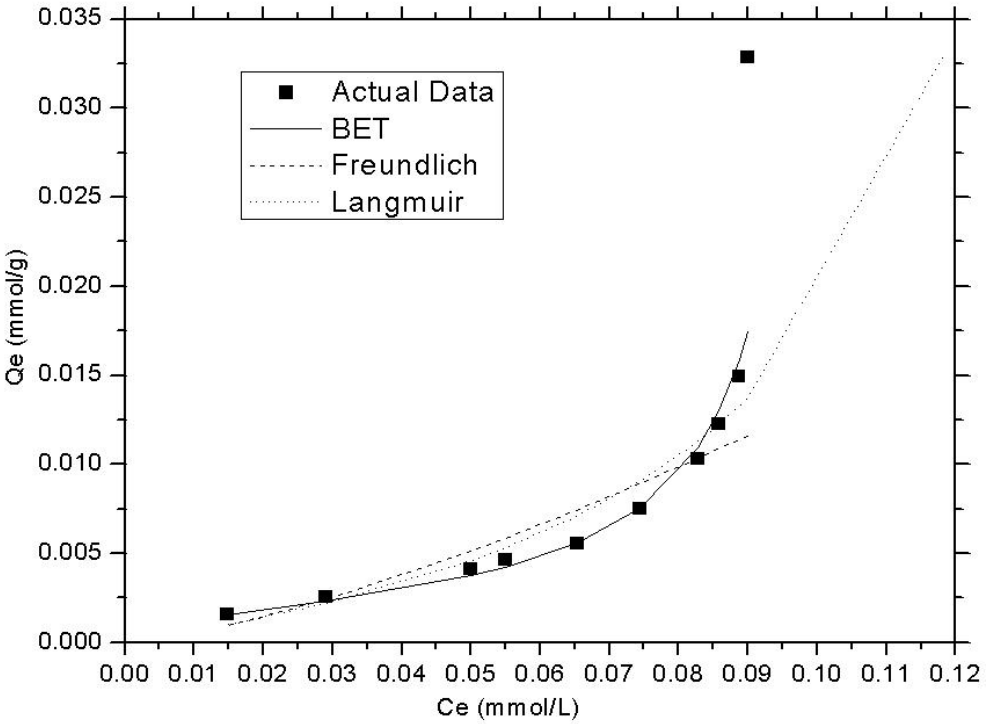

Figure 3.26: Experimental data and fitting of sorption isotherms CD ICS 6(16) using p-nitrophenol at pH 5.0 in 0.1 M CH_3COOH/CH_3COONa buffer.

Among the various models, the BET model gave the best fit for all CD ICS materials, the nature of the adsorption can be interpreted as that of multilayer adsorption. For higher Q_e values (i.e. for lower mass of adsorbent), the error is greater. On the other hand, error is lower for smaller Q_e values (i. e. for higher mass of adsorbent). Adsorption is more prominent in the region of higher mass of adsorbent. Consequently, the adsorption isotherm models generally fit better for lower Q_e values i.e. the region in which maximum adsorption occurs and vice versa for higher Q_e values. As a result, in most of the isotherms the uppermost points i.e. the value with highest Q_e does not fit with any isotherm model (see Figures 3.23 to 3.26).

Figure 3.27 shows a comparison of adsorption capacity for materials synthesized using same surfactant but with different CD loading.

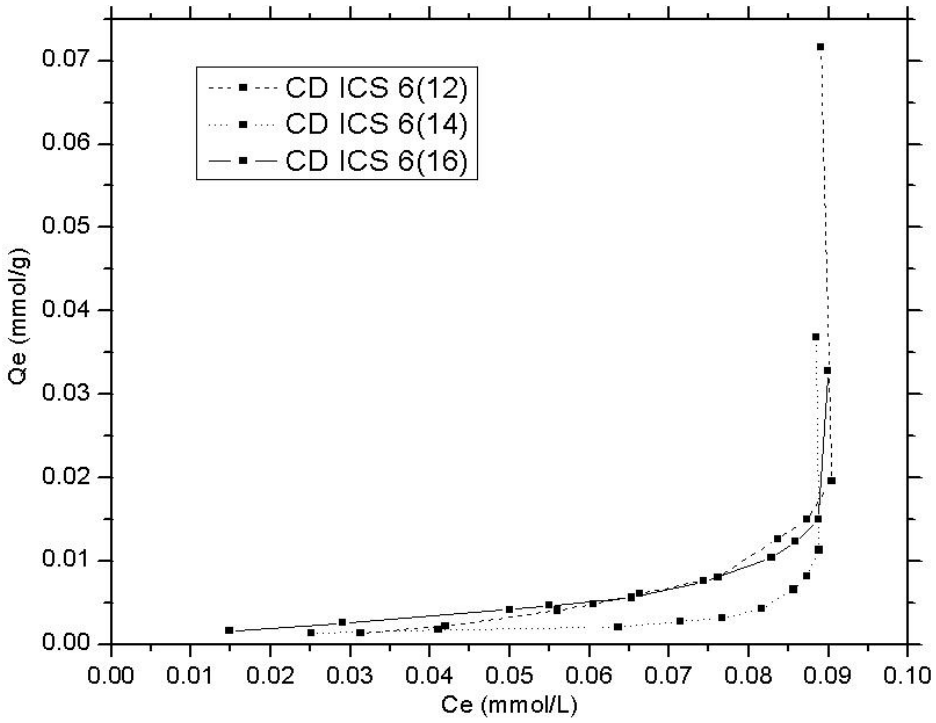

Figure 3.27: Comparison of adsorption capacity of CD ICS 2(12), CD ICS 4(12) and CD ICS 6(12) for sorption of p-nitrophenol at room temperature.

With an increase of CD loading, the value of C_e the equilibrium concentration of p-nitrophenol decreases accordingly. When pristine HMS silica was treated with p-nitrophenol, no p-nitrophenol adsorption was observed. Similar observations were found by Mercier *et al.*[60] for CD HMS materials due to an adsorption process solely driven by the non-covalent interactions of the guest p-nitrophenol and host adsorbent. Therefore the observed sorption can be attributed to cyclodextrin inclusion of p-nitrophenol.

With an increase of CD loading, the adsorption of p-nitrophenol increases, as observed for an increase in adsorption for CD ICS 6(12) in comparison to CD ICS 2(12). Although the increase is not very high, the reason is that for CD ICS materials prepared by same surfactant, the pore volume and surface area

decrease despite the increase in CD loading. Such changes in surface properties are reflected in the sorption property of the materials synthesized with same SDA. As the surface area and pore volume decreases, the degree of sorption decreases. This is understood in terms of the steric restriction of p-nitrophenol molecules in accessing the CD molecules located deep inside the silica mesostructure.

An increase of the alkyl chain length of SDA provides larger mesostructures with higher surface area and pore volume characteristics. The result is a remarkable increase in sorption capacity for system with different alkyl chain length of SDA with the same CD loading, as shown below (see Figure 3.28). For a given value of C_e, the equilibrium concentration of p-nitrophenol decreases from 3×10^{-2} mmol/L for CD ICS 6(12) to 5×10^{-3} mmol/L for CD ICS 6(16).

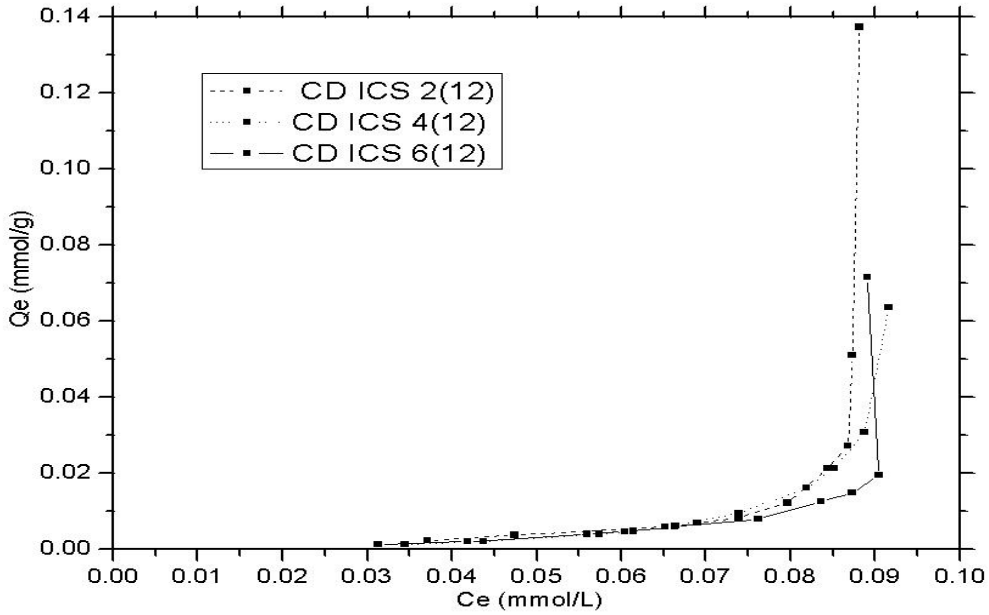

Figure 3.28: Comparison of experimental adsorption capacity of CD ICS 6(12), CD ICS 6(14) and CD ICS 6(16) for sorption of p-nitrophenol at room temperature.

Among all the nine CD ICS materials, the CD ICS 6(16) is the material which has both highest CD loading and highest surface area and pore volume. So, it gives the maximum sorption.

Distribution coefficients

The distribution coefficient K_d is defined as follows

$$K_d = \frac{(C_i - C_f)V_{sol}}{C_f m_{ads}}) \ldots\ldots\ldots\ldots\ldots\ldots\ldots\ldots\ldots\ldots (3.2)$$

C_i is initial concentration of p-nitrophenol in solution (mmol)

C_f is final concentration of p-nitrophenol after adsorption (mmol)

V_{sol} is the volume of solution (mL)

m_{ads} is the amount of adsorbent used (g).

The value of log K_d against the mass of adsorbent was plotted. With increase of mass of adsorbent the value of logK_d decreases in a monotonic fashion (see Figure 3.29).

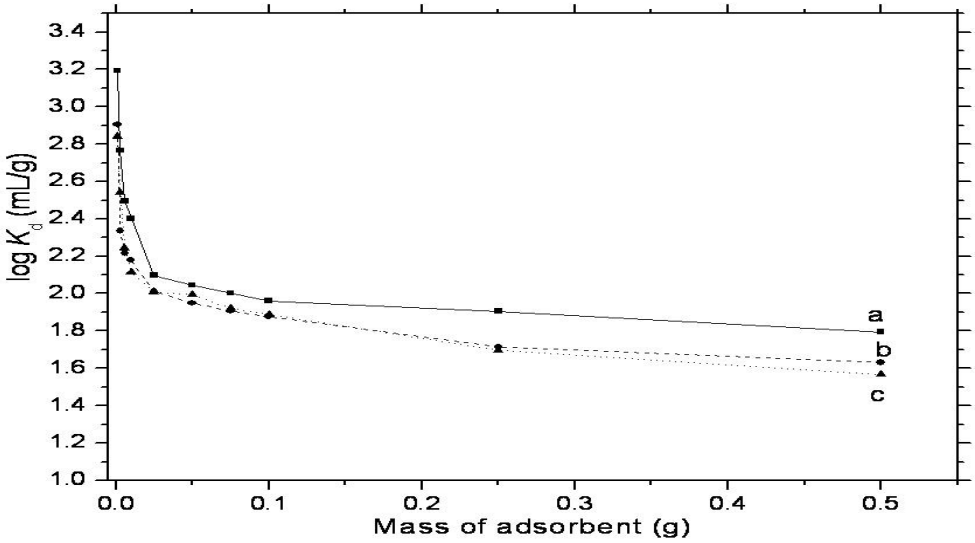

Figure 3.29: Plot of log K_d vs. Mass of adsorbent for a) CD ICS 2(12) b) CD ICS 4(12) and c) CD ICS 6(12) for sorption of p-nitrophenol at room temperature.

.

This type of adsorption behavior is typical for materials that have appreciable binding interactions with targeted guest compounds because adsorbents with specific binding sites are most effective for binding when these sites are largely unoccupied by the adsorbate. As the number of available sites become occupied, the binding affinity of the material decreases, in accordance with the predictions according to the Langmuir equilibria. Similar observation were reported by others.[95, 96]

Kinetics of adsorption

Kinetic adsorption of p-nitrophenol with CD ICS at room temperature yielded the following plot (see Figure 3.30).

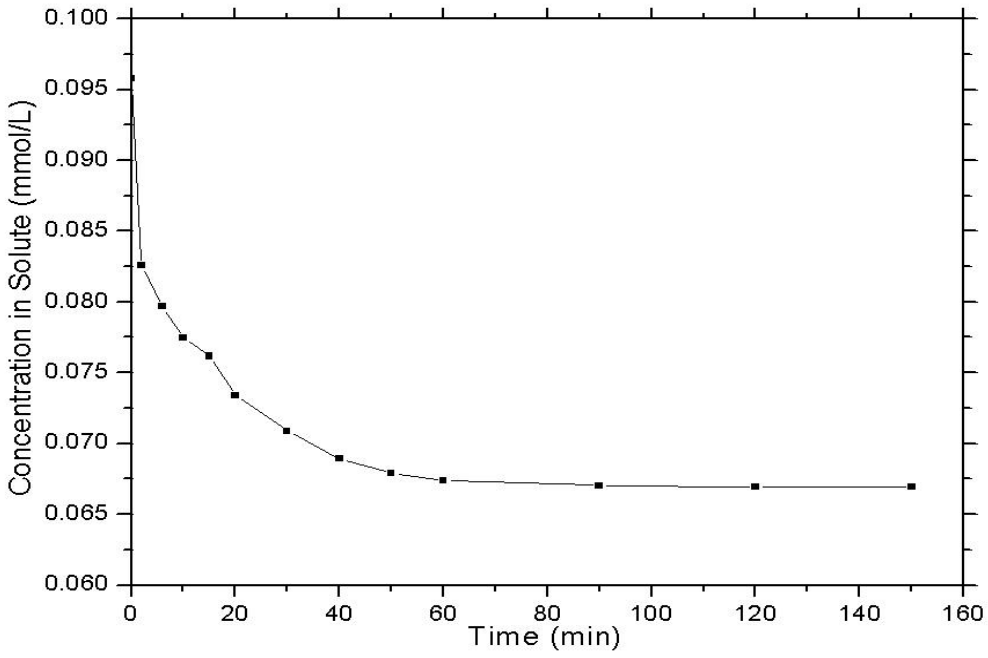

Figure 3.30: Kinetic sorption isotherm of CD ICS 6(16) with p-nitrophenol at pH 5.0 in 0.1 M CH_3COOH/CH_3COONa buffer obtained at room temperature.

The uptake of p-nitrophenol by CD ICS is relatively rapid reaches the maximum adsorption capacity near a 60 min of exposure time. The fast adsorptivity exhibited by CD ICS can be attributed to the open framework nature of the mesoporous adsorbents, resulting in greatly improved access of the targeted adsorbate molecules to the cyclodextrin binding sites.

Figure 3.31 shows the fitting of the kinetic data where ln (X_e – X) versus time was plotted. X_e refers to the amount of adsorbate adsorbed within the sorbent material after reaching equilibrium, while X is the amount of adsorbate adsorbed at any particular time (t). The resulting adsorption rate constant is 5.9×10^{-2} min^{-1}.

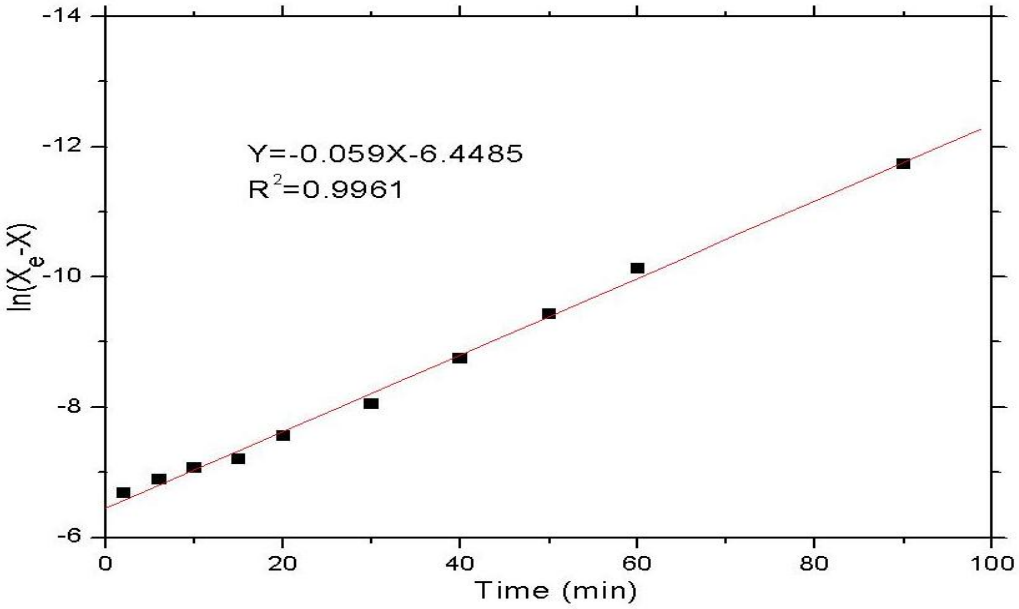

Figure 3.31: Linearized fitting of CD ICS 6(16) with first order kinetic model for data obtained at room temperature as described in Figure 3.30.

The fitting of experimental data with first order kinetic model indicates that the adsorption of p-nitrophenol is governed by the concentration of p-nitrophenol only. For such process the rate expression is given by equation (3.3),

$$Rate = -\left(\frac{\partial[pNP]}{dt}\right) = k_{obs}[pNP]..... .....(3.3)$$

where k_{obs} is rate constant and $[pNP]$ is the concentration of *p*-nitrophenol in the solution at any time (*t*).

The integrated form of the above equation is as follows

$$\ln[pNP] = \ln[pNP]_0 - k_{obs}t..... .....(3.4)$$

$$\ln[X_e - X] = \ln[X]_0 - k_{obs}t..... .....(3.5)$$

where $[X_e - X]$ is the concentration of p-nitrophenol at any time (*t*), $[X_e]$ is the concentration of p-nitrophenol after reaching equilibrium, $[X]_0$ is the initial concentration of p-nitrophenol before adsorption.

Consequently, a plot of *t* vs. $\ln[X_e - X]$ will give a straight line, where, the slope k_{obs} denotes the observed rate constant.

Mercier *et al.*[60] incorporated CD within the mesoporous framework by using the following triethoxysilane linker APS β-CD with dodecylamine surfactant.

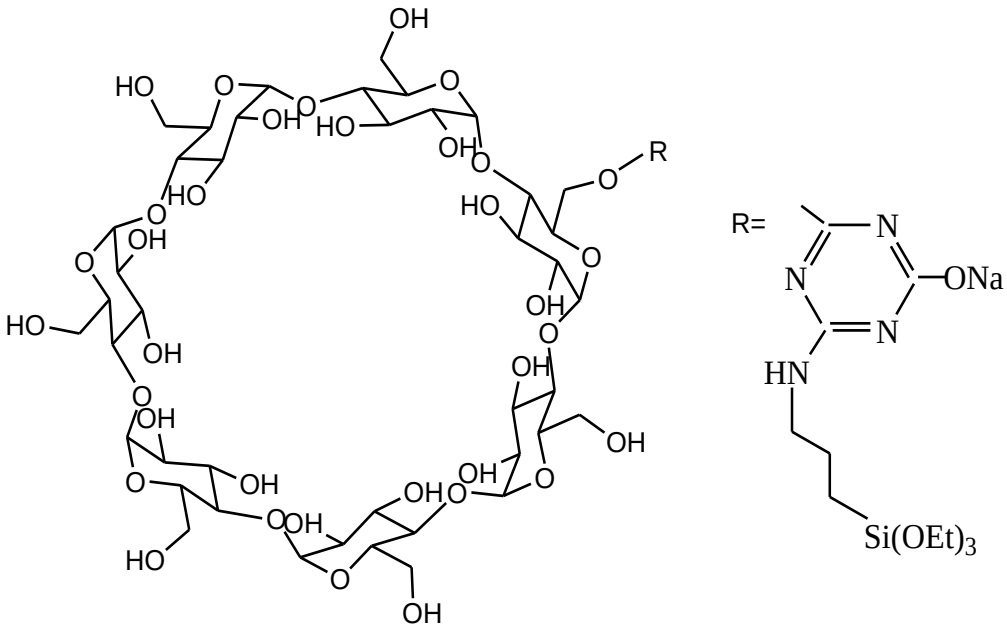

APS β–CD

Figure 3.32: APS β-CD reported by Mercier *et al.*[60]

In this study, we have used the ICL linker because the materials described by Mercier (see Figure 3.32) were found to be unstable in aqueous solution. The CD ICL precursor outlined in Figure 3.33 was utilized because the urethane bond linker and β-cyclodextrin was anticipated to withstand hydrolysis and have greater stability.

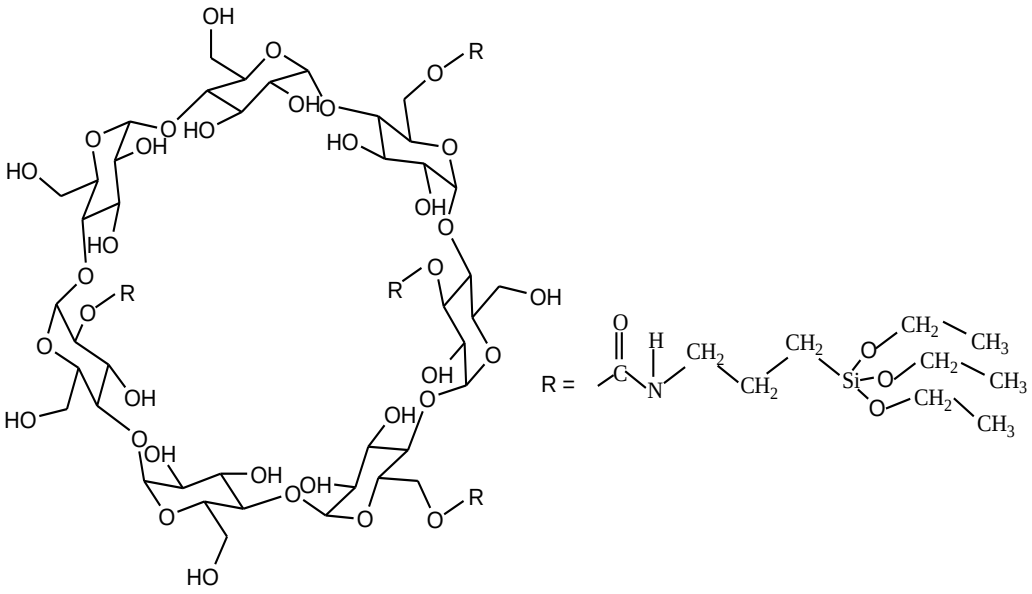

Figure 3.33: Molecular structure of CD ICL, the silica precursor used in the co-condensation with TEOS to form hybrid silica materials with grafted β-cyclodextrin.

We have independently synthesized CD HMS materials and confirmed Mercier's results. However, the CD HMS materials do not have favorable sorption properties as previously reported in aqueous solution because of hydrolysis of MCT linker. APS β-CD was used for synthesis of CD HMS. 3-aminopropyltriethoxysilane (APS) part of the molecule of APS β-CD interacts with p-nitrophenol[97] via hydrogen bonding and results in shifts of the λ_{max} as shown by the following UV-Visible spectra (Figure 3.34).

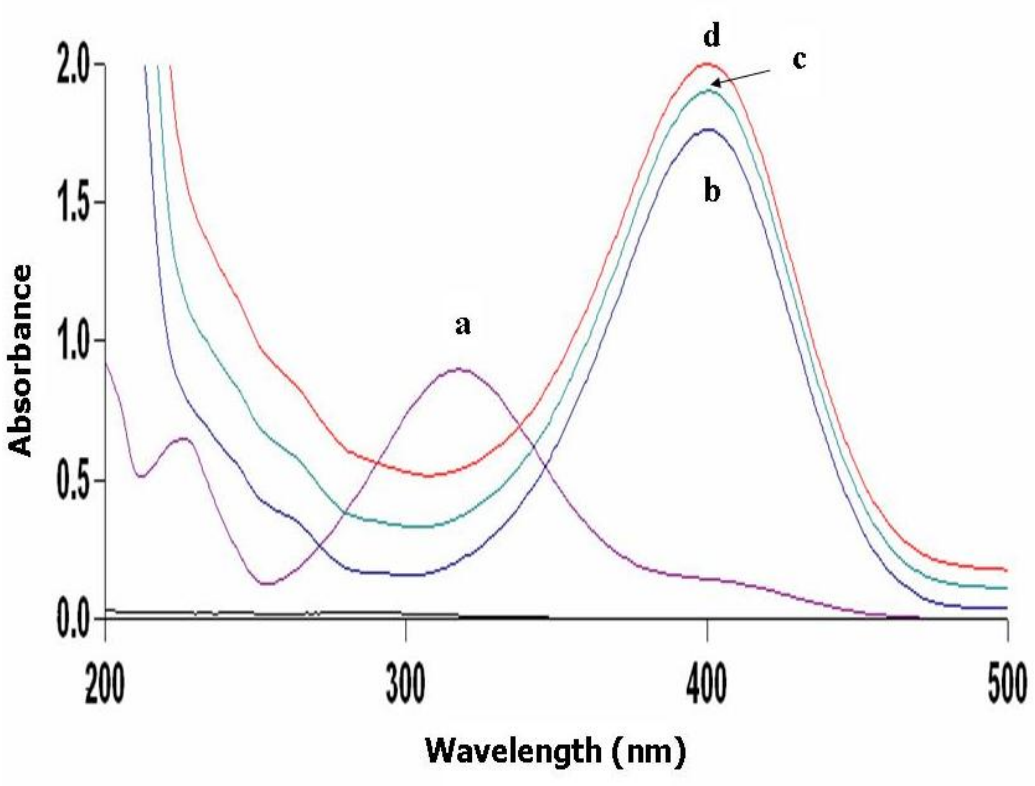

Figure 3.34: UV-Visible spectra showing the effect of APS on p-nitrophenol. a) 10^{-4} M neutral p-nitrophenol without APS, b) 100 µL (~ 100 mg) APS with 10 ml 10^{-4} M p-nitrophenol, c) 200 µL (~ 200 mg) APS with 10 ml 10^{-4} M p-nitrophenol, and d) 300 µL (~ 300 mg) APS with 10 ml 10^{-4} M p-nitrophenol.

As the content of APS increases, the peak at 400 nm for basic p-nitrophenol increases in intensity. The λ_{max} at 400 nm is typically observed for p-nitrophenol at elevated pH values, when it is in its ionized form. The appearance of the ionized form of the p-nitrophenol was prevented by carrying out the sorption experiments in aqueous solutions buffered at reduced pH = 7.45.

The result was also supported by IR spectroscopy. IR spectra of CD HMS were taken before and after adsorption of p-nitrophenol from aqueous solution. After the adsorption of p-nitrophenol, IR bands around 1600 cm^{-1} due to C=N stretching frequency and 1512 cm^{-1} due to C-C aromatic skeletal vibration of cyanuric chloride from APS β-CD are lost with concomitant increase of the

vibrational band around 1080 cm^{-1} due to Si-O-Si stretching from silica network (see Figure 3.35).

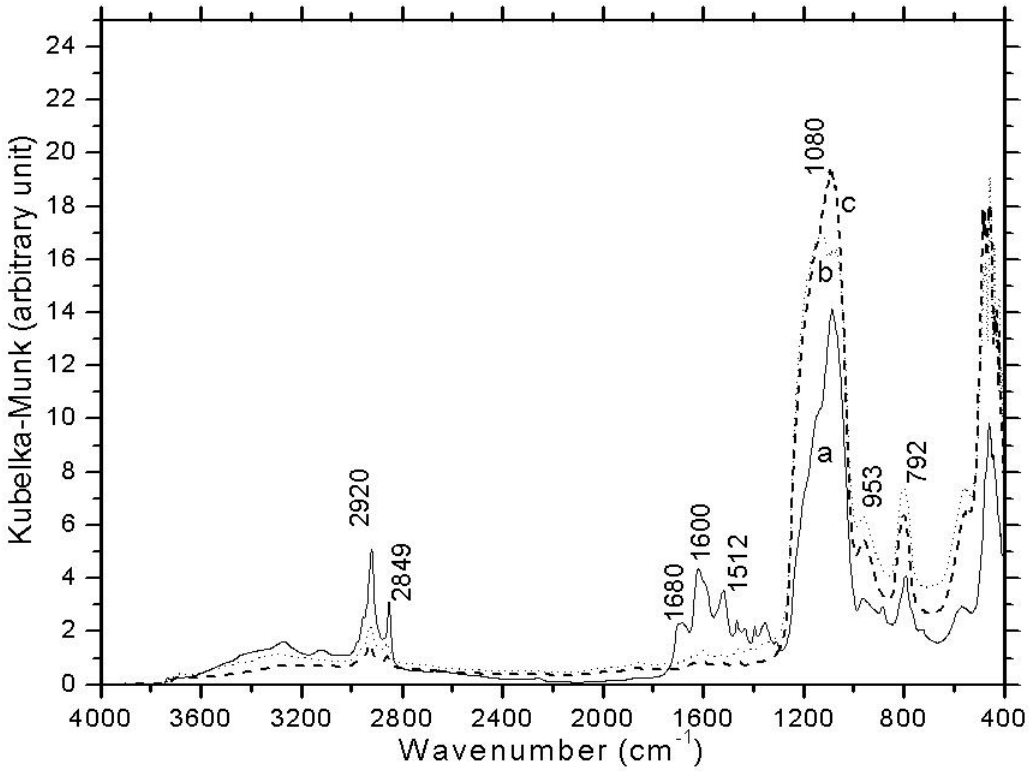

Figure 3.35: IR spectra of CD HMS a) before adsorption of p-nitrophenol b) after adsorption of p-nitrophenol in millipore water c) after adsorption of p-nitrophenol at pH 7.45 in 0.1 M KH_2PO_4/NaOH buffer at room temperature.

Table 3.6 shows the comparison of surface properties of CD HMS materials synthesized by Mercier *et al.*[60] with an equivalent amount of CD ICS (12) materials synthesized using dodecylamine as SDA.

Table 3.6: Comparison of Surface Properties of CD ICS Materials with CD HMS materials as obtained from nitrogen porosimetry

Material	BET Surface Area (m^2/g)	Pore Volume (cm^3/g)
CD ICS 2(12)	630.3	0.67
CD HMS 2%[a]	547.0	0.51
CD ICS 4(12)	504.3	0.51
CD HMS 4%[a]	319.0	0.26
CD ICS 6(12)	307.0	0.21
CD HMS 6%[a]	197.0	0.21

[a] From Reference 60

CD ICS materials have greater surface area and pore volume compared to CD HMS materials. The reason for superior surface properties of CD ICS is due to use of different linker, i.e. CD ICL, and is smaller than the bulky linker APS β-CD used by Mercier *et al.*[60]

One of the prime objectives of this research was to synthesize a mesoporous material with higher CD loading, but also possessing a greater surface area and pore volume. By increasing the alkyl chain length of the SDA, these objectives have been met in this research. Table 3.7 shows the variation of the length of alkyl chain length of SDA considerably changes the surface properties.

Table 3.7: Variation of Surface Properties with change of surfactant.

Material	BET Surface Area (m^2/g)	Pore Volume (cm^3/g)
CD HMS 6%[a]	197.0	0.21
CD ICS 6(12)	307.0	0.21
CD ICS 6(14)	591.8	0.42
CD ICS 6(16)	656.8	0.47

[a] From Reference 60

CD ICS and CD HMS materials show comparable sorption from the gas phase. Figure 3.36 below shows the CH_3Cl sorption isotherm of CD ICS and CD HMS materials.

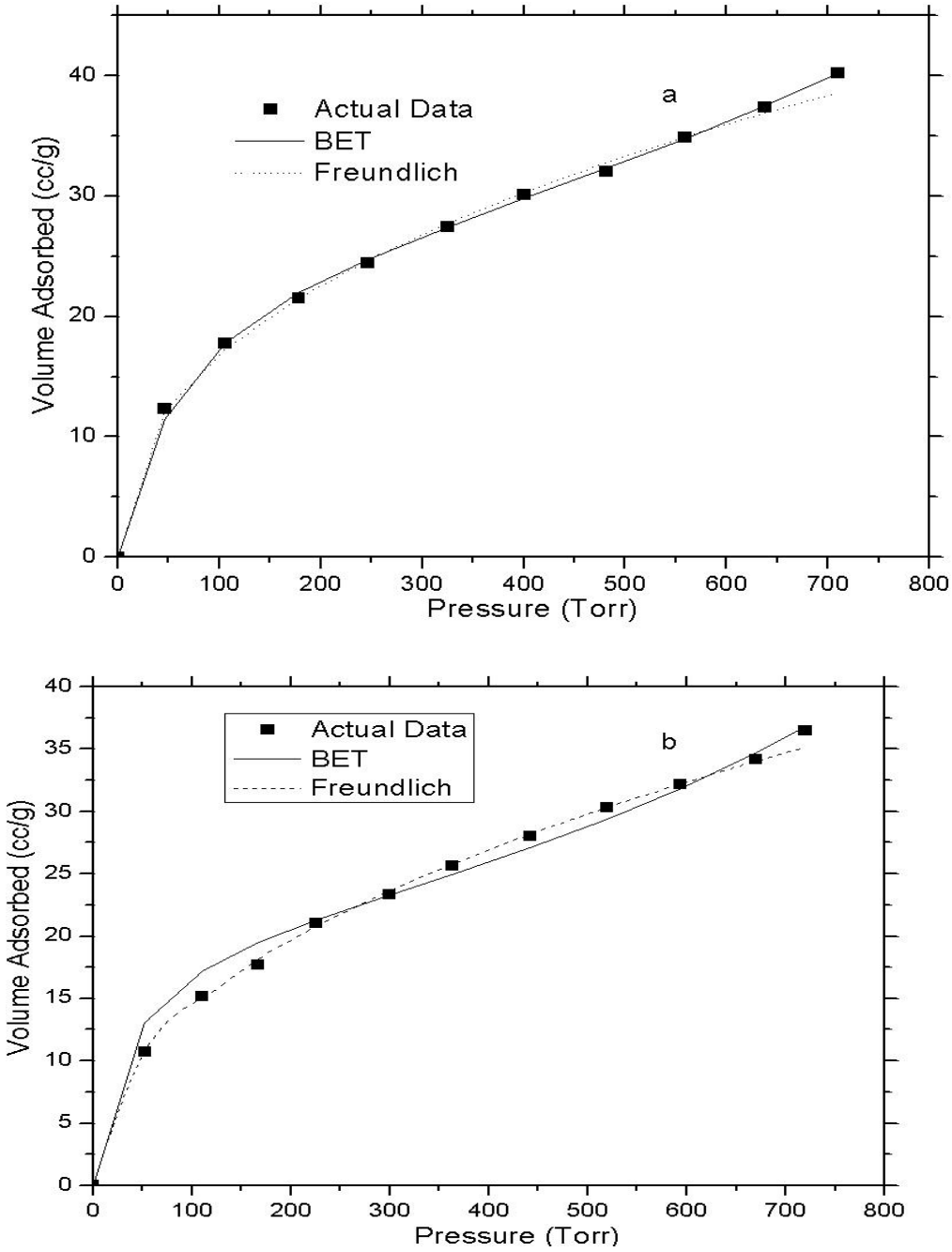

Figure 3.36: Comparison of CH_3Cl sorption of a) CD ICS with b) CD HMS at ambient temperature. The poor fits are not shown because they do not have a suitable sum of square of residuals.

CD ICS materials show superior sorption affinity towards p-nitrophenol than the CD HMS materials. Table below is showing the comparison of sorption of p-nitrophenol from solution for CD ICS and CD HMS materials.

Table 3.8: Comparison of p-nitrophenol sorption of CD ICS with CD HMS obtained at room temperature.

Material (500 mg)	**Adsorption capacity (mmol/g)**	**p-nitrophenol adsorbed (mol%)**
CD ICS 2	5.7×10^{-3}	61%
CD HMS 2%[a]	3.3×10^{-3}	Not reported
CD ICS 4	6.2×10^{-3}	65%
CD HMS 4%[a]	2.1×10^{-3}	Not reported
CD ICS 6	6.5×10^{-3}	68%
CD HMS 6% [a]	3.4×10^{-3}	Not reported
CD ICS 6(14)	6.6×10^{-3}	73%
CD ICS 6(16)	7.6×10^{-3}	84%

[a] From reference 60

$C_0 = 10.0 \times 10^{-2}$ mmol/L.

CHAPTER 4
CONCLUSIONS AND FUTURE WORK
4.1 Conclusions

Composite mesoporous silica materials containing microporous β-cyclodextrin were prepared by covalently grafting β-CD to the walls of the mesoporous silica channels. The materials were synthesized by a sol-gel process that utilized three different neutral surfactants with variable alkyl chain length (dodecylamine, tetradecylamine and hexadecylamine). β-cyclodextrin functionalized mesoporous silica (CD ICS) materials were synthesized by co-condensation of a β-CD functionalized triethoxysilane (CD ICL) with TEOS in the presence of a structure directing agent (SDA) or surfactant and a pore expander (TMB). In total, nine CD ICS materials were synthesized by varying the molar percentage of β-CD incorporation with respect to TEOS at 2%, 4% and 6% of β-CD.

CD ICL was prepared by reacting β-CD with 3-isocyanatopropyl triethoxy silane (ICL) at 70^0C in dry pyridine. The identity of the product CD ICL was confirmed by IR spectroscopy due to the complete disappearance of the isocyanato group at 2270 cm^{-1}. According to the ^{1}H NMR results of CD ICL, four isocyanate linkers were covalently attached to one molecule of β-CD at random positions 2-, 3-, or 6- hydroxyl groups of the β-cyclodextrin macrocycle.

The incorporation of β-cyclodextrin within the mesoporous framework was supported by IR, Raman, MALDI TOF MS and solid state ^{13}C NMR CP MAS results. The IR spectra of CD ICS showed vibrational bands at 1050-1150 cm^{-1}, and are characteristic of siloxane condensation. The bands observed in the IR spectra of CD ICL overlapped with the characteristic bands of CD ICS thereby showing successful incorporation of β-cyclodextrin within the mesostructure framework. The Raman spectra showed characteristic peaks at 3650-3000 cm^{-1} and 3000-2800 cm^{-1} which are attributed to O-H and C-H stretching, respectively. Incorporation of β-cyclodextrin within the mesostructure was also supported by MALDI TOF mass spectrometry results from the two peaks at m/z 1157 a.m.u. and 1173 a.m.u. values due to $[\beta\text{-CD} + Na]^+$ and $[\beta\text{-CD} + K]^+$, respectively. The mass spectrometry results provide direct evidence of the desorption of covalently bound β-CD from the mesoporous framework. The solid state ^{13}C NMR CP MAS results showed ^{13}C NMR peaks in the region δ = 60-110 ppm due to the ^{13}C nuclei of β-cyclodextrin. The higher field ^{13}C NMR signals $\delta < 60$ ppm were attributed to those of the ICL linker and provide further support for covalent immobilization of β-CD onto the silica framework. Additional peaks at 14, 126 and 130 ppm were due to TMB (pore expander), indicating incomplete removal of the pore expander because of occlusion within the framework during the sol-gel synthesis.

Small angle X-ray diffraction patterns of the CD ICS materials showed a large intensity and sharp low angle diffraction peak at $2\theta \approx 2.2^0$, corresponding to the presence of an ordered silica mesostructure framework. TGA of the

surfactant containing CD ICS materials showed a weight loss in the region 100^0C to 200^0C, which is attributed to loss of physisorbed surfactant and the pore expander. The differential thermograms revealed that the decomposition temperature of the cyclodextrin in the composite silica CD ICS materials (324^0C) was higher than the melting point of native β-CD (280^0C), providing additional evidence of successful covalent attachment of β-cyclodextrin onto the silica network.

Nitrogen adsorption-desorption isotherms showed that an increase in alkyl chain length of the surfactants resulted in larger mesostructures with greater surface areas and pore volumes. CD ICS materials were found to be effective as sorbents for adsorbates in the gas (CH_3Cl) and aqueous (p-nitrophenol) phases respectively. BET and Freundlich models gave the best fits for adsorption of CH_3Cl gas. Sorption isotherms of p-nitrophenol from aqueous solution conformed to the BET model. The results suggest that the adsorption of CH_3Cl and p-nitrophenol in CD ICS materials adopts a multilayer adsorption profile.

The composite materials (CD ICS) will contribute positively to industrial applications related to sorption phenomena and chemical separations involving the remediation of water and other aqueous phases containing organic compounds, namely, p-nitrophenol. They will also be effective in the removal of gas phase adsorbates or volatile organic compounds (e.g. CH_3Cl).

4.2 Future Work

Future research in the area of composite silica mesoporous materials could be addressed in the three specific areas: synthesis, characterization and sorption studies.

A major drawback of the synthesis of CD ICS materials described in this thesis is the incomplete removal of the pore expander (TMB). Synthesis of CD ICS may be done without a pore expander by careful selection of the appropriate SDA. Instead of neutral amine surfactant, alternative structure directing agents, such as, quaternary ammonium surfactants,[98-100] anionic surfactants,[101-104] nonionic triblock copolymers[105-108] may be employed. Alternative supramolecular compounds, such as, crown ethers, [109] or calixarenes[65, 110] or cyclams[111] hosts may be attached to the silica framework instead of cyclodextrins. Calixarenes or cyclams covalently bound to the silica network will be effective for the extraction of metal ions from aqueous solution.[112]

Further characterization of CD ICS materials can be addressed by using solid state ^{29}Si NMR MAS spectroscopy. In order to explore the morphology of CD ICS materials, in further details, polarization dependence studies using micro-Raman spectroscopy may be employed[113] These structural studies will provide information about the silica framework and the nature of the attachment of macrocycles to the surface of the mesoporous network.

The sorption properties of CD ICS materials may be investigated using other aqueous contaminants, for example, dibenzofuran, naphthenic acids and other types of PAH's. Variable temperature sorption studies can be performed in

order to exploit the effectiveness of sorption of the CD ICS materials at these conditions to further understand the thermodynamics of the sorption process. The kinetics of sorption can be obtained by studying the time dependence of sorption phenomena to further understand the mechanism of sorption of such composite mesoporous materials.

REFERENCES

1. Sing, K. S. W.; Everett, D. H.; Haul, R. A. W.; Moscou, L.; Pierotti, R. A.; Rouquerol J.; Siemieniewska, T. *Pure & Appl. Chem*, **1985**, *57*, 603-619.
2. Meier, W. M.; Olson, D. H.; Baerlocher, Ch. *Zeolites*, **1996**, *17*, 1-230.
3. Ying, J. Y.; Mehnert, C. P.; Wong, M. S. *Angew. Chem. Int. Ed.*, **1999**, *38*, 56-77.
4. Beck, J. S.; Vartuli, J. C.; Roth, W. J.; Leonowicz, M. E.; Kresge, C. T.; Schmitt, K. D.; Chu, C. T. W.; Olson, D. H.; Sheppard, E. W.; McCullen, S. B.; Higgins, J. B.; Schlenker, J. L. *J. Am. Chem. Soc.*, **1992**, *114*, 10834-10843.
5. Hatton, B.; Landskron, K.; Whitnall, W.; Perovic, D.; Ozin, G. A. *Acc. Chem. Res.*, **2005**, *38*, 305-312.
6. Schmidt, H. *J. Non-Cryst. Solids*, **1985**, *73*, 681-691.
7. Lim, M. H.; Blanford C. F.; Stein, A. *Chem. Mater.* **1998**, *10*, 467-470.
8. Lim, M. H.; Stein A., *Chem. Mater.* **1999**, *11*, 3285-3295.
9. Inagaki, S.; Guan, S.; Fukushima, Y.; Ohsuna, T.; Terasaki, O. *J. Am. Chem. Soc.* **1999**, *121*, 9611-9614.
10. Melda, T.; Holland, B. T.; Blanford, C. F.; Stein, A. *Chem. Mater.* **1999**, *11*, 3302-3308.
11. Asefa, T.; MacLachan, M. J.; Coombs, N.; Ozin, G. A., *Nature* **1999,** *402*, 867-871.
12. Szetjili, J. *Chem Rev*, **1998**, *98*, 1743-1753.
13. Villiers, A. *Compt. Rend.*, **1891**, *112*, 536.
14. Valle E. M. M. D. *Process Biochemistry*, **2004**, *39*, 1033-1046.
15. Crini G.; Morcellet M. *J. Sep. Sci.*, **2002**, *25*, 789-813.
16. Loftsson, T; Brewster M. E. *J Pharm Sci*, **1996**, *85*, 1017–1025.
17. Connors, K. A. *Chem. Rev.*, **1997**, *97*, 1325-1357.
18. Bertrand, G. L.; Faulkner, J. R.; Han, S. M.; Armstrong, D. W. *J. Phys. Chem.* **1989**, *93*, 6863-6867.
19. Lipkowitz, K. B. *Chem. Rev.* **1998**, *98*, 1829-1873.
20. Rajewski, R. A.; Stella, V. J. *J. Pharm. Sci*, **1996**, *85*, 1142-1169.
21. Uekama, K.; Hirayama, F.; Irie, T. *Chem. Rev.* **1998**, *98*, 2045-2076.
22. Hedges, A. R. *Chem. Rev.* **1998**, *98*, 2035-2044.
23. Breslow, R.; Dong, S. D. *Chem Rev.*, **1998**, *98*, 1997-2011.
24. Rekharsky, M. V.; Inoue, Y. *Chem Rev.*, **1998**, *98*, 1875-1917.
25. Li, S.; Purdy, W. C. *Chem Rev.*, **1992**, *92*, 1457-1470.
26. Khan, A. R.; Forgo, P.; Stine, K. J.; DSouza, V. T. *Chem Rev.*, **1998**, *98*, 1977-1996.
27. Takahashi, K. *Chem Rev.*, **1998**, *98*, 2013-2033.
28. Harata, K. *Chem Rev.*, **1998**, *98*, 1803-1827.
29. Saenger, W.; Jacob, J.; Gessler, K.; Steiner, T.; Hoffman, D.; Sanbe, H., Koizumi, K.; Smith, S. M.; Takaha, T. *Chem Rev.*, **1998**, *98*, 1787-1802.
30. Gattuso, G.; Nepogodiev, S. A.; Stoddart, J. F. *Chem Rev.*, **1998**, *98*, 1919.

31. Baciocchi, R.; Attina, M.; Lombardi, G.; Boni, M. R. *J. Chromatogr.* **2001**, *911*, 135-141.
32. Bagheri, H.; Saraji, M. *J. Chromatogr.* **2001**, *910*, 87-93.
33. Rodriguez, I.; Llompart, M. P.; Cela R. *J. Chromatogr.* **2000**, *885*, 291-304.
34. Fitzpatrick, L. J.; Dean, J. R.; Comber, M. H. I.; Harradine, K.; Evans, K. P.; Pearson, S. *J. Chromatogr.* **2000**, *873*, 287-291.
35. Ohlemeir, L. A.; Gavlick, W. K. *J. Liq. Chromatogr.* **1995**, *18*, 1833-1849.
36. Marce, R. M.; Borull, F. *J. Chromatogr.* **2000**, *885*, 273-290.
37. Delval, F.; Vebrel J.; Point, P.; Morcellet, M.; Janus, L.; Crini, G. *Polym. Recycling*, **2000**, *5*, 137-143.
38. Crini, G.; Bertini, S.; Tori, G.; Naggi, A.; Sforzini, D.; Vecchi, C.; Janus, L.; Lekchiri, Y.; Morcellet, M. *J. Appl. Polym. Sci.*, **1998**, *68*, 1973-1978.
39. Crini, G.; Janus, L.; Morcellet, M.; Tori, G.; Naggi, A.; Bertini, S.; Vecchi, C. *J. Appl. Polym. Sci.*, **1998**, *69*, 1419-1427.
40. Furton, K. G.; Jolly, E.; Pentzke, G. *J. Chromatogr.* **1993**, *642*, 33-45.
41. Belyakov, V. N.; Belyakova, L. A.; Varvarin, A. M.; Khora, O. V.; Vasilyuk, S. L.; Kazdobin, K. A.; Maltseva, T. V.; Kotvitsky, A. G.; Namor, A. F. D. *J. Coll. Interface Sci.*, **2005**, *285*, 18-26.
42. Li D. and Ma M., *CHEMTECH*, **1999**, *29*, 31-37.
43. Ma M. and Li D., *Chem. Mater.*, **1999**, *11*, 872-874.
44. Harada A., Li J. and Kamachi M., *Nature*, **1993**, *364*, 516-518.
45. Zhu X. X., Brizard F., Wen C. C. and Brown G. R., *J. Macromol. Sci. Pure Appl. Chem.*, **1997**, *A34*, 335-347.
46. Crini G., Cosentino C., Bertini S., Naggi A., Torri G., Vecchi C., Janus L. and Morcellet M., *Carbohydr. Res.*, **1998**, *308*, 37-45.
47. Zhao X. B. and He B. L., *React. Polym.*, **1994**, *24*, 9-16.
48. Sreenivasan K., *J. Appl. Polym. Sci.*, **1996**, *60*, 2245-2249.
49. Tanaka M., Yoshinaga M., Ito M. and Ueda H., *Anal. Sci.*, **1995**, *11*, 227-231.
50. Ciucanu I. and König W. A., *J. Chromatogr. A*, **1994**, *685*, 166-171.
51. Ciucanu I., *J. Chromatogr. A*, **1996**, *727*, 195-201.
52. Crini G., Morcellet M. and Torri G., *J. Chromatogr. Sci.*, **1996**, *34*, 477-484.
53. Sébille B., Guillaume M., Madjar C. V. and Thuaud N., *Chromatographia*, **1997**, *45*, 383-389.
54. Zhang L., Wong Y., Chen L., Ching C. B. and Ng S., *Tetrahedron Lett.*, **1999**, *40*, 1815-1818.
55. Phan T. N. T., Bacquet M., Laureyns J. and Morcellet M., *Phys. Chem. Chem. Phys.*, **1999**, *1*, 5189-5195.
56. Crini, G.; Lekchiri, Y.; Janus, L.; Morcellet, M.; Morin, N. *Chromatographia*, **1999**, *50*, 661-669.
57. Phan, T. N. T.; Bacquet, M.; Morcellet M. *J. Incl. Phenom.*, **2000**, *38*, 345-359.
58. Akiyama, T.; Hishiya, T.; Asanuma, H.; Komiyama, M. *J. Incl. Phenom.*, **2001**, *41*, 149-153.
59. Li, D.; Ma, M. *Filtration & Separation* **1999**, *36(10)*, 26-28.
60. Huq, R.; Mercier, L.; Kooyman P. J., *Chem. Mater.*, **2001**, *13*, 4512-4519.

61. Liu, C.; Lambert, J. B.; Fu, L. *J. Am. Chem. Soc.*, **2003**, *125*, 6452-6461.
62. Liu, C.; Lambert, J. B.; Fu L. *J. Org. Chem.*, **2004**, *69*, 2213-2216.
63. Liu, C.; Lambert J. B. *Polymer Preprints.*, **2004**, *45(2)*, 746-747.
64. Liu, C.; Naismith, N.; Economy, J. *J. Chromatogr. A*, **2004**, *1036*, 113-118.
65. Liu, C.; Wang, J.; Economy, J. *Macromol. Rapid Commun.*, **2004**, *25*, 863-866.
66. Wight, A. P.; Davis, M. E. *Chem. Rev.* **2002**, *102*, 3589-3614.
67. Mercier, L.; Pinnavia, T. J. *Chem Mater*, **2000**, *12*, 188-196.
68. Tanev, P. T.; Pinnavaia, T. J. *Chem. Mater.* **1996**, *8*, 2068-2079.
69. Langmuir, I. *J. Am. Chem. Soc.*, **1916**, *38*, 2221-2295.
70. Freundlich, H. *Colloid and Capillary Chemistry, London,* **1926**, p 120.
71. Brunauer, S.; Emmet, P. H.; Teller, E. *J. Am. Chem. Soc.*, **1938**, *60*, 309-319.
72. Richer, R.; Mercier L. *Chem. Commun.*, **1998**, 1775-1776.
73. Richer, R.; Mercier L. *Chem. Mater.*, **2001**, *13*, 2999-3008.
74. Harwood, L. M.; Moody, J. M. *Experimental Organic Chemistry, Blackwell Scientific Publication, London,* **1990**, p 137.
75. Wenz, G. *Angew. Chem. Int. Ed. Engl.* **1994**, *33*, 803-822 and references cited therein.
76. Kortum, G. *Reflectance Spectroscopy, Springer Verlag, Heidelberg - New York, NY,* **1969**.
77. Krivacsy, Z.; Hlavayb, J. *Journal of Molecular Structure*, **1995**, *349*, 289-292.
78. Long, D. A. *Raman Spectroscopy, McGraw Hill International Book Company, New York, NY*, **1997**.
79. Jaffe, H. H.; Orchin M., *Theory and Applications of Ultraviolet Spectroscopy, John Wiley and Sons, Inc. New York, NY*, **1962**.
80. Sing, K. S. W. *Pure and Applied Chemistry*, **1982**, *54*, 2201-2218.
81. Toreci, I.; Tezel, F. H.; Yong, Y.; Sayari, A. *Adsorption Science and Technology*, **2006**, *24 (1),* 79-99.
82. Sismanoglu, T.; Ercag, A.; Pura, S; Ercag, E. *J. Braz. Chem. Soc.*, **2004**, *15(5)*, 669-675.
83. Schneider, H. J.; Hacket, F.; Rudiger V.; Ikeda, H. *Chem. Rev.* **1998**, *98*, 1755-1785.
84. Egyed, O. *Vibrational Spectroscopy*, **1990**, *1*, 225-227.
85. Williams, D. H.; Fleming, I. *Spectroscopic Methods in Organic Chemistry, 5th Ed., McGraw-Hill Companies, New York, NY*.
86. Jung, H. Y.; Gupta, R. K.; Oh, E. O.; Kim, Y. H.; Whang, C. M. *Journal of Non-crystalline Solids*, **2005**, *351*, 372-379.
87. Ponchel, A.; Abramson, S.; Quartararo, J.; Bormann, D.; Barbaux, Y.; Monflier, E. *Microporous and Mesoporous Materials*, **2004**, *75*, 261-272.
88. Yoo, S.; Lunn, J. D.; Gonzalez, S.; Ristich, J. A.; Simanek, E. E.; Shantz, D. F *Chem. Mater*. **2006**, 18*(13)*, 2935-2942.
89. Bauer, F.; Ernst, H.; Hirsch, D.; Naumov, S.; Pelzing, M.; Sauerland, V.; Mehnert, R. *Macromolecular Chemistry and Physics*, **2004**, *205(12)*, 1587-1593.
90. Bauer, F.; Glasel, H. J.; Decker, U.; Ernst, H.; Freyer, A.; Hartmann, E.; Sauerland, V.; Mehnert, R. *Progress in Organic Coatings*, **2003**, *47(2)*, 147-153.

91. Bauer, F.; Glasel, H. J.; Hartmann, E.; Bilz, E.; Mehnert, R. *Nuclear Instruments & Methods in Physics Research, Section B: Beam Interactions with Materials and Atoms* **2003**, *208*, 267-270.
92. Vuluga, D. M.; Hamaide, T.; Pantiru, M.; Novat, C. *Polymer Bulletin (Berlin, Germany)* **2002**, *47(5)*, 399-405.
93. Brunel, D.; Cauvel, A.; Fauja, F.; DiRenzo, F. *Studies in Surface Science and Catalysis*, **1995**, *97*, 173-180.
94. Kruk, M.; Jaroniec, M. *Chem. Mater.*, **2001**, *13*, 3169-3183.
95. Burleigh, M. C.; Dai, S.; Hagaman, E. W.; Lin, J. S. *Chem. Mater.*, **2001**, *13*, 2537-2546.
96. Hossain, K. Z.; Mercier L. *Adv. Mater.*, **2002**, *14*, 1053-1056.
97. Belyakova, L. A.; Vlasova, N. N.; Golovkova, L. P.; Varvarin, A. M.; Lyashenko, D. Y.; Svezhentsova, A. A.; Stukalina, N. G.; Chuiko, A. A. *J. Coll. Interface Sci.*, **2003**, *258*, 1-9.
98. Lin, H. P.; Mou, C. Y. *Acc. Chem. Res.*, **2002**, *35*, 927-935.
99. Che, S.; Lai, H.; Lim, S.; Sakamoto, Y.; Terasaki, O.; Tatsumi, T. *Chem. Mater.*, **2005**, *17*, 4103-4113.
100. Pang, J.; Na, H.; Lu, Y. *Microporous and Mesoporous Materials*, **2005**, *86*, 89-95.
101. Yokoi, T.; Yoshitake, H.; Yamada, T.; Kubota, Y.; Tatsumi, T. *J. Mater. Chem.*, **2006**, *16*, 1125-1135.
102. Chen, D.; Li, Z.; Wan, Y.; Tu, X.; Shi Y.; Chen, Z.; Shen, W.; Yu, C.; Tu, B.; Zhao, D. *J. Mater. Chem.*, **2006**, *16*, 1511-1519.
103. Tarafdar, A.; Pramanik, P. *Microporous and Mesoporous Materials*, **2006**, *91*, 221-224.
104. Che, S.; Garcia-Bennet, A. E.; Yokoi, T.; Sakamoto, K; Kunieda, H; Terasaki, O; Tatsumi, T. *Nature*, **2003**, *2*, 801-805.
105. Hu, Q.; Hampsey, J. E.; Jiang, N.; Li, C.; Lu, Y. *Chem. Mater.*, **2005**, *17*, 1561-1569.
106. Cho, E. B.; Char, K. *Chem. Mater.*, **2004**, *16*, 270-275.
107. Kimura, T. *Chem. Mater.*, **2005**, *17*, 5521-5528.
108. Li, D.; Guan, X.; Song, J.; Di, Y.; Zhang, D.; Ge, X.; Zhao, L.; Xiao S. *Colloids and Surfaces A: Physicochem. Eng. Aspects*, **2006**, *272*, 194-202.
109. Christian, D.; Guoying, X.; Normand, V.; Suzanne, G.; Serge, K. *Revue Roumaine de Chimie*, **2000**, *44*, 1011-1023.
110. Liu, C.; Lambert, J.; Fu, L. *J. Mater. Chem.*, **2004**, *14*, 1303-1309.
111. Yinhan, G.; Kee, L. H. *Analytical Chemistry*, **2003**, *75*, 1348-1354.
112. Franck, D.; Geraud, D.; Raphael, T.; Stephane, B.; Roger, G; *Phosphorus, Sulfur and Silicon and the Related Elements*, **2001**, *168-169*, 151-156.
113. Dag O.; Ozin, G. A. *Advanced Materials*, **2001**, *13*, 1182-1185.

APPENDICES

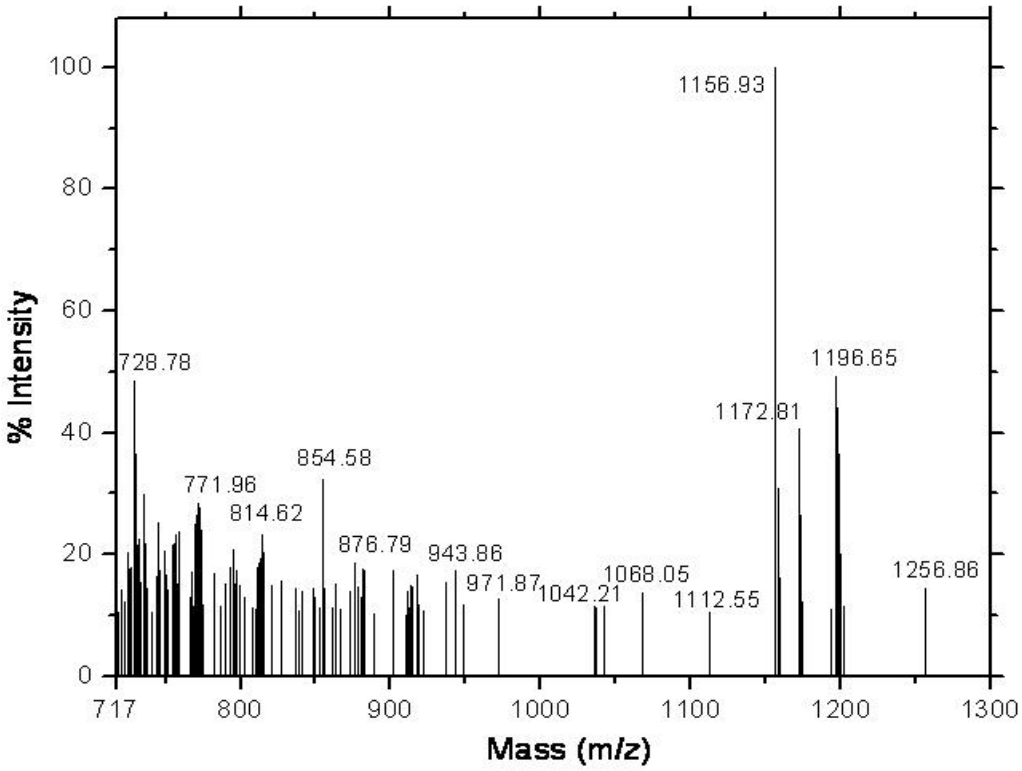

A.1: MALDI TOF MS of CD ICS 2 (12).

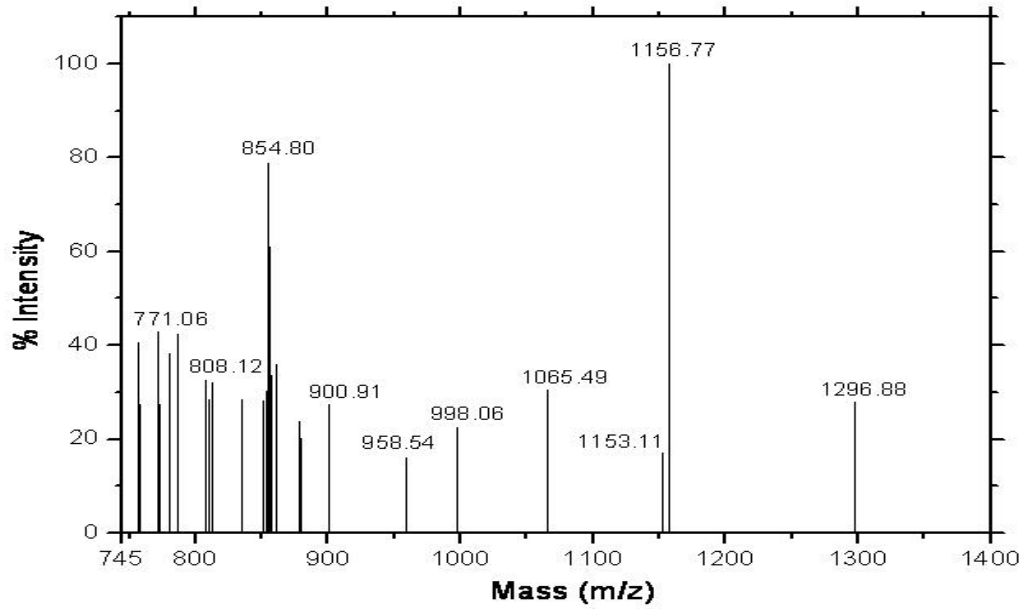

A.2: MALDI TOF MS of CD ICS 6 (12).

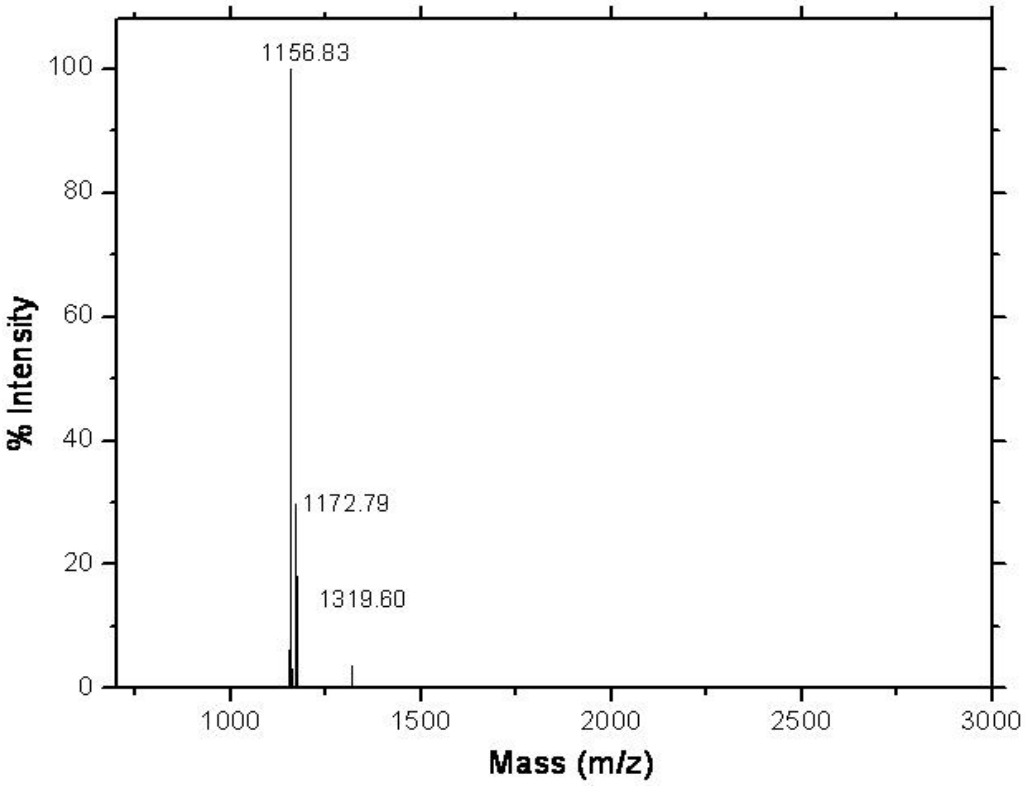

A.3: MALDI TOF MS of CD ICS 2 (14).

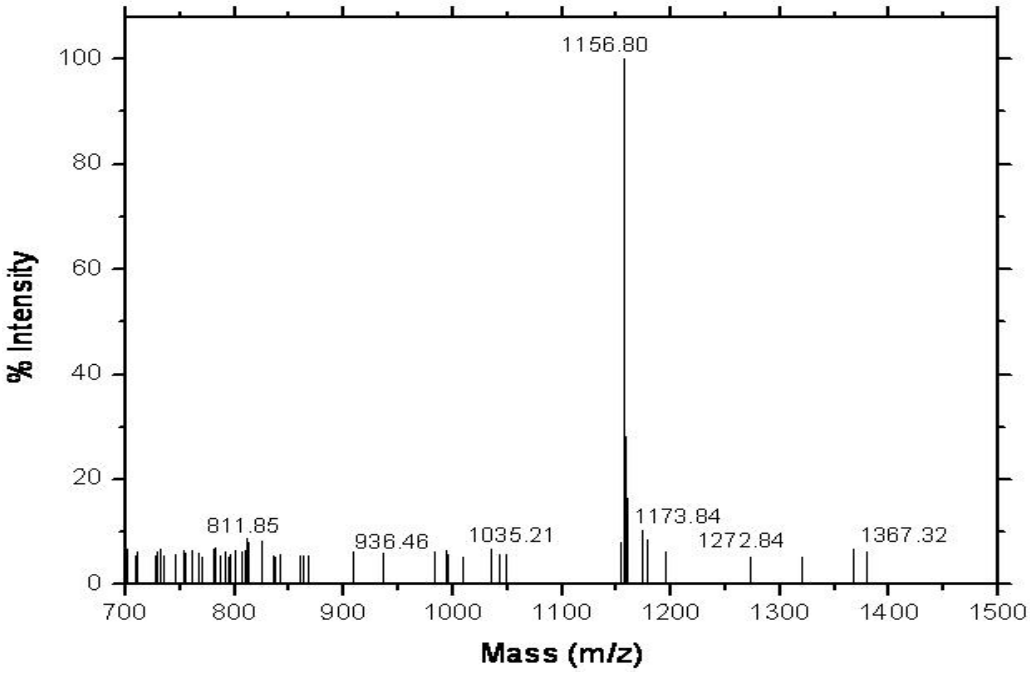

A.4: MALDI TOF MS of CD ICS 4 (14).

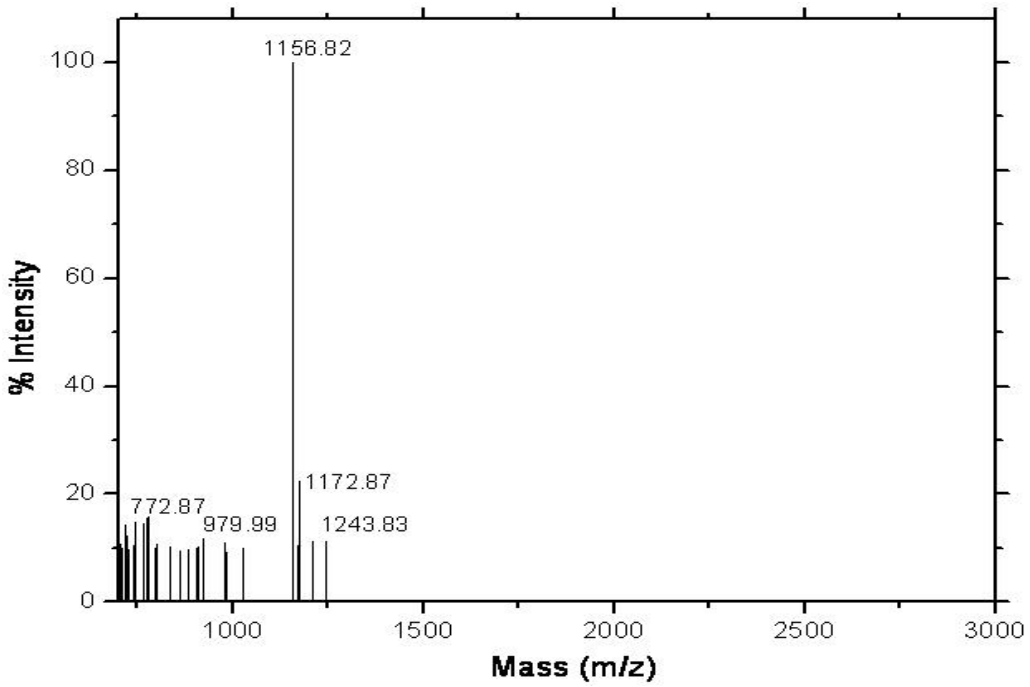

A.5: MALDI TOF MS of CD ICS 6 (14).

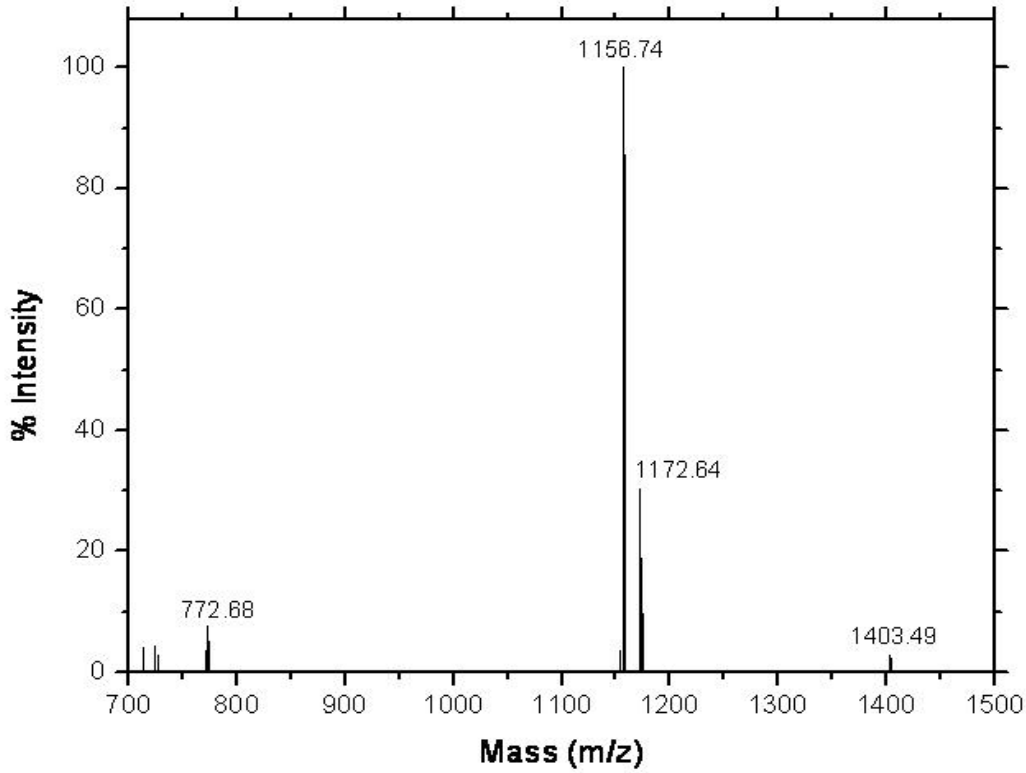

A.6: MALDI TOF MS of CD ICS 4 (16).

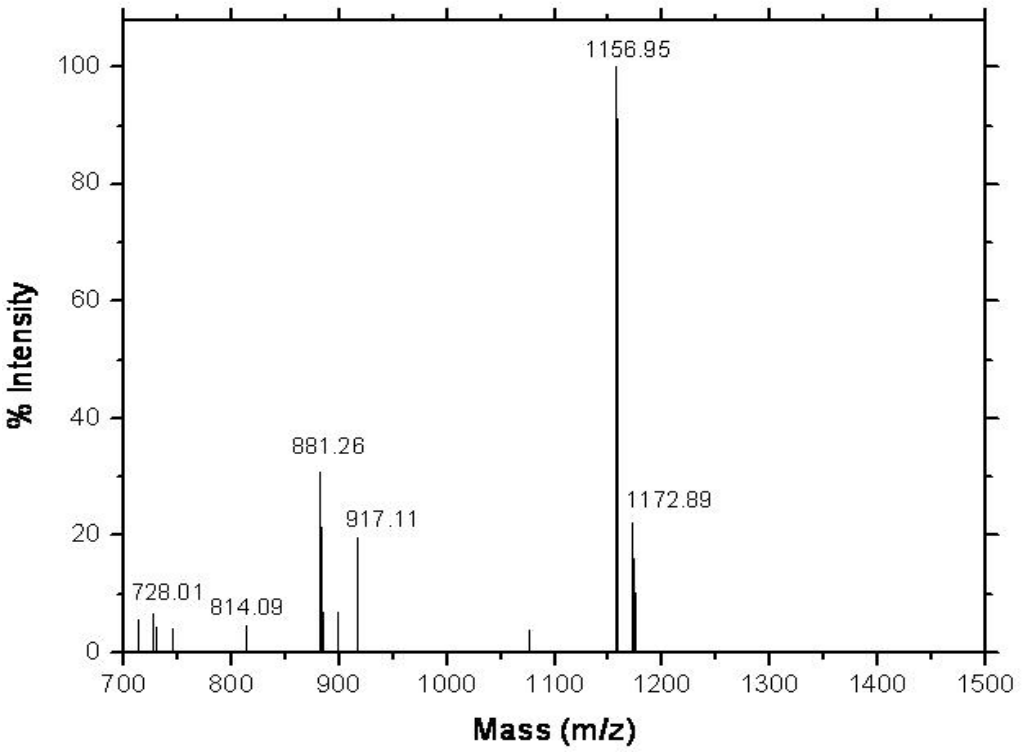

A.7: MALDI TOF MS of CD ICS 6 (16).

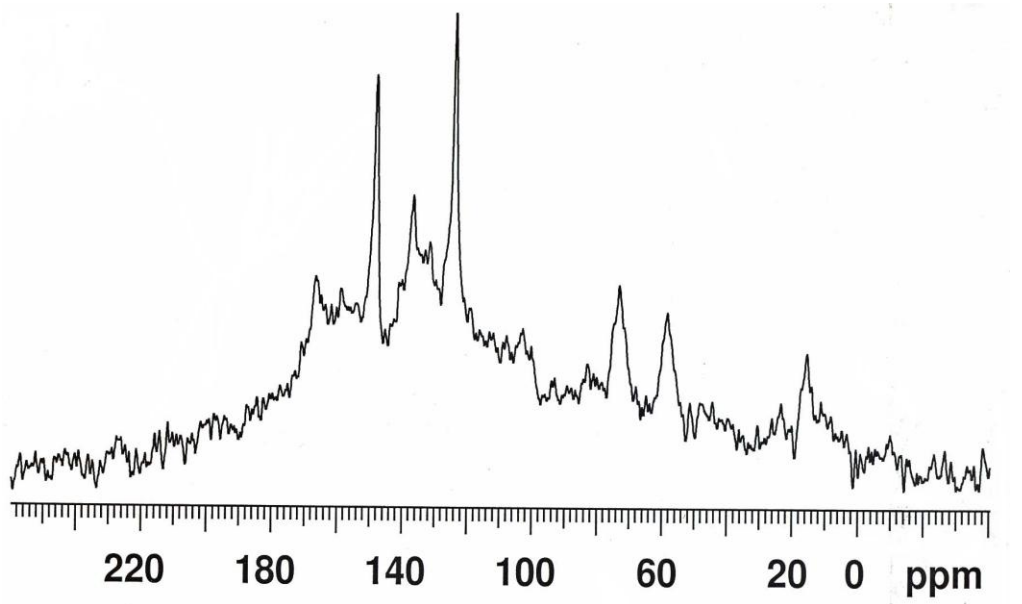

A.8: Solid state ^{13}C NMR CP MAS of CD ICS 2 (12) at room temperature obtained at 150.8 MHz and room temperature with a spinning speed of 16 kHz.

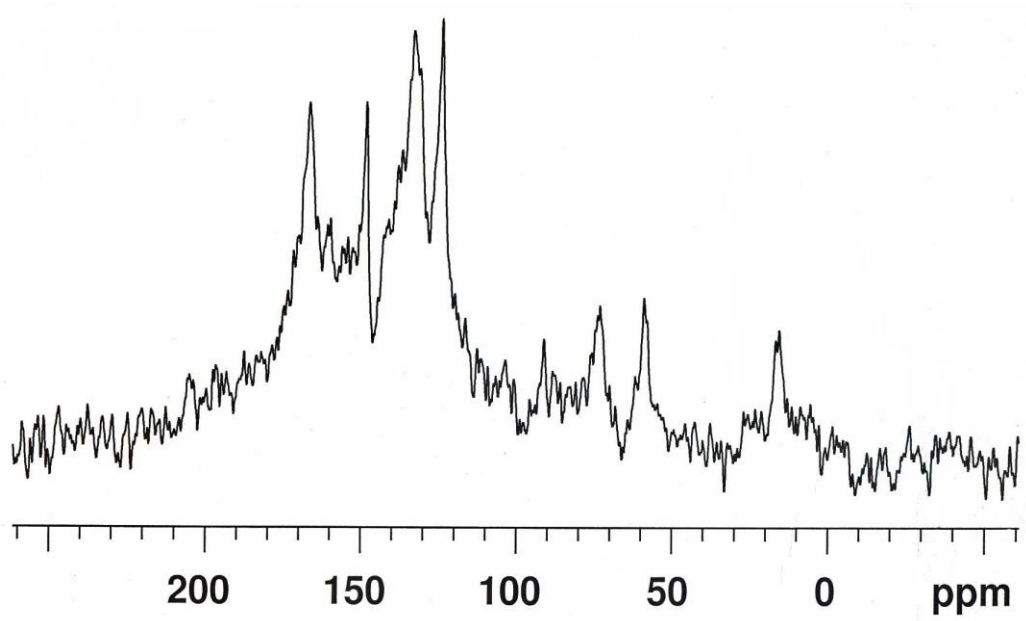

A.9: Solid state ^{13}C NMR CP MAS of CD ICS 4 (12) at room temperature obtained at 150.8 MHz and room temperature with a spinning speed of 16 kHz.

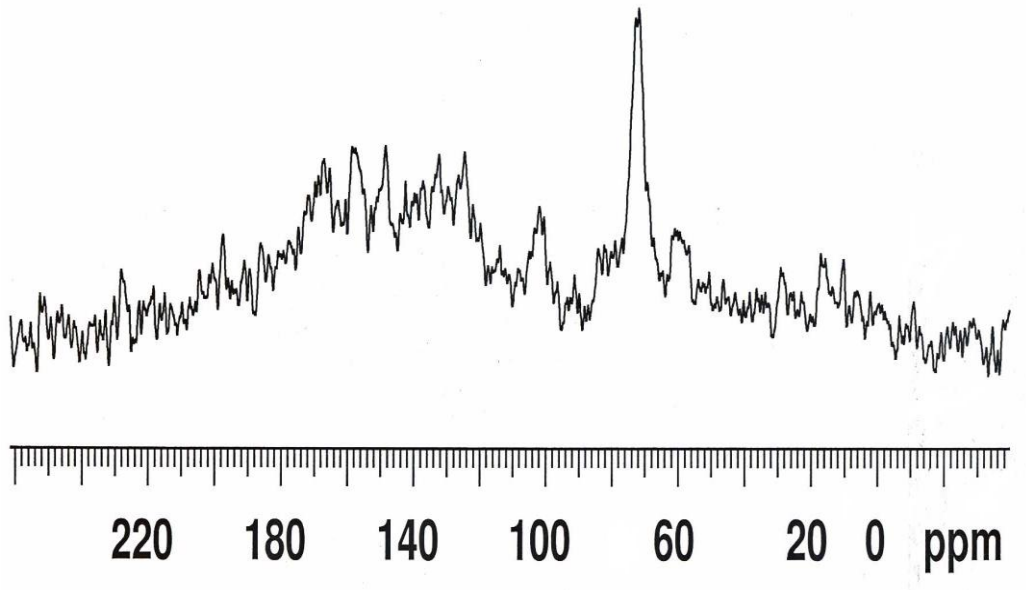

A.10: Solid state ^{13}C NMR CP MAS of CD ICS 6 (12) at room temperature obtained at 150.8 MHz and room temperature with a spinning speed of 16 kHz.

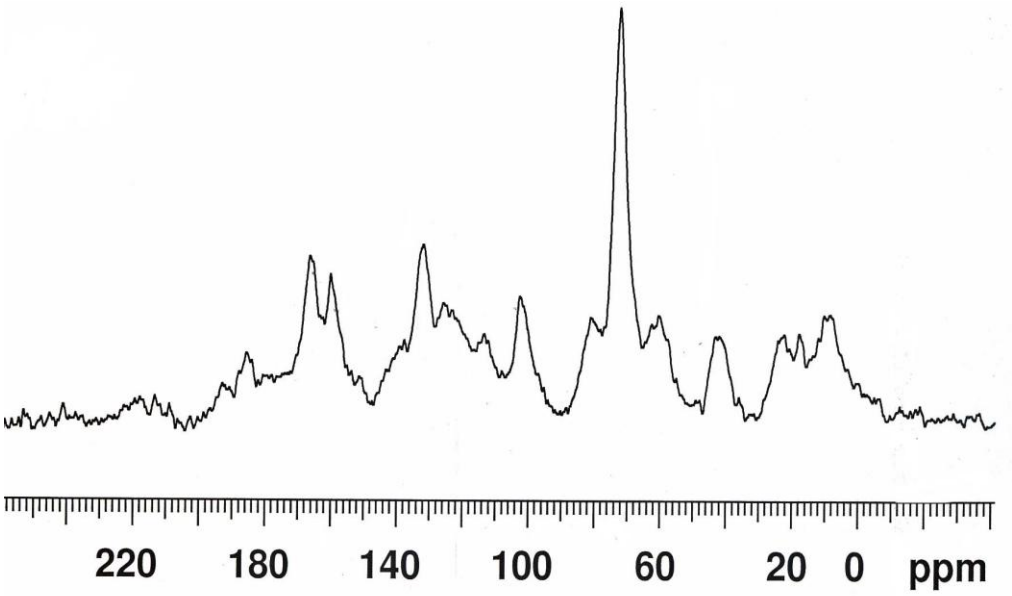

A.11: Solid state ^{13}C NMR CP MAS of CD ICS 4 (14) at room temperature obtained at 150.8 MHz and room temperature with a spinning speed of 16 kHz.

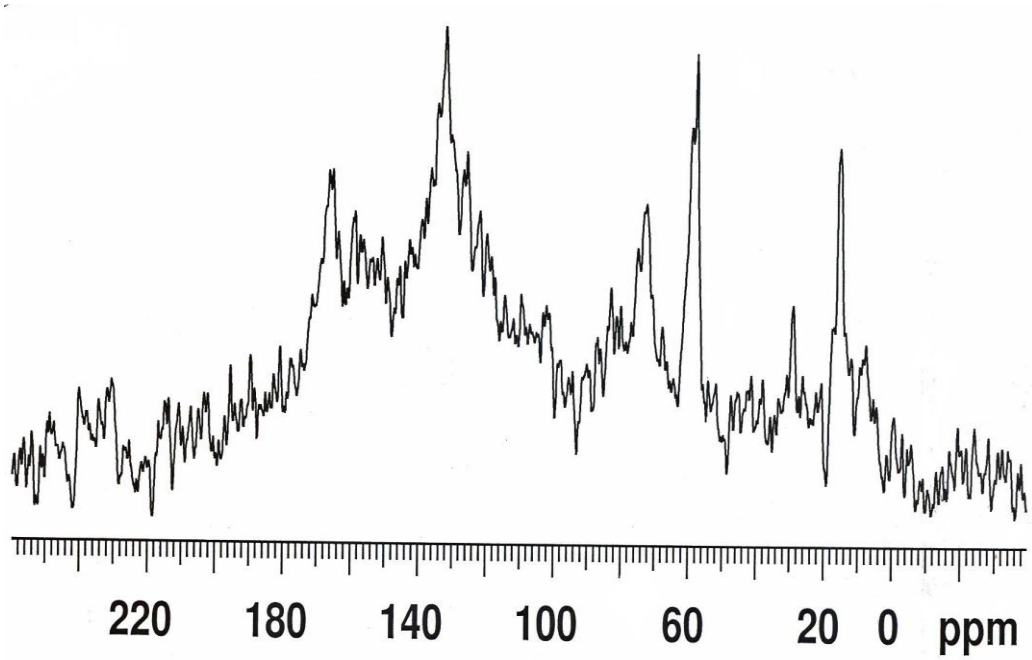

A.12: Solid state ^{13}C NMR CP MAS of CD ICS 6 (14). at room temperature obtained at 150.8 MHz and room temperature with a spinning speed of 16 kHz.

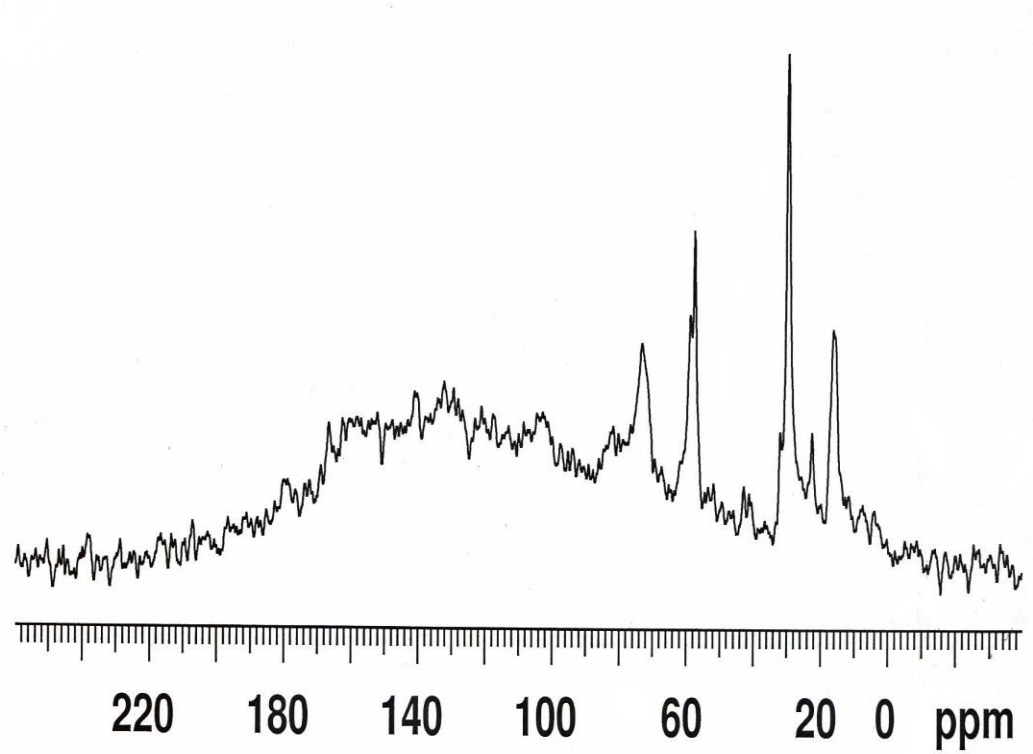

A.13: Solid state ^{13}C NMR CP MAS of CD ICS 2 (16) at room temperature obtained at 150.8 MHz and room temperature with a spinning speed of 16 kHz.

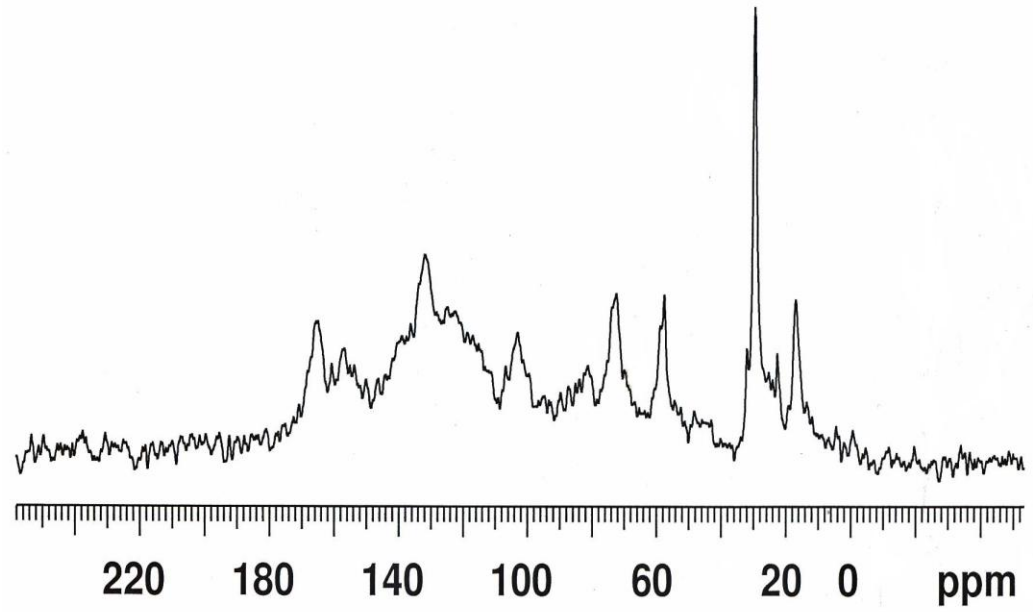

A.14: Solid state ^{13}C NMR CP MAS of CD ICS 4 (16) at room temperature obtained at 150.8 MHz and room temperature with a spinning speed of 16 kHz.

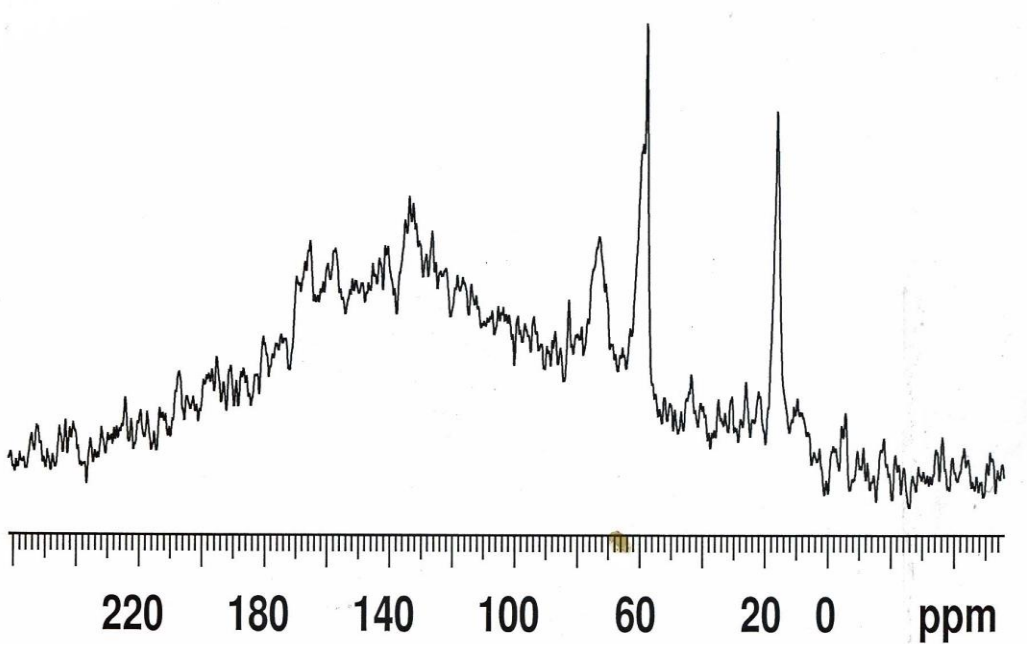

A.15: Solid state ^{13}C NMR CP MAS of CD ICS 6 (16) at room temperature obtained at 150.8 MHz and room temperature with a spinning speed of 16 kHz.

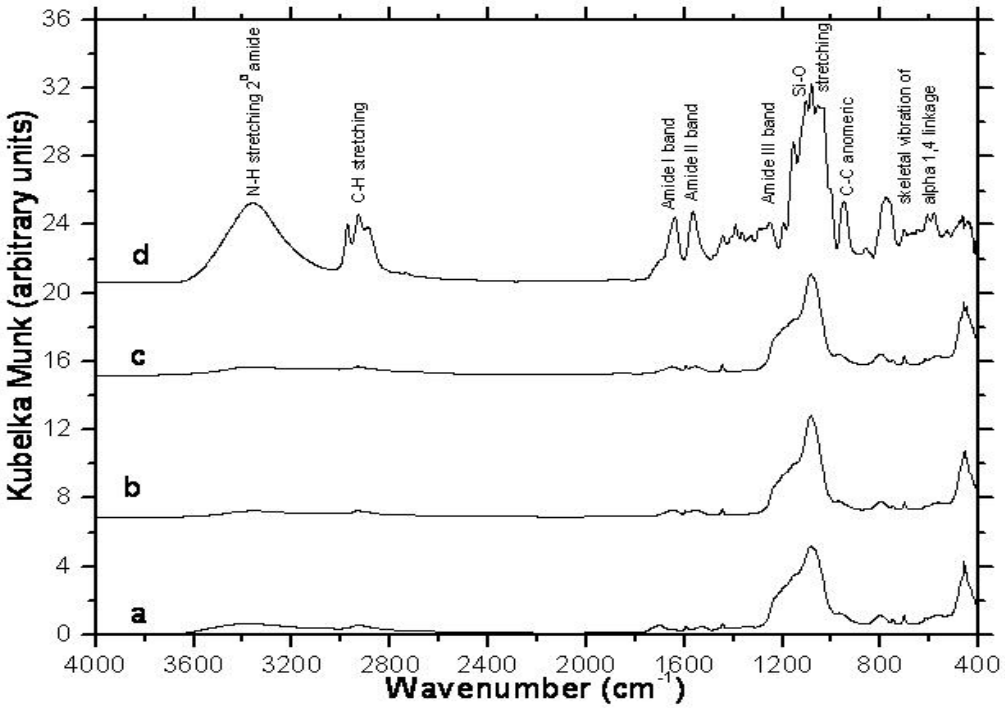

A.16: Infrared Spectra of a) CD ICS 2(12) b) CD ICS 4(12) and c) CD ICS 6(12) and d) CD ICL at room temperature.

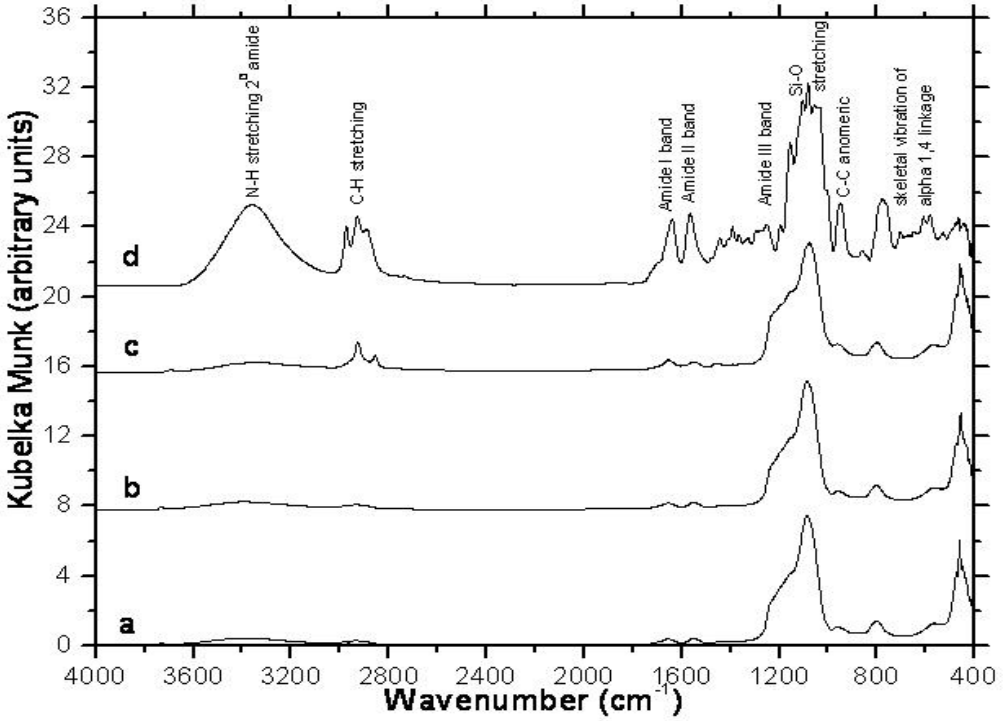

A.17: Infrared Spectra of a) CD ICS 2(16) b) CD ICS 4(16) and c) CD ICS 6(16) and d) CD ICL at room temperature.

A.18: Calculation of surface Area of CD ICS 4(12) from CH_3Cl gas adsorption at room temperature

The following example shows the calculation of surface area from Langmuir model for CD ICS 4(12).

According to Langmuir isotherm $\frac{P}{V} = \frac{P}{V_u} + \frac{1}{bV_u}$.....(*A*.1)

From nonlinear Langmuir fitting V_u = 49.16 cm^3/g

$V_{STP} = \frac{RT_{STP}}{P_{STP}}$..... .(*A*.2)

R = universal gas constant = 0.08206 $dm^3atmK^{-1}mol^{-1}$

T_{STP} = absolute temperature = 298.15 K

P_{STP} = absolute pressure = 0.98685 atm

Putting the value of R, T_{STP} and P_{STP} in the equation, $V_{STP} = \frac{RT_{STP}}{P_{STP}}$, the value of

V_{STP}= 24792.40 cm^3

No of molecules in unimolecular layer = $\frac{V_u N_A}{V_{STP}}$..... ...(*A*.3)

Where N_A = Avogadro number = 6.02214×10^{23}

Putting the value of V_u, N_A and V_{STP} the number of molecules in unimolecular layer = 1.19×10^{21}

Assuming that molecule has same volume as a molecule in liquid state, the volume of one gas molecule can be calculated from the following equation

Volume of one gas molecule of CH_3Cl is $V_{molecule} = \frac{MolarMass}{N_A \rho_{CH_3Cl}}$……...(*A*.4)

Molar mass of CH_3Cl = 50.488 a.m.u., $N_A = 6.02214 \times 10^{23}$

And density of CH_3Cl = 0.9159 g/cm^3

From these values,

Volume of one gas molecule of CH_3Cl is $V_{molecule} = 9.1535 \times 10^{-23}$ cm^3

surface area of a single molecule (assuming cubic geometry)

Area = $(V_{molecule})^{2/3} = 4.3758 \times 10^{-15}$ cm^2

Surface area per gram of adsorbent can be calculated as

Area/g = (Area) (number of molecules) = 5.21×10^6 cm^2/g = 521 m^2/g

A.19: Experimental data and equation for analysis of error for sorption of p-nitrophenol in CD ICS

The following equation was used to calculate the value of χ^2 (as it appears in Tables A.8)

$$\chi^2 = \sum_{i=1}^{10} \frac{\left(Q_{e,experimental} - Q_{e,theoritical}\right)^2}{Q_{e,theoritical}} \text{..... .}(A.5)$$

where, $Q_{e,\ experimental}$ and $Q_{e,\ theoretical}$ are observed and expected value of the equilibrium concentration of p-nitrophenol adsorbed in CD ICS.

A.20: Experimental data and value of $\chi_{distribution}^{*}$ for sorption of p-nitrophenol in CD ICS 2(12)

Mass (g)	**C_o (mmol/L)**	**C_e (mmol/L)**	**Q_e (mmol/g)**	**$\chi_{distribution}$**
1.000×10^{-3}	9.499×10^{-2}	8.812×10^{-2}	1.374×10^{-1}	9.870×10^{-1}
3.000×10^{-3}		8.733×10^{-2}	5.110×10^{-2}	9.969×10^{-1}
6.000×10^{-3}		8.682×10^{-2}	2.721×10^{-2}	9.988×10^{-1}
1.000×10^{-2}		8.434×10^{-2}	2.130×10^{-2}	9.991×10^{-1}
2.500×10^{-2}		7.966×10^{-2}	1.226×10^{-2}	9.996×10^{-1}
5.000×10^{-2}		7.388×10^{-2}	8.442×10^{-3}	9.997×10^{-1}
7.500×10^{-2}		6.900×10^{-2}	6.923×10^{-3}	9.998×10^{-1}
1.000×10^{-1}		6.522×10^{-2}	5.953×10^{-3}	9.998×10^{-1}
2.500×10^{-1}		4.740×10^{-2}	3.807×10^{-3}	9.999×10^{-1}
5.000×10^{-1}		3.715×10^{-2}	2.314×10^{-3}	9.999×10^{-1}

*obtained using 3 degrees of freedom (C_e, Q_e, and m) according to the calculation provided within the built in χ function provided by MS Excel®

A.21: Experimental data and value of $\chi_{distribution}^{*}$ for sorption of p-nitrophenol in CD ICS 2(16)

Mass (g)	C_o (mmol/L)	C_e (mmol/L)	Q_e (mmol/g)	$\chi_{distribution}$
1.000×10^{-3}	9.340×10^{-2}	8.802×10^{-2}	5.376×10^{-2}	9.967×10^{-1}
3.000×10^{-3}		8.623×10^{-2}	2.389×10^{-2}	9.990×10^{-1}
6.000×10^{-3}		8.344×10^{-2}	1.659×10^{-2}	9.994×10^{-1}
1.000×10^{-2}		7.996×10^{-2}	1.344×10^{-2}	9.996×10^{-1}
2.500×10^{-2}		7.190×10^{-2}	8.601×10^{-3}	9.998×10^{-1}
5.000×10^{-2}		6.503×10^{-2}	5.674×10^{-3}	9.999×10^{-1}
7.500×10^{-2}		5.995×10^{-2}	4.460×10^{-3}	9.999×10^{-1}
1.000×10^{-1}		5.537×10^{-2}	3.803×10^{-3}	9.999×10^{-1}
2.500×10^{-1}		3.616×10^{-2}	2.290×10^{-3}	9.999×10^{-1}
5.000×10^{-1}		2.252×10^{-2}	1.418×10^{-3}	9.999×10^{-1}

*obtained using 3 degrees of freedom (C_e, Q_e, and m) according to the calculation provided within the built in χ function provided by MS Excel®

A.22: Experimental data and value of $\chi_{distribution}^{*}$ for sorption of p-nitrophenol in CD ICS 4(12)

Mass (g)	C_o (mmol/L)	C_e (mmol/L)	Q_e (mmol/g)	$\chi_{distribution}$
1.000×10^{-3}	9.798×10^{-2}	9.161×10^{-2}	6.371×10^{-2}	9.958×10^{-1}
3.000×10^{-3}		8.872×10^{-2}	3.086×10^{-2}	9.985×10^{-1}
6.000×10^{-3}		8.514×10^{-2}	2.140×10^{-2}	9.991×10^{-1}
1.000×10^{-2}		8.185×10^{-2}	1.613×10^{-2}	9.995×10^{-1}
2.500×10^{-2}		7.388×10^{-2}	9.637×10^{-3}	9.997×10^{-1}
5.000×10^{-2}		6.642×10^{-2}	6.311×10^{-3}	9.999×10^{-1}
7.500×10^{-2}		6.144×10^{-2}	4.871×10^{-3}	9.999×10^{-1}
1.000×10^{-1}		5.746×10^{-2}	4.051×10^{-3}	9.999×10^{-1}
2.500×10^{-1}		4.372×10^{-2}	2.170×10^{-3}	9.999×10^{-1}
5.000×10^{-1}		3.446×10^{-2}	1.270×10^{-3}	9.999×10^{-1}

*obtained using 3 degrees of freedom (C_e, Q_e, and m) according to the calculation provided within the built in χ function provided by MS Excel®

A.23: Experimental data and value of $\chi_{distribution}^{*}$ for sorption of p-nitrophenol in CD ICS 4(16)

Mass (g)	C_o (mmol/L)	C_e (mmol/L)	Q_e (mmol/g)	$\chi_{distribution}$
1.000×10^{-3}	9.340×10^{-2}	8.912×10^{-2}	4.281×10^{-2}	9.977×10^{-1}
3.000×10^{-3}		8.703×10^{-2}	2.124×10^{-2}	9.992×10^{-1}
6.000×10^{-3}		8.464×10^{-2}	1.460×10^{-2}	9.995×10^{-1}
1.000×10^{-2}		7.986×10^{-2}	1.354×10^{-2}	9.996×10^{-1}
2.500×10^{-2}		7.190×10^{-2}	8.601×10^{-3}	9.999×10^{-1}
5.000×10^{-2}		6.493×10^{-2}	5.694×10^{-3}	9.999×10^{-1}
7.500×10^{-2}		5.577×10^{-2}	5.017×10^{-3}	9.999×10^{-1}
1.000×10^{-1}		5.179×10^{-2}	4.161×10^{-3}	9.999×10^{-1}
2.500×10^{-1}		2.948×10^{-2}	2.556×10^{-3}	9.999×10^{-1}
5.000×10^{-1}		1.864×10^{-2}	1.495×10^{-3}	9.999×10^{-1}

*obtained using 3 degrees of freedom (C_e, Q_e, and m) according to the calculation provided within the built in χ function provided by MS Excel®

A.24: Experimental data and value of $\chi_{distribution}^{*}$ for sorption of p-nitrophenol in CD ICS 6(12)

Mass (g)	C_o (mmol/L)	C_e (mmol/L)	Q_e (mmol/g)	$\chi_{distribution}$
1.000×10^{-3}	9.629×10^{-2}	8.912×10^{-2}	7.168×10^{-2}	9.950×10^{-1}
3.000×10^{-3}		9.041×10^{-2}	1.958×10^{-2}	9.993×10^{-1}
6.000×10^{-3}		8.733×10^{-2}	1.493×10^{-2}	9.995×10^{-1}
1.000×10^{-2}		8.364×10^{-2}	1.264×10^{-2}	9.996×10^{-1}
2.500×10^{-2}		7.618×10^{-2}	8.044×10^{-3}	9.998×10^{-1}
5.000×10^{-2}		6.632×10^{-2}	5.993×10^{-3}	9.999×10^{-1}
7.500×10^{-2}		6.045×10^{-2}	4.779×10^{-3}	9.999×10^{-1}
1.000×10^{-1}		5.597×10^{-2}	4.032×10^{-3}	9.999×10^{-1}
2.500×10^{-1}		4.193×10^{-2}	2.174×10^{-3}	9.999×10^{-1}
5.000×10^{-1}		3.128×10^{-2}	1.338×10^{-3}	9.999×10^{-1}

*obtained using 3 degrees of freedom (C_e, Q_e, and m) according to the calculation provided within the built in χ function provided by MS Excel®

A.25: Experimental data and value of $\chi_{distribution}^{*}$ for sorption of p-nitrophenol in CD ICS 6(14)

Mass (g)	C_o (mmol/L)	C_e (mmol/L)	Q_e (mmol/g)	$\chi_{distribution}$
1.000×10^{-3}	9.221×10^{-2}	8.852×10^{-2}	3.683×10^{-2}	9.981×10^{-1}
3.000×10^{-3}		8.882×10^{-2}	1.128×10^{-2}	9.997×10^{-1}
6.000×10^{-3}		8.733×10^{-2}	8.130×10^{-3}	9.998×10^{-1}
1.000×10^{-2}		8.563×10^{-2}	6.570×10^{-3}	9.999×10^{-1}
2.500×10^{-2}		8.165×10^{-2}	4.221×10^{-3}	9.999×10^{-1}
5.000×10^{-2}		7.667×10^{-2}	3.106×10^{-3}	9.999×10^{-1}
7.500×10^{-2}		7.140×10^{-2}	2.774×10^{-3}	9.999×10^{-1}
1.000×10^{-1}		6.363×10^{-2}	2.041×10^{-3}	9.999×10^{-1}
2.500×10^{-1}		4.104×10^{-2}	1.711×10^{-3}	9.999×10^{-1}
5.000×10^{-1}		2.511×10^{-2}	1.342×10^{-3}	9.999×10^{-1}

*obtained using 3 degrees of freedom (C_e, Q_e, and m) according to the calculation provided within the built in χ function provided by MS Excel®

A.26: Experimental data and value of $\chi_{distribution}^{*}$ for sorption of p-nitrophenol in CD ICS 6(16)

Mass (g)	C_o (mmol/L)	C_e (mmol/L)	Q_e (mmol/g)	$\chi_{distribution}$
1.000×10^{-3}	9.320×10^{-2}	8.992×10^{-2}	3.285×10^{-2}	9.984×10^{-1}
3.000×10^{-3}		8.872×10^{-2}	1.493×10^{-2}	9.995×10^{-1}
6.000×10^{-3}		8.583×10^{-2}	1.228×10^{-2}	9.996×10^{-1}
1.000×10^{-2}		8.285×10^{-2}	1.035×10^{-2}	9.997×10^{-1}
2.500×10^{-2}		7.439×10^{-2}	7.526×10^{-3}	9.998×10^{-1}
5.000×10^{-2}		6.533×10^{-2}	5.574×10^{-3}	9.999×10^{-1}
7.500×10^{-2}		5.497×10^{-2}	4.662×10^{-3}	9.999×10^{-1}
1.000×10^{-1}		4.999×10^{-2}	4.115×10^{-3}	9.999×10^{-1}
2.500×10^{-1}		2.909×10^{-2}	2.564×10^{-3}	9.999×10^{-1}
5.000×10^{-1}		1.485×10^{-2}	1.567×10^{-3}	9.999×10^{-1}

*obtained using 3 degrees of freedom (C_e, Q_e, and m) according to the calculation provided within the built in χ function provided by MS Excel®

A.27: Error analysis for p-nitrophenol sorption in CD ICS materials

CD ICS	Langmuir		BET		Freundlich	
	χ^2 $\times 10^{-1}$	SSR $\times 10^{-4}$	χ^2 $\times 10^{-1}$	SSR $\times 10^{-4}$	χ^2 $\times 10^{-1}$	SSR $\times 10^{-4}$
CD ICS 2(12)	9.99	2.29	9.99	82.6	9.99	125
CD ICS 2(16)	10.0	0.759	10.0	2.04	9.99	14.2
CD ICS 4(12)	10.0	0.193	10.0	3.81	9.99	13.5
CD ICS 4(16)	10.0	6.09	10.0	2.50	9.99	7.59
CD ICS 6(12)	9.99	29.0	9.99	29.2	9.99	31.3
CD ICS 6(14)	9.99	6.92	9.99	6.90	9.99	9.27
CD ICS 6(16)	10.0	3.75	10.0	2.40	9.99	4.74